DISCLAIMER

Project Technical Progress Report

for

US Department of Energy

Award Number: DE-EE0009162.000

Project Title: Membrane-based Ionic Liquid Absorption System for Ultra-Efficient Dehumidification and Heating

Project Period: April 1st, 2020 – March 31st, 2025

Date of Report: July 30th, 2025

Recipient Organization: University of Florida

33 Tigert Hall

Gainesville, FL 32611-3001

DUNS: 969663814

Partner: GTI Energy

Technical Contact: Saeed Moghaddam, (352) 392-0889, saeedmog@ufl.edu

Business Contact: Stephanie Gray, (352) 392-9267, ufproposals@ufl.edu

Table of Contents

Table of Figures

List of Tables

Summary

The project team – comprising the University of Florida (UF), GTI Energy, and Modine Manufacturing – sought to develop a highly efficient heat-powered absorption cycle with combined dehumidification and heat pumping. This DOE-supported project advanced the technology from a TRL of 3 to 6, culminating in the development of a 1,000 CFM system. Key innovations implemented in the system addressed the low efficiency, size, cost, and reliability challenges of conventional absorption cycles. Specifically, the system was enabled by: (1) a semi-open cycle that allowed simultaneous dehumidification and heat recovery, (2) non-crystallizing ionic liquids (ILs) that enabled "double-effect" operation at elevated temperatures without the need for costly control equipment, (3) a compact membrane-based absorber that confined the IL and directly cooled it to achieve low dew points, and (4) a novel, highly integrated desorber–condenser assembly that reduced size, weight, and cost. The technology was developed with commercial HVAC applications in mind, particularly for separate sensible and latent cooling (SSLC), an innovation aimed at achieving independent and more efficient humidity control.

Introduction

Project Background and Motivation

Commercial HVAC is a major end use for natural gas and propane in buildings, with forced-air type equipment (e.g. RTUs) the primary means of heating/cooling. The Advanced RTU Campaign (DOE) estimates that more than 60% of commercial building area is conditioned by RTUs, either processing makeup air, mixed outdoor/makeup air, or as a dedicated outside air system (DOAS) configuration. For RTUs processing outside air, to remove moisture from air, vapor compression systems must overcool air to saturation conditions. This is a thermodynamically inefficient process particularly in the DOAS application in which cooled air is often reheated. The ability to directly remove moisture from air, without cooling it, enables more efficient HVAC systems capable of separate sensible and latent cooling (SSLC). This is particularly the case when latent load constitutes majority of the ventilation load, in many parts of US (See Figure 1). The idea of SSLC is not new; however, despite decades of work, implementation of this technology within the HVAC market space has remained limited. Liquid desiccant technology can play a key role in achieving this objective but this potential has not materialized; high efficiency, low-cost, scalable and robust systems must be developed.

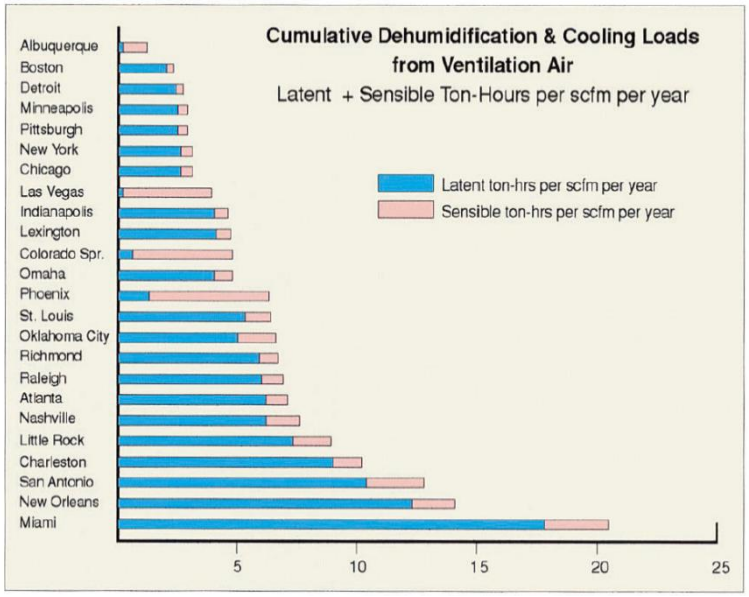

Figure 1: Building Cooling Loads by Location [Harriman, 1997].]

For this effort, the project team developed a highly efficient gas-fired absorption cycle with combined dehumidification and heat pumping functions with $COP_{combined}$ ~ 4. The system can utilize ventilation or indoor humidity load for water and/or space heating. DOE funds was used to advance this technology from a TRL of 3 to 6. A 1000 CFM system was developed: The system benefits from advancements made to enable multiple functionality and address low efficiency, size, cost, and reliability of the existing absorption cycles. Specifically, the system is enabled by 1) a semi-open cycle that allows combined dehumidification and heating, 2) non-crystallizing ionic liquids (ILs) that allow double-effecting the cycle and operation at elevated temperatures (~160 °C) without costly control equipment, 3) compact membrane-based absorber to contain IL and directly cool it for a high system COP, and 4) novel highly integrated double-effect desorbers and condensers design to reduce, size, weight and cost. These advancements have transformational impact on RTU (Figure 2) technology. Example applications include DOAS for dehumidification combined with building zones reheating and/or hot water supply, handling indoor humidity in tight buildings combined with ventilation air and/or space heating in winter, and handling humidity in indoor pools combined with pool water and/or space heating.

Figure 2: Rooftop units developed and tested in prior R&D efforts of the team.

Technical Potential

In developing this advanced IL-based DOAS commercial HVAC solution, the team projected several benefits, including an expansion of natural gas and propane use, reduction in peak electrical power consumption, ~2x increase in energy efficiency of liquid desiccant-based latent cooling cycles, and ~3x increase in heat pumping energy efficiency. The system is based on a compact, efficient latent cooling cycle for separate sensible and latent cooling (SSLC) applications, which can improve indoor air quality (IAQ) at a lower cost. Team estimates indicate a potential for an 85% reduction in operating costs, potential for negative payback vs. expensive EHP-based equipment, primarily based on the substitution of natural gas or propane for electricity when handling high dehumidification loads. If deployed widely in the U.S., the team also projects a reduction of source energy consumption by 0.80 quads. The details of this potential are further explored in this report.

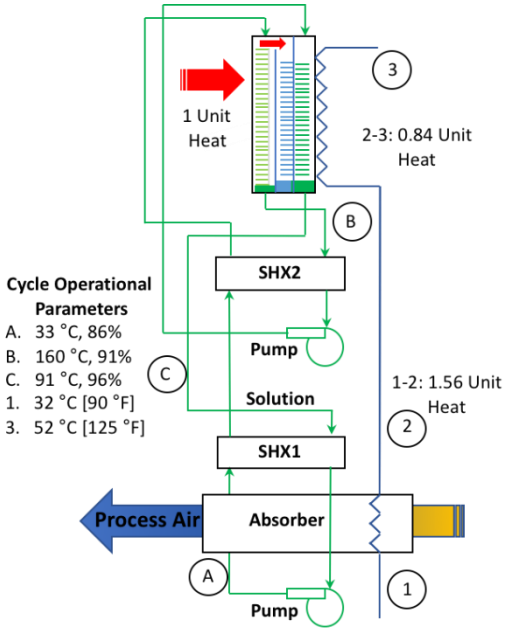

Figure 3: Semi-open absorption system.

Further detail on projected unit cost, the average cost of commercial grade DOAS equipment is $15/cfm. This estimate results in a unit cost of typical new technology of $15,000 for a 1000 cfm DOAS unit. University of Florida estimated the production costs of the sorption module and extended to that of a 1000 cfm commercial grade DOAS unit, with the assumption of a high-volume production environment, a conservative production cost of a 1000 cfm DOAS using our proposed technology is estimated to be $9,280. DOE's composite markup value for HVAC systems of 1.34, this represents a $12,436 retail cost. Thus, the first cost of our proposed DOAS technology is less than the existing typical new DOAS technology. The incremental initial cost of our proposed technology at scale, results in cost of (-$2,564). This indicates that the proposed technical solution has a lower cost at volume.

GTI's Contributions

With experience and expertise in the design and evaluation of thermally-driven HVAC systems, GTI's overall contributions to the project were as follows:

- **Provide Commercial HVAC Subject Matter Expertise**: With experience in the design and demonstration of commercial HVAC equipment, including innovative sorption-based heat pumps and desiccant dehumidification equipment, GTI provided subject matter expertise concerning the design, use, installation, and production of dedicated outdoor air system (DOAS) type rooftop units (RTU). This included support with product definition, competitive assessments, codes/standards analyses, and system design/controls.
- **Hot Side" Technical Support**: Responsible for the design, assessment, and demonstration of the "hot side" of the DOAS RTU, including the combustion system, flue/air side heat exchange, and indirect heating system (if used), to meet performance and emissions targets as defined.
- **Alpha Prototype Packaging and Assessment**: Using a custom RTU test stand, GTI intended to support the packaging, installation, and shakedown of the prototype 1,000 CFM DOAS RTU, using the cycle shown below, and characterize performance through steady-state and cycling tests.

A more detailed breakdown of the efforts are provided below:

- Provide commercial HVAC expertise to the team during the initial product definition, competitive assessment, and determination of operating conditions. Additionally, perform a codes and standards analysis to identify any possible non-technical barriers to DOAS RTU system design and deployment.
- In support of the detailed design of the desorbers and condensers, perform limited modeling (e.g. CFD) and analysis to provide insight into fuel/air-side impacts on these "hot side" components and initiate design activities in preparation for later testing. This analysis will focus on natural gas as fuel but will evaluate how propane can also be best integrated.
- In parallel to the project team's integration of the first double-effect system for evaluation of individual heat and mass exchangers, evaluate the technical feasibility and comparative performance of options for direct (preferred) and indirect-fired (steam/oil) desorbers.
- With design guidance from the project team, design and fabricate "simulators" for the desorber(s) to evaluate multiple combustion system design options and to assess the ability to meet or exceed performance and emission targets.
- Develop an experimental test plan, including simulator design, "hot side" design options, and measurement schemes. Upon team approval, construct the simulator test rig, procure cost-effective options for the combustion system (burner, gas valve/controls, ignition system, blower/inducer), and shakedown the test rig. This test rig will be designed for flexible operation.
- Execute the test plan, analyze the data, compare the performance of each system combination in support of meeting performance and emission targets, and make initial recommendations to the project team to proceed to system prototyping.
- Demonstrate a small scale (200 cfm) Proof-of-Concept double-effect IL absorption system in a lab environment
- Show performance of $COP_{cooling} > 1.2$ & $COP_{heating} > 2.0$

However, the full system 1,000 CFM prototype testing was extensively delayed, due in large part to the COVID-19 pandemic and the associated supply chain disruptions. These tasks to be performed under future projects:

- With the prototype installed at GTI, perform a shakedown to assure the RTU, instrumentation, and controls are all functioning correctly. Ability of the test rig to create and sustain the desired environmental conditions will also be verified.
- Execute the DOAS RTU experimental test plan, fully characterizing the DOAS RTU prototype unit. All testing will be done using natural gas as fuel, but the accompanied analytical analysis of testing results will also consider propane fuel.
- Following the completion of testing analyze the data, compare the performance of the prototype RTU against performance goals, for the interior systems and the overall RTU, issues a summary report, and make recommendations to the project team for future design modifications.

Figure 4: 1,000 CFM prototype under assembly.

KPIs associated with these later tasks include the team demonstrating the first full scale (1,000 cfm) breadboard system and show its performance to meet or exceed $COP_{cooling}$ > 1.4 & $COP_{heating}$ > 2.4. These adjustments to the project task level timing were necessary, due to several challenges overcome during the execution of the tasks. Later results from the testing of the 1,000 CFM prototype will be provided to DOE.

Analysis of Ionic Liquid HVAC System

Ionic liquid desiccants (ILD) are an emerging class of sorbent materials being evaluated for air conditioner (AC) applications. Longstanding public and private sector research, development, and deployment (RD&D) objectives have sought to introduce new AC technologies that separate the treatment of sensible cooling (temperature reduction) loads and latent cooling (moisture removal or dehumidification) loads, as well as shift much of these loads to compressor-less-based technologies. Meeting these objectives with ILDAC technology would provide the required dehumidification in many building applications and climatic locations, while reducing the compressor-based technology portion of the AC capacity requirements and avoiding its oversizing and wasting of operating energy from overcooling and reheating processes using those conventional chilled water (CW) or direct expansion (DX) refrigerant AC systems. Buildings that apply dedicated outside air systems (DOAS), especially in more humid climatic locations, to process 100% OA as ventilation air to maintain building indoor air quality (IAQ), or as makeup air to compensate for exhaust to maintain neutral/slightly positive building pressurization, are early market opportunities for alternative enhanced dehumidification systems such as ILDACs.

The UF and GTI Energy project team has progressed its ILDAC RD&D project sufficiently with its joint sponsors, U.S. Department of Energy (DOE) and GTI's utility industry Utilization Technology

Development (UTD) consortium, to provide preliminary insights for initial discussion with these sponsors as well as with potential heating, ventilating, and air conditioning (HVAC) manufacturing partners in the following areas:

- early market opportunities for alternative enhanced dehumidification systems such as ILDACs;
- ILDAC system configurations and performance comparisons with CW and DX only counterpart systems; and
- standards and codes applicable to the design and operation of ILDACs and to their performance test methods and ratings.

The next several pages summarize the preliminary insights in those three (3) areas.

Early Market Opportunities

The emergence of DOAS over the last couple of decades has been driven in large part by the substantial standard and code driven increases in OA requirements of the 1990's that resulted from preceding issues with sick building syndrome (SBS) and building related illnesses (BRI)[1]. The coincident emergence of weather data providing humidity design conditions in the 1990's has allowed those increases in OA to maintain building IAQ to be readily quantified in terms of moisture loads on HVAC systems, with a heavy emphasis on the V for ventilation and the large dehumidification loads that result from outside air, especially in more humid climates[2]. Various HVAC systems with enhanced dehumidification capabilities have been researched, developed, and deployed over the years[3,4] in an effort to provide more energy efficient DOAS designs for commercial and institutional buildings.

Desiccant-based HVAC systems have a long and successful history dating back to the 1930's for meeting cost effective dehumidification needs in industrial manufacturing and storage applications that require lower humidity control levels. As needs emerged in the 1990's for cost effective dehumidification of OA for commercial and institutional buildings, significant inroads were made by desiccant-based DOAS, primarily in buildings with refrigeration processes that benefitted from lower humidity control levels below conventional comfort conditioning applications including:

- hospital operating room suites
- supermarkets
- refrigerated warehouses
- ice arenas/curling rinks

---

[1] ASHRAE Bookstore, Dehumidification Issues of Standard 62-1989, Kosar D, Witte M, Shirey D, Hedrick R, https://www.techstreet.com/ashrae/standards/dehumidification-issues-of-standard-62-1989?product_id=1712868

[2] ASHRAE Bookstore, Dehumidification and Cooling Loads from Ventilation Air, Harriman L, Plager D, Kosar D, https://www.techstreet.com/ashrae/standards/dehumidification-and-cooling-loads-from-ventilation-air?product_id=1713677

[3] ASHRAE Bookstore, Evaluating Active Desiccant Systems for Ventilating Commercial Buildings, Harriman L, Czachorski M, Witte M, Kosar D, https://www.techstreet.com/ashrae/standards/evaluating-active-desiccant-systems-for-ventilating-commercial-buildings?product_id=1713670

[4] ASHRAE Bookstore, Dehumidification System Enhancements, Kosar D, https://www.techstreet.com/ashrae/standards/dehumidification-system-enhancements?product_id=1718687

Much more limited inroads were made with desiccant-based DOAS in more mainstream applications with higher humidity control levels typical of conventional comfort conditioning. Improvements to conventional compressor- based DOAS to enhance dehumidification were also increasingly competitive on performance and cost in these higher humidity control applications. These more mainstream applications for DOAS to provide building ventilation include:

- retail stores (generally "big box")
- schools
- theaters
- sports arenas
- non-surgical healthcare facilities
- day care centers

Other buildings require similar 100% OA systems, known as a make-up air unit (MAU) to supply OA to compensate for exhaust and maintain neutral or slightly positive building pressurization. Some examples of building types that use MAUs are:

- hotels and multifamily buildings (corridors)
- health club facilities
- restaurants or any commercial/institutional kitchens

System Configurations

UF has developed a small laboratory scale ILDAC apparatus to provide preliminary data on which to base analytical models of the absorber and its dehumidification performance. This absorber model has been integrated with other well-established HVAC component models to generate projections of inlet/outlet state point performance for the following three (3) DOAS configurations:

1. 100% OA ILD absorber coupled with downstream mixed air (MA) CW coil
2. 100% OA DX coil coupled with downstream 100% OA ILD absorber
3. 100% OA compressor-less (NO DX/CW) ILD absorber with ambient heat exchanger (HX) and downstream building energy recovery HX

The performance was evaluated at the following two (2) design conditions for Gainesville FL:

1. **1% Cooling Dry Bulb (DB) Temperature/Mean Coincident Wet Bulb (WB) Temperature**
    - **92.2 °F DB**
    - **75.8 °F WB**
    - 69.4 °F DP
    - 108.5 gr/lb HR
    - 47.3 % Relative Humidity (RH)

2. **1% Dehumidification Dew Point (DP) Temperature/Humidity Ratio (HR)/Mean Coincident Dry Bulb (DB) Temperature**

    - **76.4 ºF DP**
    - **138.5 gr/lb HR**
    - **81.9 ºF DB**
    - 77.8 ºF WB
    - 83.2 % Relative Humidity (RH)

For brevity, only the 1% dehumidification condition performance is presented.

ILDAC systems 1 and 2 are compared to their CW and DX only counterparts in these enhanced dehumidification DOAS applications to illustrate their system design (lower overall capacity) advantages, and in turn potential operation (lower energy consumption/cost) advantages that will be addressed later in the ILDAC development process.

CW System

One of the early market opportunities identified for the ILDAC is its use in DOAS applications with humidity control levels below conventional comfort conditioning practices, which are typically on the order of 75 ºF DB and 55% RH (57.8 ºF DP/71.8 gr/lb HR). For CW based systems, this is exemplified by an operating room (OR) suite in a hospital application with lower setpoints in the space of 68 ºF DB and 50% RH (48.7 ºF DP/51 gr/lb HR). Standard practice has a CW system alone applied that often requires the CW plant to provide lower temperature CW just to satisfy the dehumidification needs of the OR. In that CW only system, deep row CW coils are utilized to reach the supply air (SA) DP/HR necessary to meet the dehumidification loads and maintain the humidity control levels in the space, along with reheat to avoid overcooling the space. The UF staff prepared system schematics, psychometric process plots and/or process state tables, and performance comparison summary tables to document the design advantages of using the ILDAC in this application.

In the system schematic that follows is a general layout of a 100% OA ILD absorber coupled with a downstream MA CW coil. The conventional CW only system would have a similar schematic with a reheat coil downstream of the cooling coil but without the ILD absorber pretreating the OA.

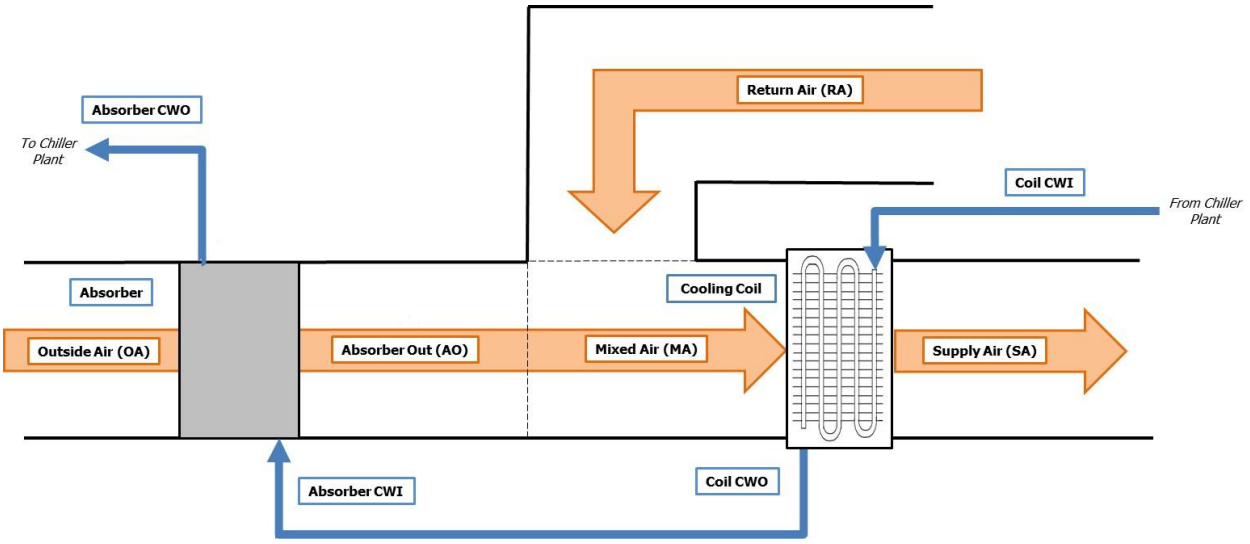

Figure 5: System schematic for IL DOAS HVAC.

At the 1% dehumidification design condition, the process state point tables below show the psychrometric conditions through the ILDAC/CW system on top and CW only system on bottom.

Table 1: Process State Points for IL DOAS HVAC

Outside Air		Absorber Outlet		Return Air		Mixed Air		Coil Leaving Air/Supply Air	
T_DB [F]	81.9	T_DB [F]	73.366	T_DB [F]	68	T_DB [F]	69.035	T_DB [F]	62.738
T_WB [F]	77.803	T_WB [F]	58.035	T_WB [F]	56.79	T_WB [F]	57.033	T_WB [F]	54.535
T_dp [F]	76.4	T_dp [F]	46.886	T_dp [F]	48.69	T_dp [F]	48.35	T_dp [F]	48.35
W [grains/lb]	138.3	W [grains/lb]	47.7	W [grains/lb]	51	W [grains/lb]	50.4	W [grains/lb]	50.4
h [BTU/lb]	41.337	h [BTU/lb]	25.052	h [BTU/lb]	24.277	h [BTU/lb]	24.426	h [BTU/lb]	22.884
v [cu.ft/lb]	14.081	v [cu.ft/lb]	13.58	v [cu.ft/lb]	13.453	v [cu.ft/lb]	13.478	v [cu.ft/lb]	13.317

Outside Air		Return Air		Mixed Air		Coil Leaving Air		Supply Air with Reheat	
T_DB [F]	81.9	T_DB [F]	68	T_DB [F]	70.680	T_DB [F]	48	T_DB [F]	63
T_WB [F]	77.803	T_WB [F]	56.79	T_WB [F]	61.684	T_WB [F]	48	T_WB [F]	54.47
T_dp [F]	76.4	T_dp [F]	48.69	T_dp [F]	56.34	T_dp [F]	48	T_dp [F]	48
W [grains/lb]	138.3	W [grains/lb]	51	W [grains/lb]	67.9	W [grains/lb]	49.7	W [grains/lb]	49.7
h [BTU/lb]	41.337	h [BTU/lb]	24.277	h [BTU/lb]	27.566	h [BTU/lb]	19.207	h [BTU/lb]	22.903
v [cu.ft/lb]	14.081	v [cu.ft/lb]	13.453	v [cu.ft/lb]	13.574	v [cu.ft/lb]	12.94	v [cu.ft/lb]	13.322

Those state point tables show the two systems processing the same 1000 cfm of OA and 4000 cfm of RA at the same initial conditions and supplying the same delivered air conditions. However, as the performance comparison summary tables below show, the conventional CW only system must significantly overcool the air to achieve the required dehumidification effect and then reheat before supplying the air to avoid overcooling the space. This false loading results in dramatically greater loads overall and much more substantial cooling coils, with deeper rows and tighter fin spacing, for the CW only system. By contrast, with the ILD absorber pretreating the OA by deeply drying and precooling that airstream, the loads overall for this alternative system are reduced by 61.2% (266,430 versus 102,250 Btu/hr) and the cooling coil is simplified as well.

Table 2: Load and coil comparison for IL DOAS HVAC

LOAD COMPARISON		
	ILD Absorber & CW	CW Only
System Load [BTU/hr]	102,250	266,430
ILD Absorber Load [BTU/hr]	64,773	NA
CW Coil Load [BTU/hr]	37,477	184,746
Reheat Load [BTU/hr]	0	81,684

COIL COMPARISON			
	ILD Absorber & CW	CW Only [8 F ΔT]	CW Only [20 GPM]
Face Area [sq. FT]	9.25	9.25	9.25
Rows / FPI	2 / 6	10 / 14	12 / 13
EFT / LFT [F]	46 / 53.2	46 / 54	42 / 60.6
GPM	10.9	46.7	20
Air ΔP [in. WG]	0.13	2.29	2.38
Fluid ΔP [FT]	5.3	15.8	13.6

DX Systems

For DX based systems, this same early market opportunity for lower humidity control level applications is exemplified by a supermarket with setpoints in the space of 75 °F DB and 40% RH (49.1 °F DP/52 gr/lb HR). Common practice has a DX system alone as a specialized packaged rooftop unit (RTU) that operates as a DOAS to provide SA below space neutral DB (at 60 °F) while more deeply drying the SA DP/HR (45 °F DP/44 gr/lb HR). Multi-circuit DX coils are required to reach the lower apparatus dew point (ADP) along with reheat, from hot gas bypass and/or condenser waste heat recovered from the DX cycle, to avoid overcooling the space. As before, the UF staff prepared system schematics, psychometric process plots and/or process state tables, and performance comparison summary tables to document the design advantages of using the ILDAC in this application.

The system schematic below is a general layout of a 100% OA DX coil coupled with downstream 100% OA ILD absorber. The conventional DX only system would have a similar schematic with a reheat coil downstream of the cooling coil instead of the ILD absorber. Note that in the previous CW system design, the CW provided sensible cooling directly in the ILD absorber to dissipate its latent to sensible load conversion (heat of absorption effect) from the desiccant dehumidification process and maximize its dehumidification capacity (DP/HR reduction). That allows the ILD absorber to be placed at the front end of the DOAS OA treatment in the previous CW system design. No such practical design approach is feasible with a DX refrigerant and so the ILD absorber is moved downstream after the DX cooling coil to take advantage of its sensible cooling to maximize the incremental dehumidification capacity (DP/HR reduction) of the ILD absorber in this DX system design.

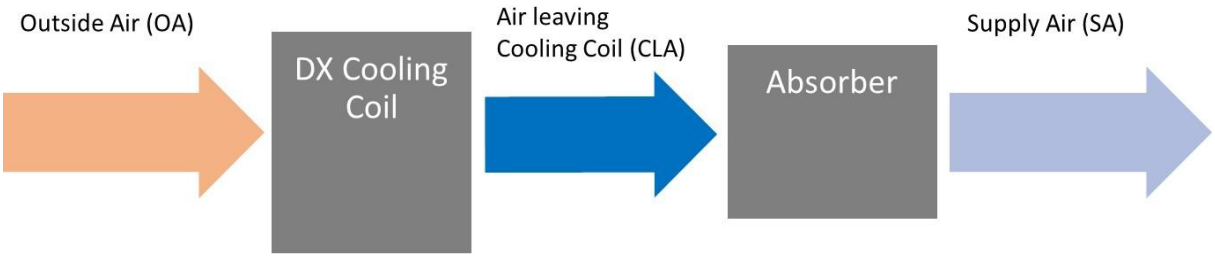

Figure 6: General layout of key components for IL DOAS HVAC.

At the 1% dehumidification design condition, the process state point tables below show the psychrometric conditions through the DX/ILDAC system on the left and DX only system on the right.

Table 3: State points for DX-ILD and DX Only systems

DX & ILD Absorber State Points				
Pts.	°F DB	°F WB	°F DP	gr/lb
OA	81.9	77.8	76.4	137.7
CLA	51.0	51.0	51.0	55.4
SA	58.3	51.1	44.9	44.1

DX Only State Points				
Pts.	°F DB	°F WB	°F DP	gr/lb
OA	81.9	77.8	76.4	137.7
CLA	45.0	45.0	45.0	44.1
SA	58.3	51.1	45.0	44.1

Those state point tables show the two systems processing the same 1000 cfm of OA at the same initial conditions and supplying the same delivered air conditions. However, as the following performance comparison summary tables show, the conventional DX only system must significantly overcool the air to achieve the required dehumidification effect and then reheat before supplying the air to avoid overcooling the space. This false loading results in significantly greater loads overall. By contrast, with the ILD absorber providing the final, incremental moisture reduction to the airstream, the loads overall for this alternative system are reduced by 18.5% (126,200 versus 102,900 Btu/hr).

Table 4: Loads for DX-ILD and DX Only systems

DX & ILD Absorber Loads	kBtu/hr
Cooling Coil Total Load	94.7
Cooling Coil Latent Load	59.8
Cooling Coil Sensible Load	34.9
Absorber Latent (to Sensible) Load	8.2
Total System Load	102.9

DX Only Loads	kBtu/hr
Cooling Coil Total Load	111.0
Cooling Coil Latent Load	68.9
Cooling Coil Sensible Load	42.1
Reheat Coil Load	15.2
Total System Load	126.2

Compressor-less Systems

Eliminating the compressor-based CW or DX components entirely from the DOAS is the ultimate goal of the earlier stated RD&D objectives. A stand-alone ILDAC could provide a mainstream

market opportunity to meet DOAS applications where humidity control requirements are at conventional comfort conditioning levels, which are typically on the order of 75 °F DB and 55% RH (57.8 °F DP/71.8 gr/lb HR). Once again, the UF staff prepared system schematics, psychometric process plots and/or process state tables, and performance comparison summary tables to document the design approach for using the ILDAC in this application.

The system schematic below is a general layout of a 100% OA ILD absorber coupled with heat exchangers (HXs) to provide heat sinks to an ambient airstream and a cooling water stream. The absorber water to air HX uses cooling water in a closed loop at a temperature that exceeds but approaches within a few degrees of the ambient DB. The building energy recovery ventilation (ERV) HX downstream of the absorber uses exhausted return air assumed to be at 75 °F DB.

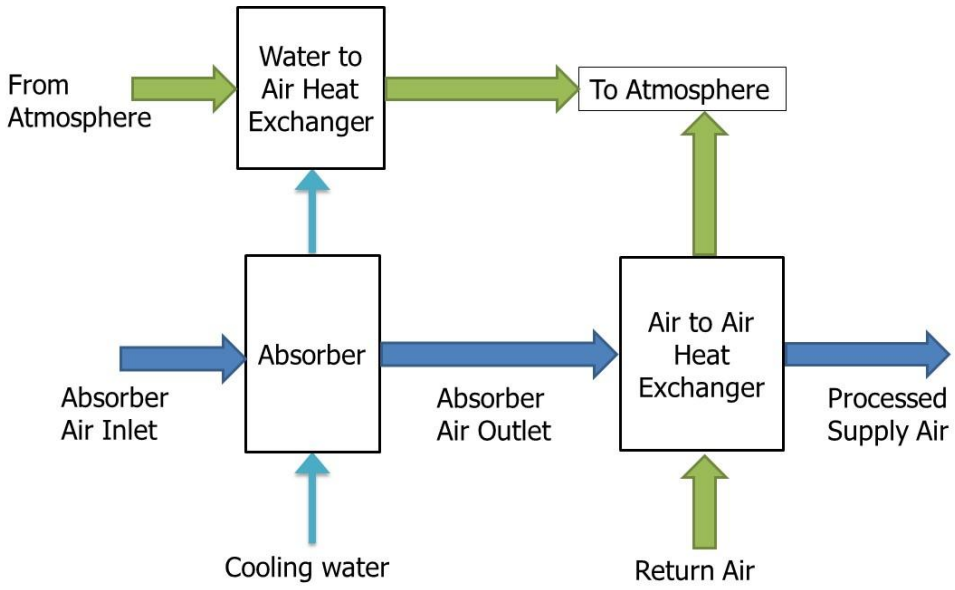

Figure 7: System schematic for compressor-less ILD HVAC system.

At the 1% dehumidification design condition, the process state point tables below show the psychrometric conditions through the ILDAC system. The first table below shows the absorber inlet and outlet conditions. The second table below shows water to air HX inlet and outlet conditions and the air to air HX inlet and outlet conditions. Those state point tables show the systems processing 1000 cfm of supply air.

Table 5: Absorber inlet/outlet and water-to-air HX inlet/outlet conditions

T air absorber inlet (°F)	RH absorber inlet (%)	W air absorber inlet (grains/lb)	T air absorber outlet (°F)	RH absorber outlet (%)	W air absorber outlet (grains/lb)
81.9	83.5	138.3	94.4	26.5	64.1

T Water-Air HX inlet (°F)	T Water-Air HX outlet (°F)	T supply Air-Air HX inlet (°F)	T supply Air-Air HX outlet (°F)
103.34	87	94.393	79.6

The following performance comparison summary table below shows the projected energy use and resulting Moisture Removal Efficiency (MRE) of 12.1. That level of MRE for a compressor-less DOAS shows indicates large potential energy savings compared to the minimum required DX only DOAS MREs in ASHRAE Standard 90.1, discussed later in this section in Applicable Standards and Codes on pages 11 - 12.

Table 6: Performance comparison summary table for compressor-less ILD HVAC system

Inlet DB (°F)	Inlet WB (°F)	Inlet DP (°F)	Outlet DB (°F)	Outlet WB (°F)	Outlet DP (°F)	Electric Power Input (kW)	Heat Input (kW)	MREeq (lbmmoisture/kWeq-hr)
81.9	77.8	76.4	79.6	64.0	54.9	0.48	8.76	12.1

Applicable Standards and Codes

Standards and codes that are generally applicable to fuel-fired or thermally driven HVAC equipment are not covered in this limited review. Rather standards and codes that are most relevant to the utilization of enhanced dehumidification component technology, especially the ILDAC absorber, are emphasized in this section. Standards generally define a best practice but lack enforcement unless those standards are referenced, or incorporated in whole or in part, into building energy codes and/or building system (equipment) efficiency regulations.

Standards applicable to the design and operation of ILDACs and to their performance test methods and ratings will influence the development of ILDACs, including their system configurations, material selections, operating schemes, and performance targets. In this context, the American Society of Heating, Refrigeration, and Air-Conditioning Engineers (ASHRAE) and its following standards[5] provide important considerations in the overall ILDAC development process.

ASHRAE/ANSI/IES Standard 90.1-2019 Energy Standard for Buildings Except Low-Rise Residential Buildings

Per its stated scope, "ASHRAE Standard 90.1 has been a benchmark for commercial building energy codes in the United States and a key basis for codes and standards around the world for more than 35 years. This standard provides the minimum requirements for energy-efficient design of most buildings, except low-rise residential buildings. It offers, in detail, the minimum energy-efficient requirements for design and construction of new buildings and their systems, new portions of buildings and their systems, and new systems and equipment in existing buildings, as well as criteria for determining compliance with these requirements."

Over the years this standard has evolved to limit the use of cooling and reheating with new energy for building humidity control and to increasingly require the use of recovered heat for reheating when allowed. The following specific standard sections, with important content highlighted in **bold**, will be the most influential for ILDAC development.

- **"6.5.2.3 Dehumidification**

[5] ASHRAE Bookstore, Standards and Guidelines, https://www.techstreet.com/ashrae/ashrae_standards.html

Where humidity *controls* are provided, such *controls* shall prevent *reheating*, mixing of hot and cold airstreams, or other means of simultaneous heating and cooling of the same airstream.

Exceptions to 6.5.2.3

1. The *system* is capable of and configured to reduce supply air volume to 50% or less of the design airflow rate or the minimum *outdoor air ventilation* rate specified in ASHRAE Standard 62.1 or other applicable federal, state, or local code or recognized standard, whichever is larger, before simultaneous heating and cooling takes place.

2. The individual fan cooling unit has a design cooling capacity of 65,000 Btu/h or less and is capable of and configured to unload to 50% capacity before simultaneous heating and cooling takes place.

3. The individual *mechanical cooling* unit has a design cooling capacity of 40,000 Btu/h or less. An individual *mechanical cooling* unit is a single *system* comprising a fan or fans and a cooling coil capable of providing *mechanical cooling*.

4. *Systems* serving *spaces* where specific humidity levels are required to satisfy process needs, such as vivariums; museums; surgical suites; pharmacies; and *buildings* with refrigerating *systems*, such as supermarkets, refrigerated warehouses, and ice arenas, and where the *building* **includes *site-recovered energy* or *site-solar energy* that provide *energy* equal to at least 75% of the annual *energy* for *reheating* or for providing warm air in mixing *systems*.** This exception does not apply to *computer rooms*.

5. At least 90% of the annual *energy* for *reheating* or for providing warm air in mixing *systems* is provided from *site-recovered energy* (including condenser heat) or *site-solar energy*.

6. *Systems* where the heat added to the airstream is the result of the use of a desiccant *system*, and 75% of the heat added by the desiccant *system* is removed by a heat exchanger, either before or after the desiccant *system*, with *energy* recovery."

The influence of standard section 6.5.2.3 on both state-of-the-art (SOA) compressor-based DX systems and desiccant-based DX coupled systems, especially DOAS, has been direct and dramatic over its history. Per exceptions 4 and 5, compressor-based DX systems have shifted from use of new energy for reheating to use of recovered energy using hot gas bypass or condenser waste heat. Per exception 6, desiccant-based DX coupled systems likewise have shifted from use of new energy for regeneration to use of recovered energy from desuperheater and/or condenser waste heat from the integrated DX system. To our best knowledge, no formal ASHRAE interpretation has been provided to date to confirm that the latent to sensible heat conversion of the desiccant dehumidification process combined with its regeneration heat recovery from the DX desuperheater/condenser waste heat stream satisfies exception 6. A formal interpretation request should be submitted to ASHRAE for confirmation as ILDAC system development proceeds further.

The influence of standard section 6.5.2.3 on both SOA compressor-based CW systems and desiccant-based CW coupled systems, especially DOAS, has been more indirect and less dramatic over its history. Per exception 4, most CW applications with enhanced dehumidification requirements tend to fall into the building categories noted, where the building overall, not the CW system alone, bears the burden to satisfy the recovered energy requirement. To the best of our knowledge, no formal ASHRAE interpretation has been provided to establish how exception 6 is to be applied in conjunction with a desiccant-based CW coupled system in those noted building categories in exception 4. A formal interpretation request should be submitted to ASHRAE for clarification.

The introduction of a compressor-less desiccant-based system will need to meet exception 6. Based on the preliminary compressor-less ILDAC shown earlier in this section, the author believes that system design will meet the requirements of exception 6, but again a formal interpretation request should be submitted to ASHRAE for confirmation.

- **"6.5.2.6 Ventilation Air Heating Control**

  Units that provide *ventilation* air to multiple zones and operate in conjunction with zone heating and cooling *systems* **shall not use heating or heat recovery to warm supply air above 60°F when** representative *building* loads or *outdoor air* temperature indicate that the **majority of zones require cooling**."

  A formal 2018 ASHRAE interpretation[6] of standard section 6.5.2.6 stated "the intention of this section is to specifically disallow use of a 'neutral' or higher temperature ventilation air control strategy in a DOAS when the zones served are mostly in cooling. The requirement does allow a higher temperature when a majority of zones do not require cooling. This can be determined by a polling of zone conditions or based on an outside air temperature representing the cooling balance point. However, when the majority of zones are in cooling, or expected to be in cooling based on outside temperature, the supply air temperature setpoint of the DOAS is limited to 60°F, even if recovered heat is used for reheat."

- These **other following sections of ASHRAE Standard 90.1** will influence the design and operation of an ILDAC system, as well as the design and operation of competing system approaches, especially for DOAS. Although relevant, these additional sections are not extensively detailed below, but the author recommends these further requirements for use of demand control ventilation (DCV) and energy recovery ventilation (ERV) be reviewed and their contents discussed with potential HVAC manufacturing partners to understand their preferred DOAS approaches using DCV and ERV and the potential fit of the ILDAC in the context of their product portfolio.

  6.4.3.8 Ventilation Controls for High-Occupancy Areas

  DCV is required for spaces above a certain size with a design occupancy for ventilation of greater than a certain number of people per unit of floor area and served by HVAC systems

[6] ASHRAE Standards Interpretations , https://www.ashrae.org/technical-resources/standards-and-guidelines/standards-interpretations,

having a design outdoor airflow greater than a certain airflow level. The prospect, with each standard revision every 3 years, is to decrease these threshold levels, so current as well as pending versions of these standard section(s) should be reviewed.

6.5.6.1 Energy Recovery Ventilation

An ERV is required by a combined threshold level is exceeded for the system design supply fan airflow rate and the percent outdoor air at full design flow. The larger the percent outside air of the system, the smaller the supply fan airflow rate threshold for the ERV requirement in the HVAC system. Again, the prospect, with each standard revision every 3 years, is to decrease these threshold levels, so current as well as pending versions of these standard section(s) should be reviewed.

ASHRAE/ANSI Standard 62.1-2019 Ventilation for Acceptable Indoor Air Quality

Per its stated scope, "ASHRAE Standard 62.1 specifies minimum ventilation rates and other measures intended to provide indoor air quality (IAQ) that is acceptable to human occupants and that minimizes adverse health effects."

Over the years this standard has evolved to increasingly emphasize the role of building humidity control measures in IAQ. The following specific standard section, with important content highlighted in **bold**, will be the most influential for ILDAC development.

- **"5.10 Maximum Indoor Air Dew Point in Mechanically Cooled Buildings**

  Buildings or spaces equipped with or served by mechanical cooling equipment shall be provided with dehumidification components and controls that limit the indoor humidity to a maximum dew point of 60°F (15°C) during both occupied and unoccupied hours whenever the outdoor air dew point is above 60°F (15°C). The dew-point limit shall not be exceeded **when system performance is analyzed with outdoor air at the dehumidification design condition (that is, design dew point and mean coincident dry-bulb temperatures)** and with the space interior loads (both sensible and latent) at cooling design values and space solar loads at zero.

  Exceptions to 5.10:

  1. Buildings or spaces that are neither equipped with nor served by mechanical cooling equipment.

  2. Buildings or spaces equipped with materials, assemblies, coatings, and furnishings that resist microbial growth and that are not damaged by continuously high indoor air dew points.

  3. During overnight unoccupied periods not exceeding 12 hours, the 60°F (15°C) dew- point limit shall not apply, provided that indoor relative humidity does not exceed 65% at any time during those hours.

  Informative Notes:

1. Examples of spaces are shower rooms, swimming pool enclosures, kitchens, spa rooms, or semi-cooled warehouse spaces that contain stored contents that are not damaged by continuously high indoor air dew points or microbial growth.

2. This requirement reduces the risk of microbial growth in buildings and their interstitial spaces because it limits the mass of indoor water vapor that can condense or be absorbed into mechanically cooled surfaces. The dew-point limit is explicitly extended to unoccupied hours because of the extensive public record of mold growth in schools, apartments, dormitories, and public buildings that are intermittently cooled during unoccupied hours when the outdoor air dew point is above 60°F (15°C).

The limitation on building indoor dew point temperature is relatively new in this standard and hence its influence over system design and operation is still forthcoming, especially given the time lag (on the order of 3 to 5 years) between standard approval and adoption in building energy code and building system efficiency regulations. The author recommends that in upcoming discussions with HVAC manufacturing partners, the ILDAC development team should discuss the influence of this standard section on building system designs and the potential adoption of enhanced dehumidification technology such as ILDs.

As noted in the section on ASHRAE Standard 90.1, DCV is required in certain system applications. The allowance for use of DCV is contained in section 6.2.6 of ASHRAE Standard 62.1. That section provides for the use of carbon dioxide (CO_2) measurements as a surrogate for occupancy levels and accommodates reductions in prescriptive ventilation rates based on reductions in those occupancy levels/CO_2 readings.

ASHRAE/ANSI Standard 174-2018 Method of Test for Rating Desiccant-Based Dehumidification Equipment

Per its stated scope, "ASHRAE Standard 174 provides a method of test (MOT) for rating the overall performance of desiccant-based dehumidification equipment. Desiccant-based systems are typically designed with moisture removal as their primary function and this method of test has been developed to assist in the measurement and documentation of variables needed to establish moisture-removal capacity per unit of energy. It is intended for equipment incorporating additional energy transfer devices that fall outside the scope of ASHRAE Standard 139, Method of Test for Rating Desiccant Dehumidifiers Utilizing Heat for the Regeneration Process."

ASHRAE/ANSI Standard 139-2019 Method of Test for Rating Desiccant Dehumidifiers Utilizing Heat for the Regeneration Process

Per its stated scope, "ASHRAE Standard 139 provides a method of test specific to the desiccant dehumidifier itself, separate from any system integration with additional energy transfer devices, which is addressed in ASHRAE Standard 174 Method of Test for Rating Desiccant-Based Dehumidification Equipment."

The system configurations described earlier in the section would be tested and rated based on ASHRAE Standard 174 and establish a Moisture Removal Efficiency (MRE) expressed as lb/hr of moisture removed per kW of system energy used. If the commercialization path for the ILDAC

with HVAC manufacturers is not exclusively based on integrated system offerings, then the ILDAC absorber (and desorber) device(s) could be additionally tested and rated based on ASHRAE Standard 139 and offered by its original equipment manufacturer (OEM) for packaging by other manufacturers into HVAC systems. Note that a counterpart MOT for DX only based DOAS is provided in ASHRAE Standard 198-2013 Method of Test for Rating DX-Dedicated Outdoor Air Systems for Moisture Removal Capacity and Removal Efficiency.

Although not addressed in this section, it is also important to note that ASHRAE MOT standards typically provide only the test procedure and not the test conditions for rating and certifying performance. The certified performance rating standards are under the control of the Air-Conditioning, Heating, and Refrigeration Institute (AHRI) and an ad hoc Consensus Standards Policy Committee (CSPC) consisting of AHRI member manufacturers of the relevant products, as well as outside stakeholders with an interest in the rating standard. The AHRI certified performance rating standard will incorporate the ASHRAE MOT standard by reference and establish rating conditions for certifying performance, if not provided in the ASHRAE MOT standard. AHRI does have an active performance rating certification program in place for DX only based DOAS[7], but no such active program for desiccant-based DOAS to the author's knowledge. AHRI/ANSI Standard 920 Performance Rating of DX Dedicated Outdoor Air System Units[8] references ASHRAE Standard 198 as its MOT standard for certified performance ratings of DX only based DOAS.

The DX only DOAS MOT Standard 198 by ASHRAE and the companion performance rating Standard 920 by AHRI also utilizes MRE, as well as an Integrated Seasonal MRE (ISMRE) based on application of weighting percentages for the MRE at different rating conditions. As a result, ASHRAE 90.1 has established a series of Section 6.8.1 tables that establish minimum MRE/ISMRE requirements for DX-only DOAS. To the author's knowledge, minimum MRE/ISMRE requirements for desiccant-based DOAS are not established in ASHRAE Standard 90.1. For DX only DOAS, minimum required MRE/ISMRE ranges from approximately 3.5 to 6.5 in ASHRAE Standard 90.1[9]. According to one current desiccant-based DOAS manufacturer Munters DryCool, these systems "can achieve an MRE as high as 10.8 during peak season. This performance exceeds ASHRAE's minimum requirement by a factor of two"[10]. Given the potential MRE/ISMRE advantages of desiccant-based DOAS, the author recommends that in support of such existing systems and ILDAC/other similar system development activities, efforts should be made on forming the necessary AHRI rating standards and certification programs to position those desiccant-based DOAS for incorporation in ASHRAE Standard 90.1 as well.

---

[7] AHRI Certification Programs , DX-Dedicated Outdoor Air System Units http://www.ahrinet.org/certification/ahri-certification-programs/dx-dedicated-outdoor-air-system-units

[8] AHRI AHRI/ANSI Standard 920 Performance Rating of DX Dedicated Outdoor Air System Units, http://ahrinet.org/App_Content/ahri/files/STANDARDS/ANSI/ANSI_AHRI_Standard_920_I-P_2015.pdf

[9] Trane Engineering Newsletter, AHRI 920 Rating Standard for DX Dedicated Outdoor-Air Units, https://www.trane.com/content/dam/Trane/Commercial/global/products-systems/education-training/engineers-newsletters/standards-codes/ADM-APN060-EN_110116.pdf

[10] Climate Technologies, Moisture Removal Efficiency of Munters DOAS Equipment Exceeds ASHRAE 90.1, https://climatetechnologies.com/news/moisture-removal-efficiency-2x-better-than-ashrae-90-1/

The ASHRAE MOT standards (and AHRI rating standards) are also typically the basis for performance testing (and rating) performance to meet federal minimum efficiency regulations, which are under the jurisdiction of DOE by a congressionally mandated rulemaking process on a roughly five (5) year cycle. DOE does not presently have a federal minimum efficiency rulemaking process in place for smaller market share HVAC products, such as desiccant-based systems or DOAS in general. However, based on a recent DOE request for information (RFI)[11], it indicates that with ASHRAE Standard 90.1 now establishing minimum MRE/ISMRE for at least DX-based DOAS, DOE will possibly follow ASHRAE's lead and also establish a federal minimum efficiency standard for those DOAS specifically. Ongoing monitoring of this potential DOE rulemaking process is strongly recommended.

Lastly from a standards perspective, the following Underwriters Laboratory (UL) standard[12] is an important consideration for material selection specifically.

UL 723 (ASTM E84) Test for Surface Burning Characteristics of Building Materials

Per its stated scope. "UL Standard 723 is a method of test for surface burning characteristics of building materials is applicable to any type of building material that, by its own structural quality or the manner in which it is applied, is capable of supporting itself in position or being supported in the test furnace to a thickness comparable to its intended use. The purpose of the test is to determine the comparative burning characteristics of the material under test by evaluating the spread of flame over its surface and the density of the smoke developed when exposed to a test fire," … and determine a flame spread and smoke developed rating that can be the basis for suitability for an intended use, such as a component in a building HVAC system.

National model building safety and fire protection codes, typically adopted in turn by state and local codes, will require that certain building materials meet different flame and smoke ratings based on UL 723 (ASTM E-84). Per UL, "building codes require that certain materials installed in a plenum or air-handling space have a flame spread index of 0 to 25 and a smoke developed index of 0 to 50"[13]. As a point of reference, the Munters DryCool solid desiccant dehumidification rotor carries a flame spread index of 0 and smoke developed index of 10[14].

Local, State, and National Building Energy Codes

Over time, national model building energy codes have merged into a single, dominant code administered by the International Code Council (ICC). ICC building energy codes directly, or by reference, incorporate many of the previous standard requirements, especially from ASHRAE Standard 90.1 and ASHRAE Standard 62.1. In turn, states and local jurisdictions adopt most/all of the national model building energy code, encouraged by various DOE funding programs requiring

[11] DOE RFI Energy Conservation Program for Certain Commercial and Industrial Equipment: Test Procedure for Certain Categories of Commercial Air Conditioning and Heating Equipment, https://www.energy.gov/sites/prod/files/2017/07/f35/ashrae-90.1-2016-tp-rfi-7-11-17.pdf

[12] UL Standards Sales Site, https://standardscatalog.ul.com/ProductDetail.aspx?productId=UL723

[13] UL Surface Burning Characteristics for Materials Used in Plenums, https://legacy-uploads.ul.com/wp-content/uploads/2014/04/ASTME84_ULCS102.2.pdf

[14] Munters DryCool™ Desiccant Dehumidification System (DDS) Engineering Catalog, https://webdh.munters.com/webdh/BrochureUploads/Engineering%20Catalog-%20DDS.pdf

state level adoption of such key codes as the International Energy Conservation Code (IECC) promulgated by ICC.

Some state level building codes are even more proactive in requiring further energy efficiency measures, including utilization of specific HVAC equipment types. For instance, in the state of Washington the building mechanical code, starting in 2017, has required the use of DOAS in certain building types[15]. Such state level initiatives are becoming more practical as ASHRAE develops documentation to help facilitate the application of DOAS, including the new ASHRAE 2020 Handbook of HVAC Systems and Equipment[16] chapter on DOAS, along with the recent ASHRAE 2017 Design Guide for DOAS[17].

[15] Washington Administrative Code (WAC), Department of Enterprise Services (Building Code Council) Title 51 Section C403.3.5—Dedicated outdoor air systems https://apps.leg.wa.gov/wac/default.aspx?cite=51-11C-40335

[16] 2020 ASHRAE Handbook--HVAC Systems & Equipment ,Chapter S51 -- Dedicated Outdoor Air Systems (I-P), https://www.techstreet.com/ashrae/standards/s51-dedicated-outdoor-air-systems-i-p?product_id=2121400

[17] ASHRAE Design Guide for Dedicated Outdoor Air Systems (DOAS) https://www.techstreet.com/ashrae/standards/ashrae-design-guide-for-dedicated-outdoor-air-systems-doas?product_id=1974732

Direct-fired Desorber

This section describes the computational fluid dynamics (CFD) modeling and analysis in support of the detailed design of the desorber. The modeling work was based on the desorber design; see Figure 8. The first set of CFD simulations looked at the flow of hot combustion or flue gases inside the plate heat exchangers and film boiling conditions outside.

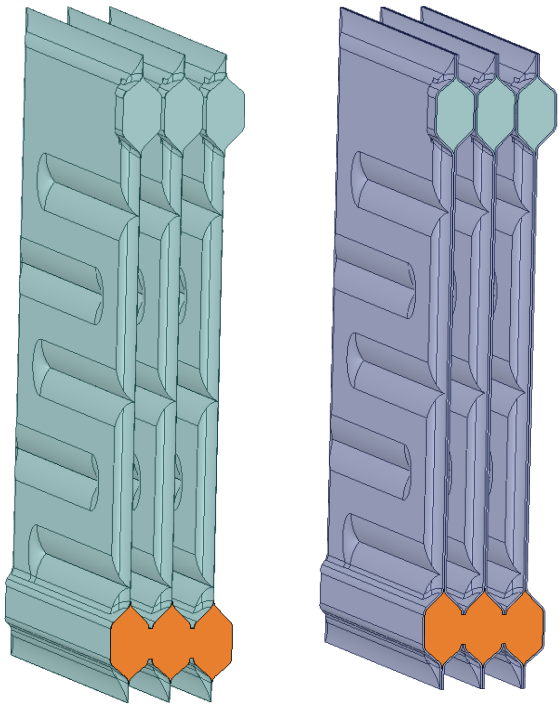

Figure 8. Desorber design without features" based on drawings from University of Florida. Left - plate heat exchangers with internal volume for flow of combustion gases; Right – internal combustion gas flow volume without the metallic plates. The combustion gas flow inlet is highlighted at the bottom.

Model Geometry and Boundary Conditions

For simplicity, only one heat exchanger plate was modeled. Further, following initial attempts with the original geometry and to improve the simulation output, a simplified geometry, as shown in Figure 9, was modeled. The primary intent behind the geometry simplification was in response to a zero-thickness geometry error that was encountered in ANSYS meshing. Further remodeling of the initial geometry was performed in order to remove curvature in the plate wall, thereby reducing the number of mesh elements required to achieve convergence. A generic mesh was generated for each of the simulation cases, with a maximum element size of 1e-03m. The total node and element count for the mesh was approximately 9.8e5 and 8.8e5, respectively.

The turbulence model used for all simulations was the k-omega SST model. This model was selected over the k-epsilon model to better handle near-wall regions and resolve vortices that are expected to form as the flow deflects and changes direction through the serpentine pathway.

The inlet combustion gas flow rate was set to achieve the desired overall heat input to the desorber and to the ionic liquid solution flowing outside the plates. Tables 1 and 2 list the initial inlet boundary conditions that were used. The values listed are based on a firing rate of 10 kW, fuel heating value of 38.2 MJ/m^3, fuel flow rate of 0.0003 m^3/s and two air-fuel ratios corresponding to 20% (λ = 1.2) and 50% (λ = 1.5) excess air.

In the current simulations, the baseline desorber was assumed to comprise of three (3) heat exchanger plates. Thus, the inlet mass flow rates used to simulate the single heat exchanger plate were one-third (1/3rd) of the mass flow rates listed in Table 7. The inlet mass flow rate was set to 0.00129 kg/s for λ = 1.2 and 0.00161 kg/s for λ = 1.5 for the baseline cases with the 3 heat exchanger plates.

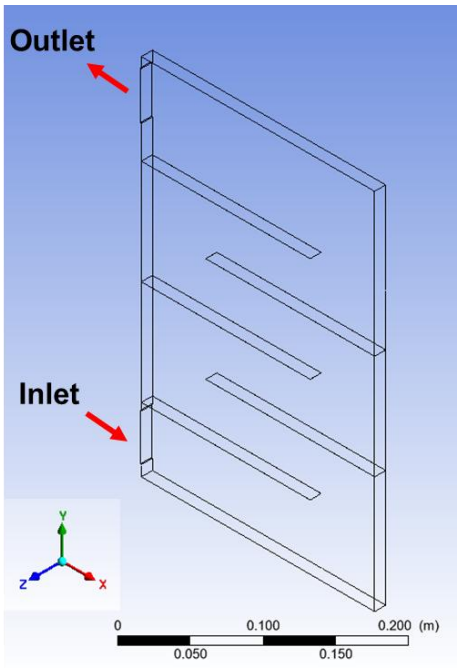

Figure 9. Simplified single-plate heat exchanger.

Table 7. Inlet combustion gas properties

λ	Air-fuel Ratio	Total Mass Flow (kg/s)	Flame Temp (°C)	Relative Mass Flow (kg/s-kW)
1.2	11.79	0.00389	2000	0.000389
1.5	14.74	0.00482	1650	0.000482

Table 8. Inlet species

λ	N_2	Ar	O_2	CO_2	H_2O
1.2	71.79%	0.92%	3.22%	8.21%	15.86%
1.5	72.95%	0.93%	6.54%	6.68%	12.90%

The solution side of the plate heat exchanger was modeled assuming falling film and pool boiling. Several cases with varying combinations of film and pool boiling were modeled. The heat transfer for both film and pool boiling was calculated using a heat transfer coefficient (h_{film}/h_{pool}) and a constant solution temperature (T_{film}/T_{pool}), which are listed in Table 9. The outlet was modeled as a pressure outlet with a gauge pressure of zero and an assumed backflow temperature of 254 °C. Lastly, these simulations neglected radiation.

Table 9. Solution side heat transfer

λ	h_{film} (W/m^2-K)	T_{film} (°C)	h_{pool} (W/m^2-K)	T_{pool} (°C)
1.2, 1.5	200	140	500	180

The simulations for all cases were initiated with a hybrid initialization, followed by a steady state treatment for approximately 500 iterations to stabilize residuals, and then completed with a transient simulation with a calculation time of at least 2 volume sweeps through the heat exchanger.

Simulation Results

Transient simulations of the different cases were performed, and the results are discussed below.

Baseline Film Boiling Cases with 3 Plates

The results of simulation of the film boiling cases with λ = 1.2 and λ = 1.5 are described here. Figure 10-Figure 12 show the contours of calculated temperature, velocity magnitude and static pressure along a vertical mid-plane along the thickness of the heat exchanger plate (i.e. an x-y plane at the mid-point of the thickness in z-direction in Figure 9).

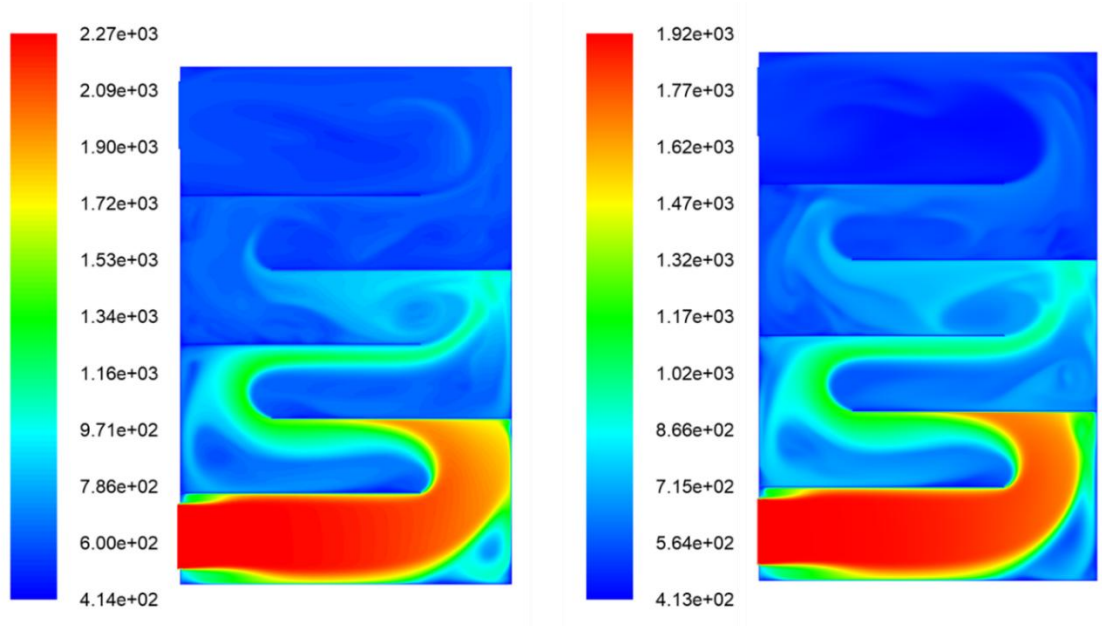

Figure 10. Temperature contours at the mid-x-y plane, in K. Left: λ = 1.2; Right: λ = 1.5.

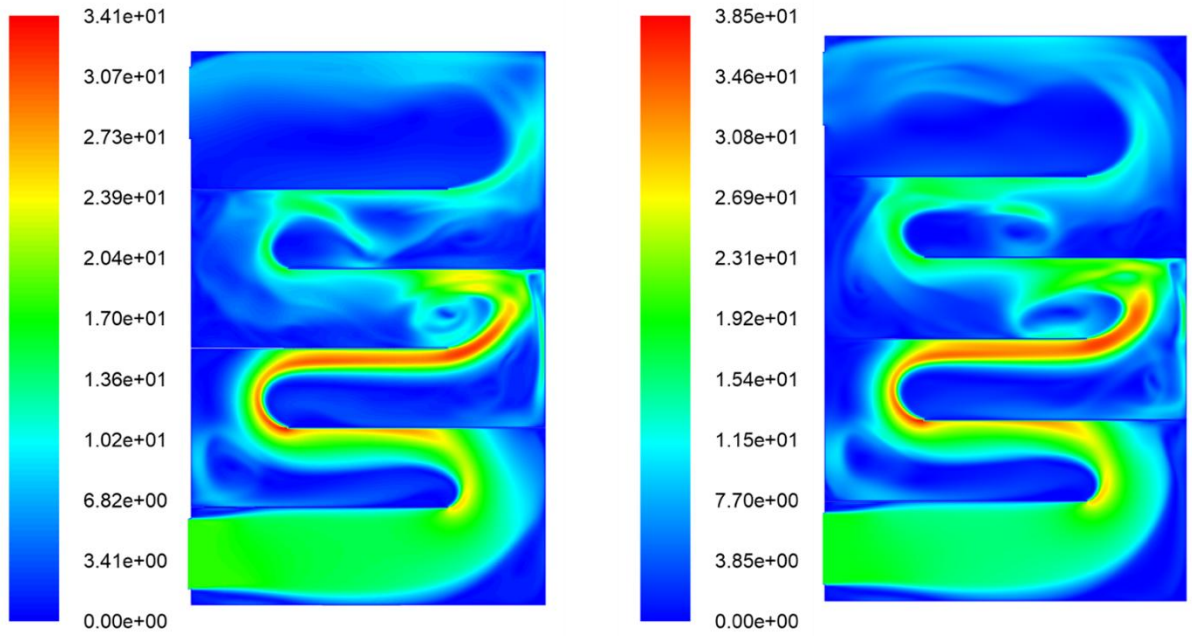

Figure 11. Velocity magnitude contours at the mid-x-y plane, in m/s. Left: λ = 1.2; Right: λ = 1.5.

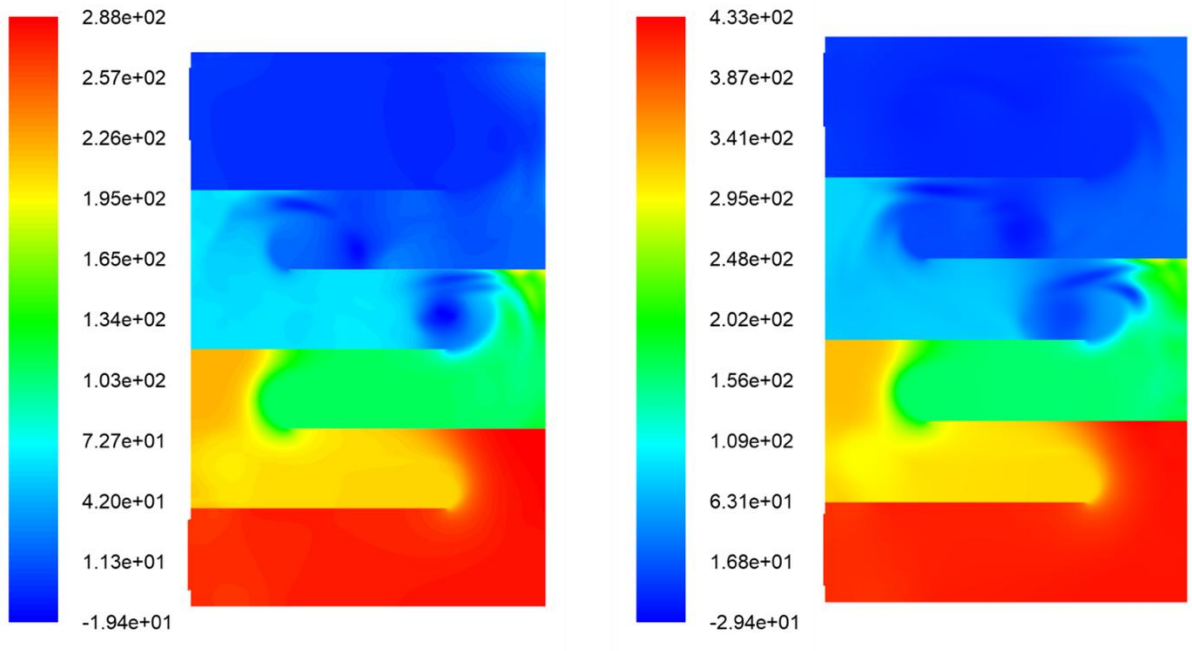

Figure 12. Static pressure contours at the mid-x-y plane, in Pa. Left: λ = 1.2; Right: λ = 1.5.

Figure 13 shows the calculated temperature distribution at the interface between the heat exchanger surfaces and the flue gases flowing inside. The temperature ranges were scaled to clearly show the hot spots on the heat exchanger surface. The maximum desired heat exchanger surface temperature is 190°C or 463 K to avoid degradation of the ionic liquid. It is clear from

Figure 13 that with film boiling only, the heat exchanger surface temperatures are much higher than desired over large area fractions.

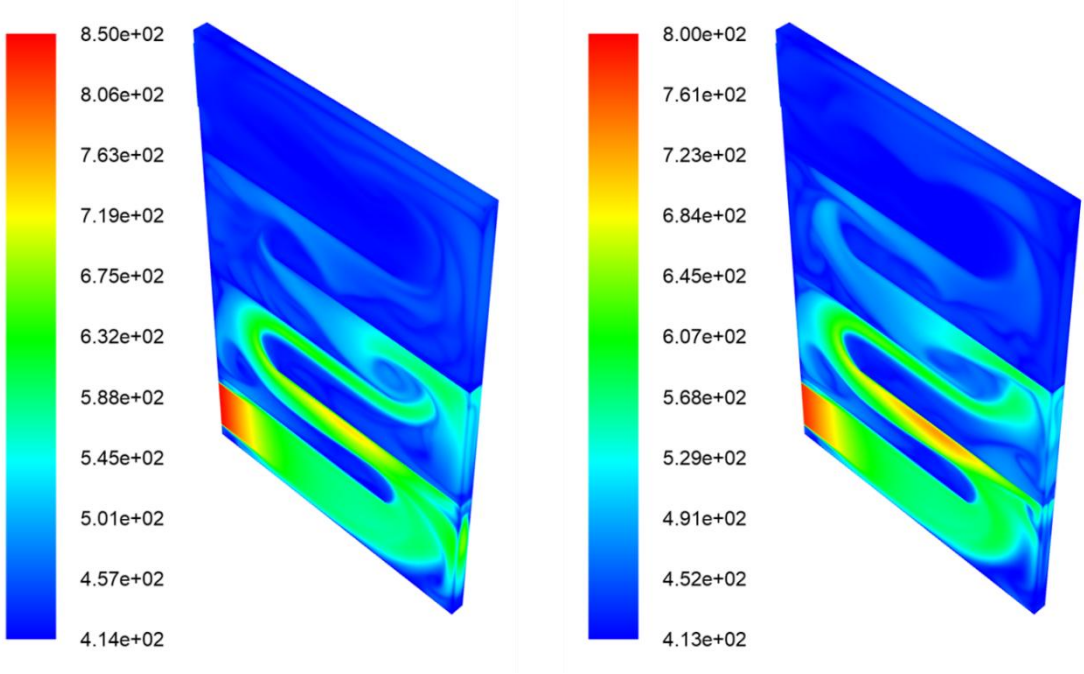

Figure 13. Temperature contours on the flue gas-wall interface, in K. Left: λ = 1.2; Right: λ = 1.5.

Mixed Film-Pool Boiling Case with 3 Plates

Next, a combined film and pool boiling case was modeled with λ = 1.5, which is deemed more suitable due to the lower flame temperature. For this case, the bottom 1/3rd of the heat exchanger was assumed be submerged in a pool of the solution and hence, exposed to pool boiling. Figure 14 shows the calculated temperature distribution at the flue-heat exchanger surface interface. Even with this scenario, the surface temperatures were much higher than desired, up to about 650 K.

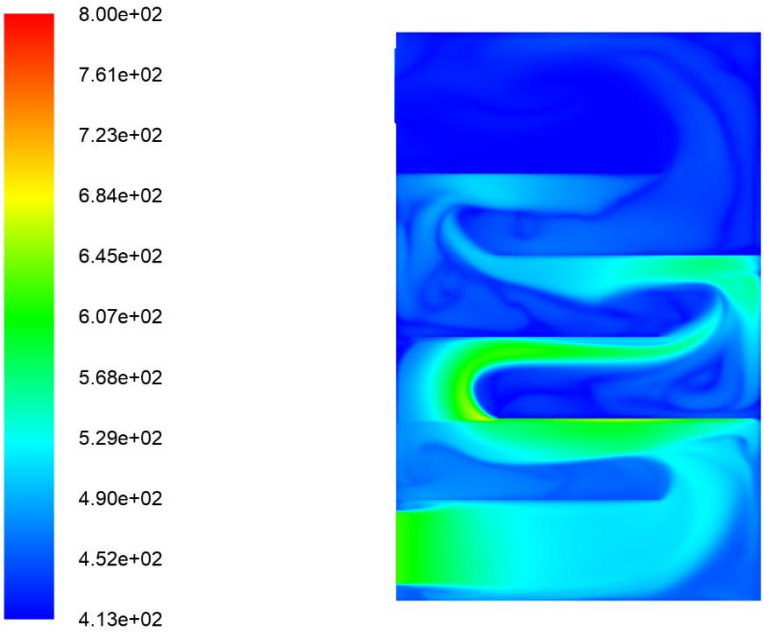

Figure 14. Temperature contours on the flue gas-wall interface for combined film and pool boiling with λ = 1.5, in K.

Pool Boiling Cases with Variable Number of Plates and Dual Inlets

Based on the high surface temperatures observed with the previous scenarios of film and mixed boiling, completely submerged or pool boiling only scenarios were modeled. In addition, since the higher temperatures were observed in the regions close to the flue gas inlet, dual flue gas inlets were considered, as shown in Figure 15. The inlet flow rates were scaled down based on the number of plates and the dual inlets to maintain the overall flue gas mass flow rate of 0.00482 kg/s for λ = 1.5. A further modification to the geometry investigated the impact of angled leading edges of the fins or flow partitions to break up the flow pattern at the turn.

Figure 16 and Figure 17 show the temperature distributions at the flue gas-heat exchanger surface interfaces for two scenarios of 3 and 6 heat exchanger plates. Compared to the film and mixed boiling scenarios, the peak temperatures and fraction of area above 190°C or 463 K are substantially reduced with the pool boiling cases. Further, with reduced flue gas mass flow rate for each plate, the 6 plate scenario showed lower surface temperatures than the 3 plates. However, a few hot spots of >463 K were still observed in both the cases. The peak hot spot temperatures were about 600 K for the 3 plates and 510 K for the 6 plates. Addition of the leading edges to the fins altered the flow pattern, but did not eliminate the hot spots.

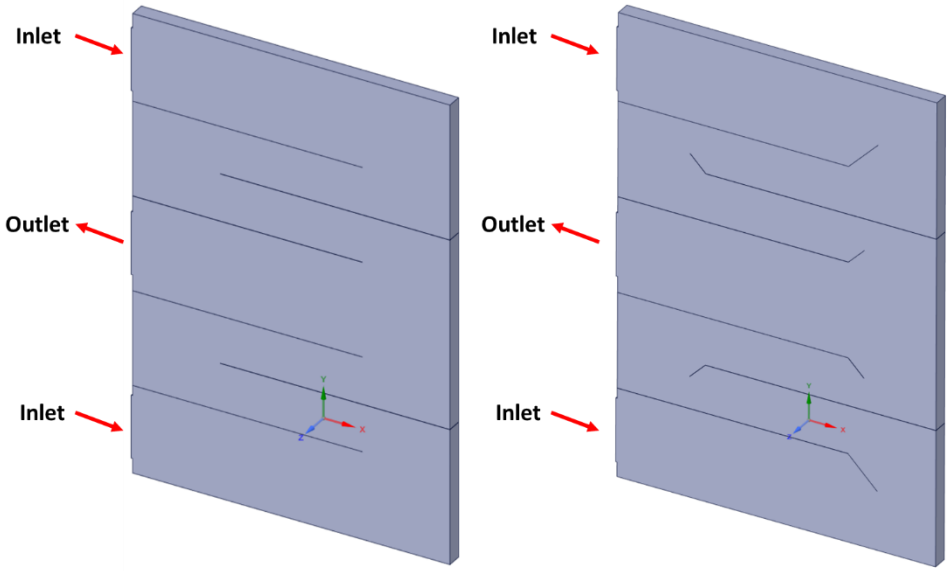

Figure 15. Heat exchanger plate with dual flue gas inlet. Left: Regular fins or flow partitions; Right: Fins with angled leading edges to break up the flow.

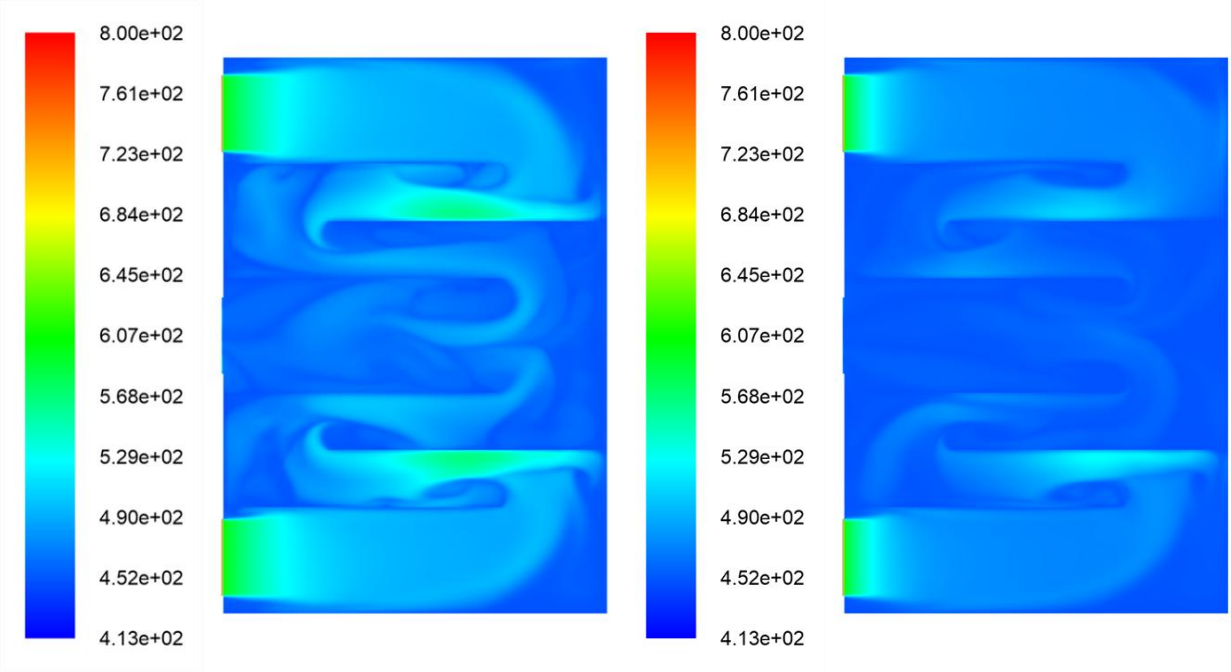

Figure 16. Temperature contours on the flue gas-wall interface for pool boiling with λ = 1.5, in K. Left: 3 plates; Right: 6 plates.

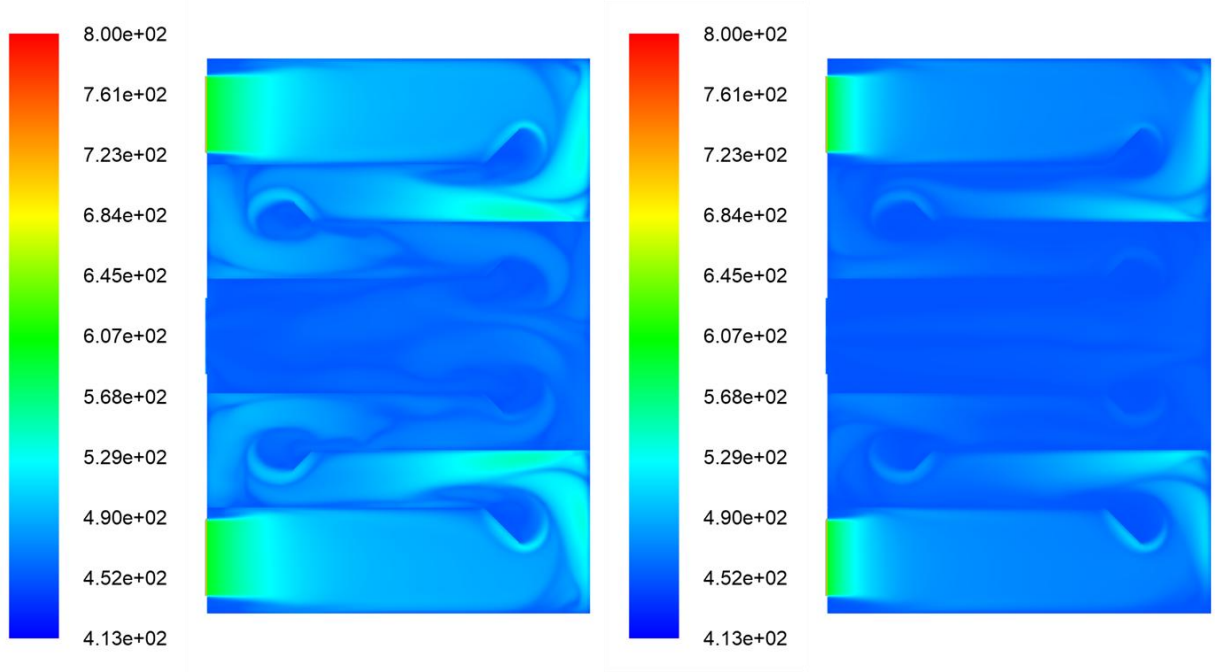

Figure 17. Temperature contours on the flue gas-wall interface for pool boiling with λ = 1.5, in K. Modified geometry with leading edges for breaking up the flow. Left: 3 plates; Right: 6 plates.

Finally, two additional scenarios with 12 and 24 plates were investigated and the results are shown in Figure 18. With the significantly reduced flue gas flow through each plate, the hot spots are nearly eliminated with only a few spots showing temperature >463 K.

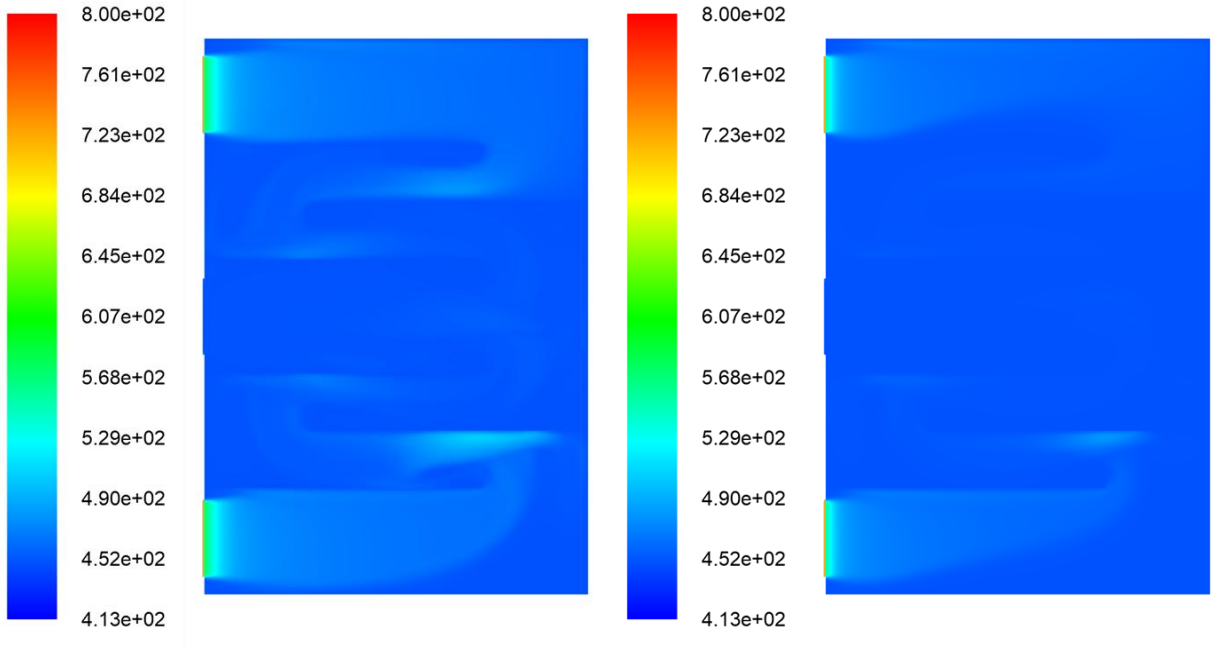

Figure 18. Temperature contours on the flue gas-wall interface for pool boiling with λ = 1.5, in K. Left: 12 plates; Right: 24 plates.

Heat Transfer and Pressure Drop

Finally, the heat transfer to the solution outside the plates and pressure drop between the inlet and outlet were calculated. The results are shown in Table 10. To reiterate, the input firing rate was 10 kW.

Table 10. Calculated heat transfer rates and pressure drops

λ	Film or pool boiling	Number of plates	Number of inlets per plate	Fins	Heat transfer (kW)		Pressure drop (Pa)
					Fluent	Theoretical	
1.2	Film	3	1	Regular	9.48	7.97	238.13
1.5	Film	3	1	Regular	8.77	7.70	409.34
1.5	Mixed	3	1	Regular	8.80	7.72	364.46
1.5	Pool	3	2	Regular	8.27	7.36	92.01
1.5	Pool	6	2	Regular	8.74	7.72	20.26
1.5	Pool	3	2	Angled edges	8.57	7.57	61.85
1.5	Pool	6	2	Angled edges	8.88	7.83	16.14
1.5	Pool	12	2	Regular	8.97	7.89	5.56
1.5	Pool	24	2	Regular	9.06	7.98	1.77

Burner Design and Gas Train Selection

The firing rate requirement for desorption was 10 kW. Based on this output requirement, bench-top, open-air testing of two radiant-style burner samples was completed. The objective of this testing was to determine an appropriate power density and burner size that would match the desorption requirement. The first test was completed on a flat, square-shaped burner fabricated out of sintered metal, as shown in Figure 19, with flameholder dimensions of approximately 4.5 in x 4.5 in. Eight operating conditions were tested spanning an air-fuel equivalence ratio (lambda, or λ) between 1.0 – 2.0 and firing rates between 8- 13 kW. A Horiba gas analyzer was used to track O_2, CO_2, NO_x, and CO emissions. The ideal range for stable operation and acceptable NO_x (< 20 ppm at 3% O_2 dilution) appeared to be a narrow lambda range of ~1.1 - 1.2 at a firing rate of 10 kW (approximately 80 W/cm^2). The lowest CO measurement was achieved at a lambda value of 1.38 with 389 ppm at 3% O_2 dilution, although the CO measurements were highly dependent on the distance of the probe from the flameholder. Excessive CO was not expected to be as high during in-situ burner operation, since a probe wouldn't be inserted into the burner chamber, thus avoiding potential flame quenching on the probe surface. A second burner, also shown in Figure 19, was tested. This burner had a flameholder that was woven rather than fabricated from sintered metal. Testing of the burner yielded similar results to the square-shaped burner and confirmed

the ideal lambda operating range of 1.1 – 1.2 to maintain acceptable NO_x emissions at a 10 kW firing rate.

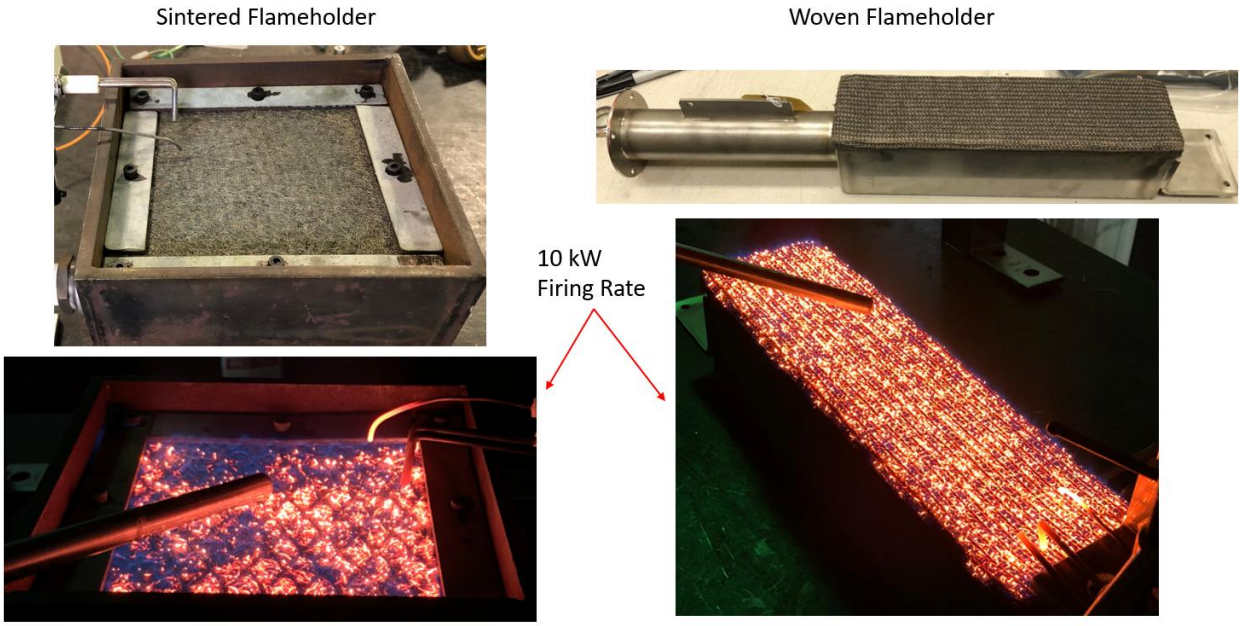

Figure 19: Open-air testing of sintered (left) and woven (right) radiant-style burners.

Following testing of the burner samples, a maximum power density of 80 W/cm^2 was selected, which translated to a burner surface area of approximately 20 in^2 for a maximum firing rate of 10 kW. Multiple manufacturers were contacted to select the most appropriate material for a radiant-style burner. Three burners with flameholders measuring approximately 2 in x 10 in were procured from different manufacturers, as shown in Figure 20. Due to limitations in time, only the burner with the sintered mesh flameholder was tested in situ with the mock desorber, which will be discussed in a later section.

The burner was installed with a gas train that included the following components:

- A FIME blower, PX118 model, with a max speed of 7,000 rpm, 56 CFM, and max outlet pressure of 10.4" W.C.
- A VK81 series gas valve, with pneumatic 1:1 air/fuel control
- A standard venturi 45.900.444-003 model, with an output range from 5 to 27 kW (17,000 to 92,000 Btu/hr)

Figure 20: Flat, rectangular-shaped, radiant-style burners procured for operating mock desorber including two woven mesh flameholders (left and center) and one sintered mesh flameholder (right).

The gas train assembly is shown with and without the burner attached in Figure 21 and Figure 22, respectively.

Figure 21: Gas train including sintered metal radiant-style burner.

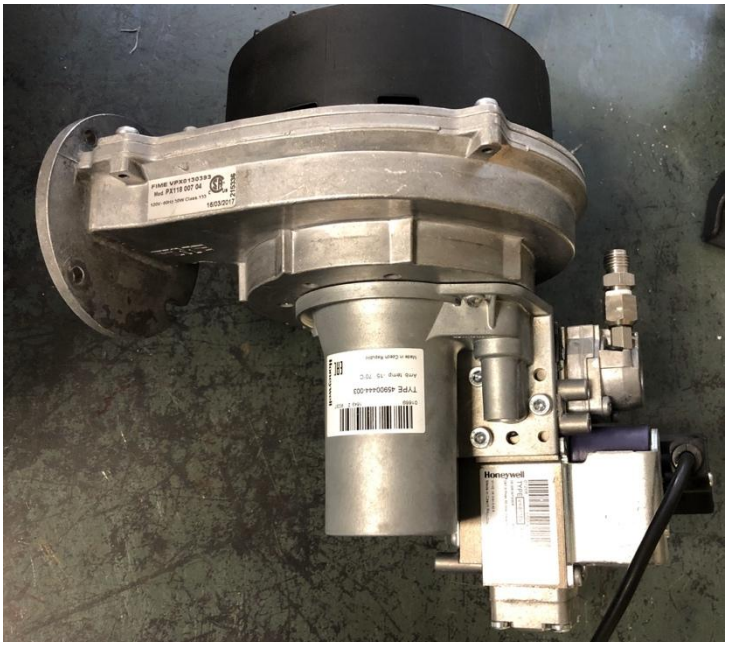

Figure 22: Gas train assembly without the burner.

The burner was installed on a combustion chamber that was in turn installed on the desorber vat (See Figure 23). Fiberglass insulation was used in between each mating surface to ensure a leak-proof seal that was compatible with high temperature flue gas.

Figure 23: Burner assembly including combustion chamber with flame sensor and hot surface ignitor installed.

To determine the potential of hot spot formation on the vat wall facing the inlet flue manifold, a simulation was performed which included the inlet flue manifold, vat wall and the first 5 inches of inlet heat exchanger tubing. Although the inlet flue manifold chamber didn't make direct contact with the vat except at the mounting flange, the simulation model was prepared with the assumption of a shared wall between the vat and the inlet flue manifold. The simulation was run with an inlet flue gas conditions as follows:

- Mass Flow Rate (kg/s): 0.002027 (based on 10 kW operating condition)

- Hydraulic Diameter: 0.0393 m
- Temperature: 1997 K (Adiabatic flame temperature based on λ = 1.25)

The walls of the inlet flue manifold were assumed to be adiabatic. As can be seen in Figure 24, hot spots of 600°F (316°C) appear outside the periphery of the intersection of the heat exchanger tubes and vat wall. This is far above the ionic liquid temperature limit beyond which it begins to break down (160°C). To avoid this hot spot formation, the decision was made to place a ceramic insulation block at the back of the inlet flue manifold. As shown in Figure 25, the ceramic insulation block has three holes measuring 2 inches in diameter to align with the heat exchanger coil inlets. The hole was machined with a 45° chamfer on the side facing the burner. This was done to prevent recirculation of flue gases inside the burner and to increase the boundary layer at the inlet of the tube and thereby reduce the potential of hot spot formation at the initial length of the inlet tube.

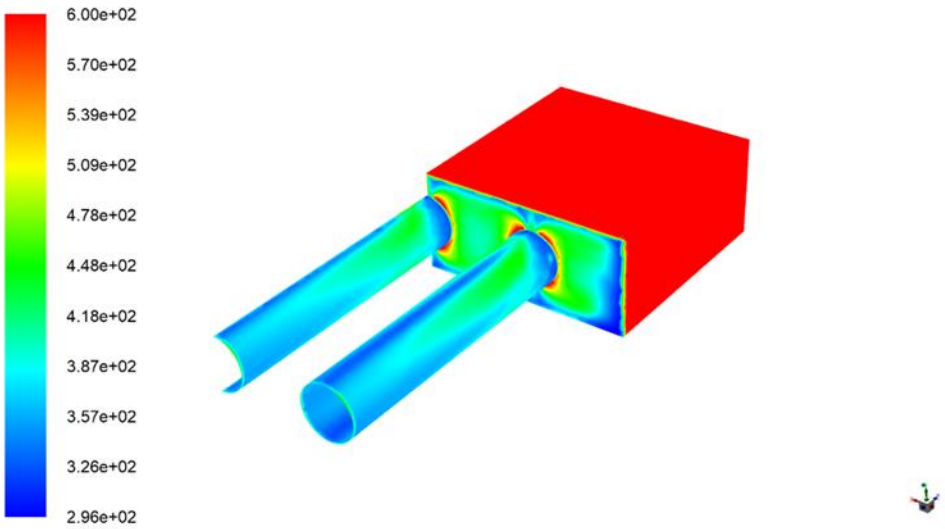

Figure 24: Simulation of 10 kW firing rate operation with uninsulated inlet flue manifold (Temperature scale in °F).

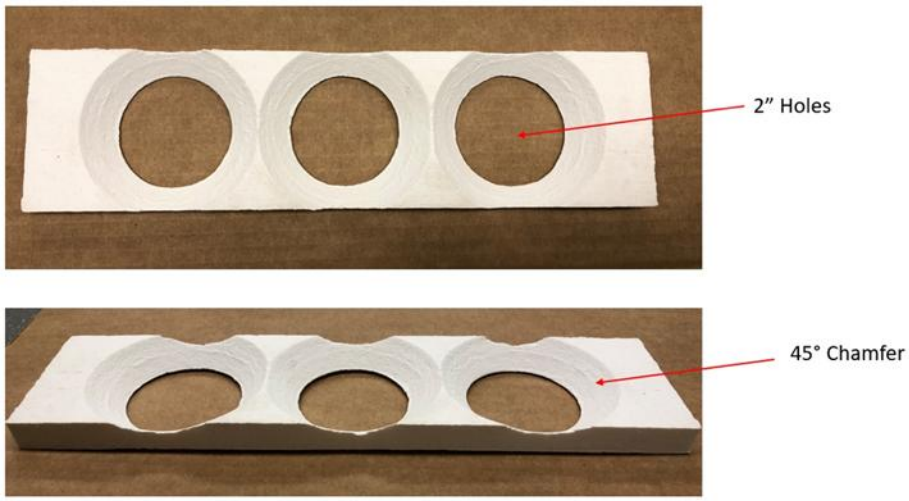

Figure 25: Ceramic insulation insert for inlet flue manifold with 2 inch diameter holes concentric with heat exchanger coil inlets and 45° chamfer.

Heat Exchanger Design

Multiple rounds of CFD simulations were performed to provide a preliminary design of the heat exchanger for the mock desorber. The initial heat exchanger design was based on a clamshell, serpentine style heat exchanger such as those found in some gas-fired furnaces. An attempt was made to fabricate clamshell heat exchanger plates using resin-filled, 3D printed molds but was ultimately unsuccessful. Due to limitations in the 3D printing, the molds were unable to withstand the expansion and heat generated by the resin, which caused warping (see Figure 26).

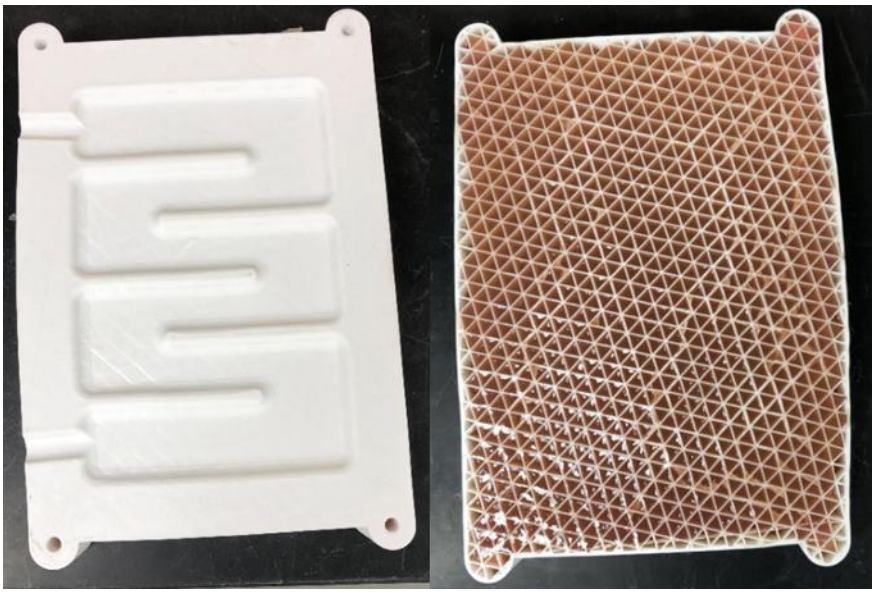

Figure 26: Top and bottom of male mold die filled with resin.

Due to these heat exchangers being designed for air-to-air applications with the flue side being under negative pressure, the construction is not liquid-tight. Also, these heat exchangers are typically sized for non-condensing applications with firing rates > 20 kW. With the goal being to test a desorber at a firing rate of up to 10 kW, the mock test stand would have been oversized. Therefore, a tubular, serpentine style heat exchanger was opted for instead, as shown on the right of Figure 27.

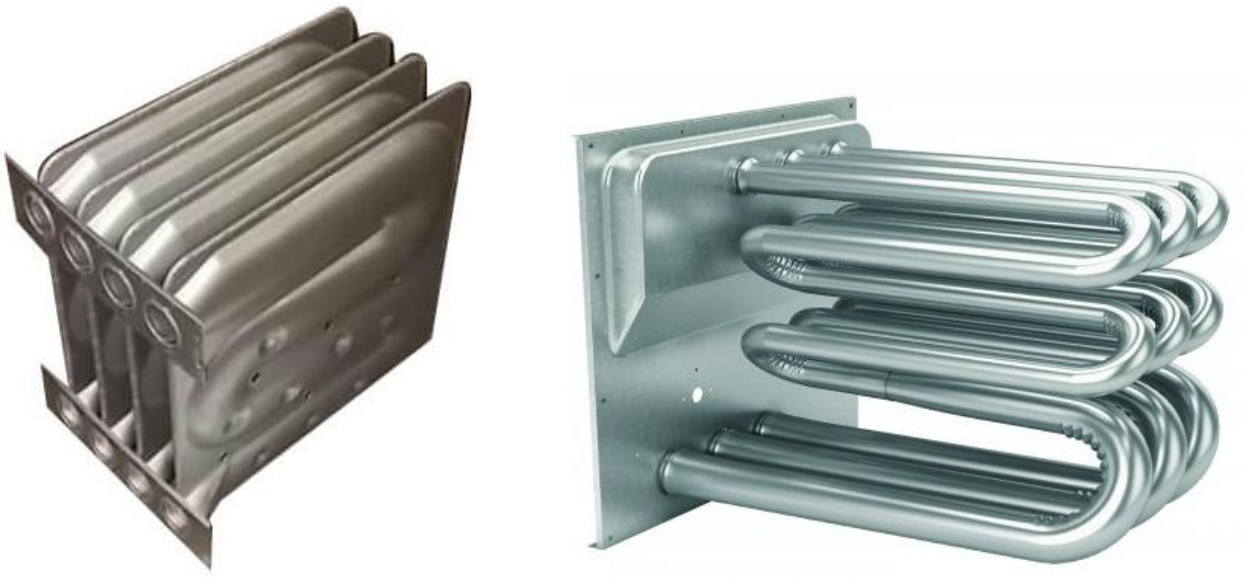

Figure 27: Clamshell style HX by Lennox (left) and Tubular style HX by Goodman (right).

Multiple off-the-shelf, tubular-style heat exchangers were purchased for possible use with the mock desorber. However, the smallest available heat exchanger was sized for 90 kBTU/hr operation (26.4 kW) and would have required a 28-gal capacity tank to accommodate the dimensions of the coils, with 25 gallons of ionic liquid. To avoid oversizing the unit and overspending on ionic liquid, a smaller, custom, tubular-style heat exchanger was designed. Using the furnace tubular style heat exchanger as a reference, a custom heat exchanger coil was designed with a 2 in. tube outer diameter and 2 in. bend radius with a volume displacement approximately half of the commercially available heat exchanger, as shown in Figure 28.

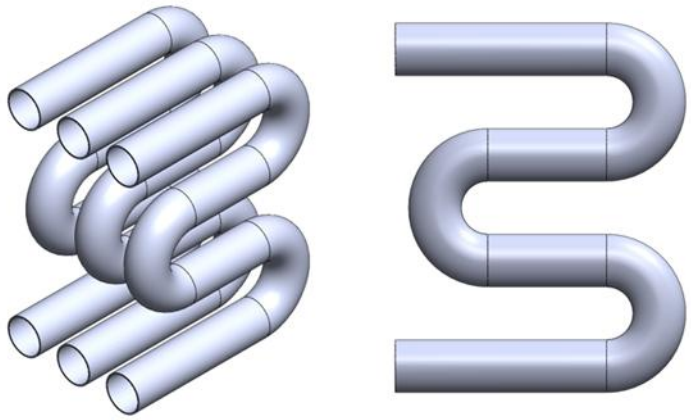

Figure 28: Custom designed heat exchanger coils with 2 in outer diameter tubing.

To minimize the amount of ionic liquid needed for the mock desorber, a custom-sized tank was also designed to provide a closer fit to the custom heat exchanger, as opposed to a commercially available tank. The tank was designed to have an overall capacity of 10 gallons with room to fit three heat exchanger coils. Refer to Figure 29 which shows the desorber assembly, including the custom designed vat, three of the custom designed heat exchanger coils, and the burner chamber.

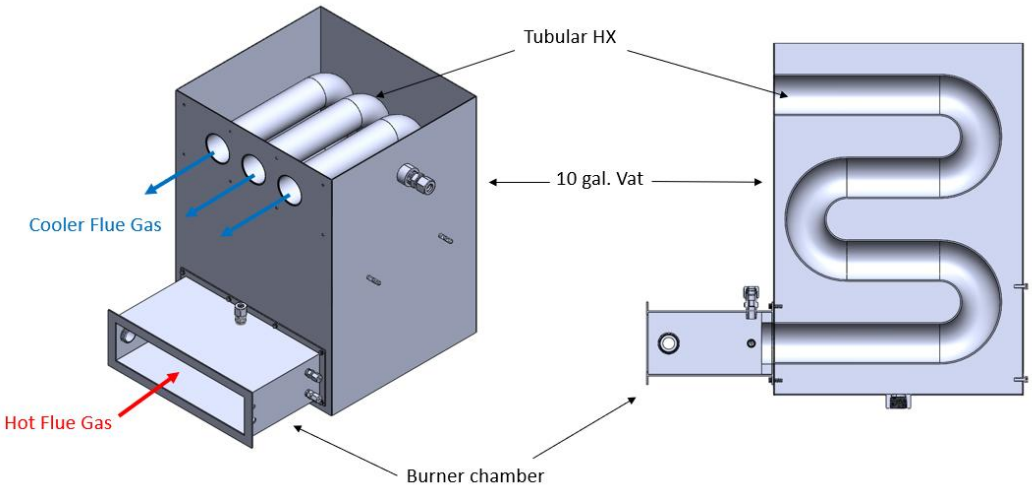

Figure 29: Custom tubular heat exchanger inside desorber vat.

One of the decisions made was to use an alternative heat transfer fluid in place of the ionic liquid, due to cost and the potential for frequent scorching of the ionic liquid. The two alternatives that were considered were Dowtherm A and peanut oil. A comparison of the thermophysical properties of ionic liquid, Dowtherm A, and peanut oil are shown in Figure 30 – Figure 33. Due to the availability of a commercial range hood with automatic sprinkler system, ease of disposal, and relatively low cost, peanut oil was used as a surrogate to the ionic liquid.

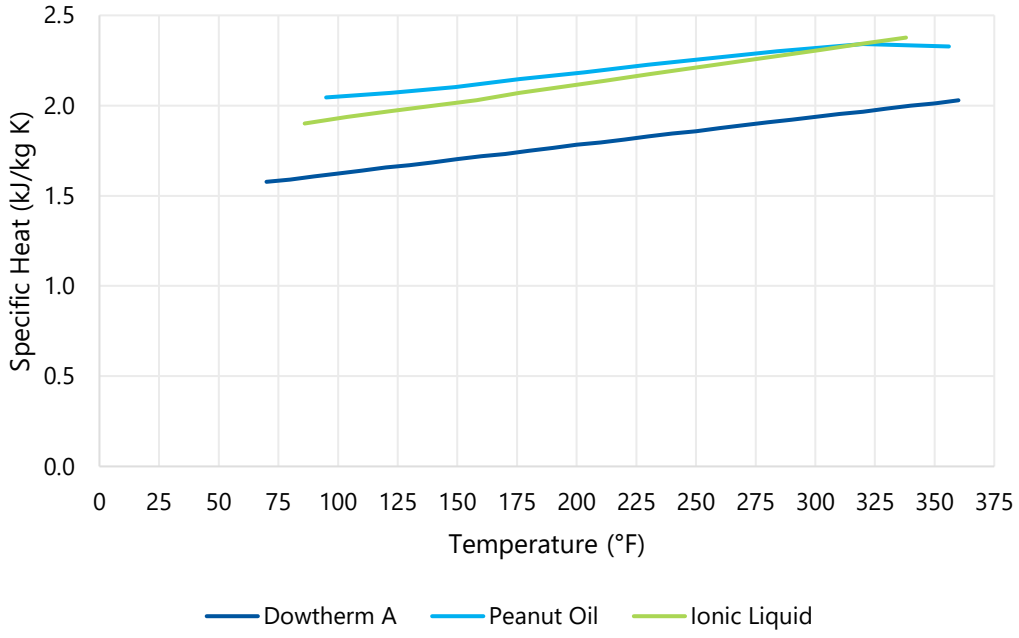

Figure 30: Specific heat of Dowtherm A, peanut oil, and ionic liquid.

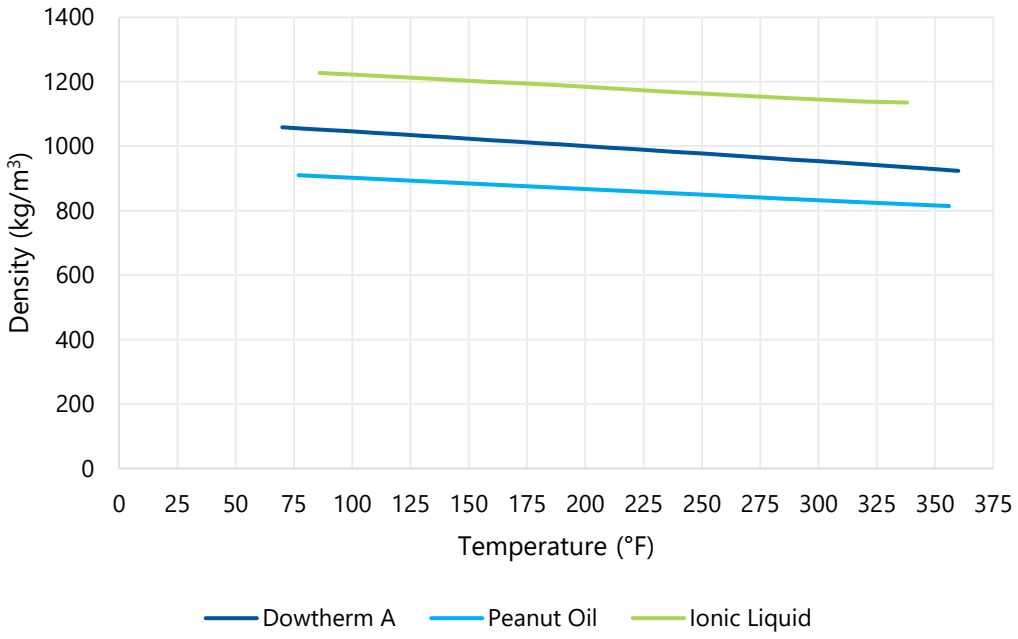

Figure 31: Density of Dowtherm A, peanut oil, and ionic liquid.

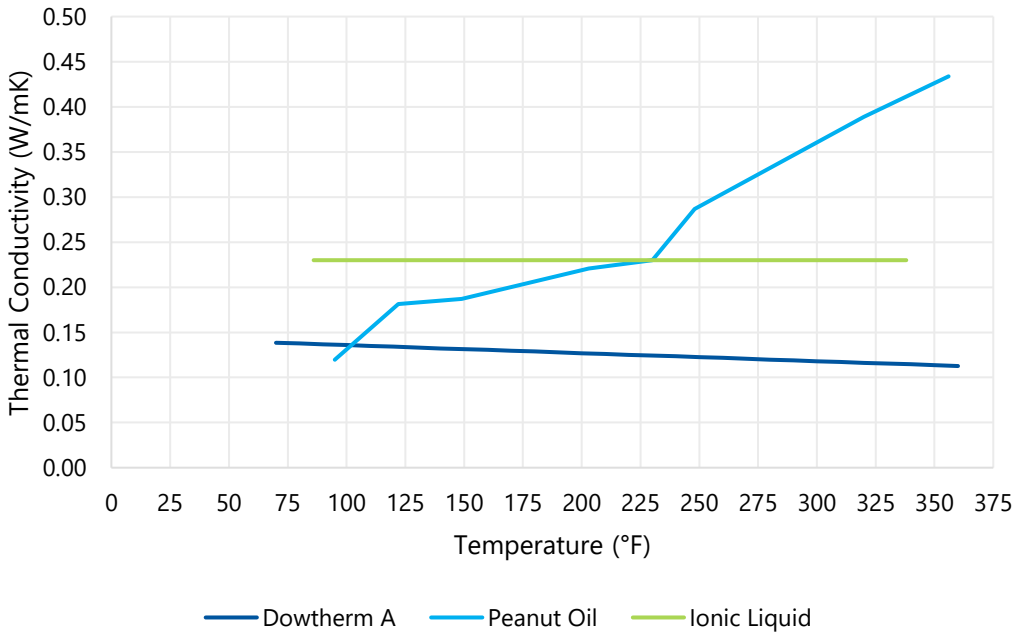

Figure 32: Thermal conductivity of Dowtherm A, peanut oil, and ionic liquid.

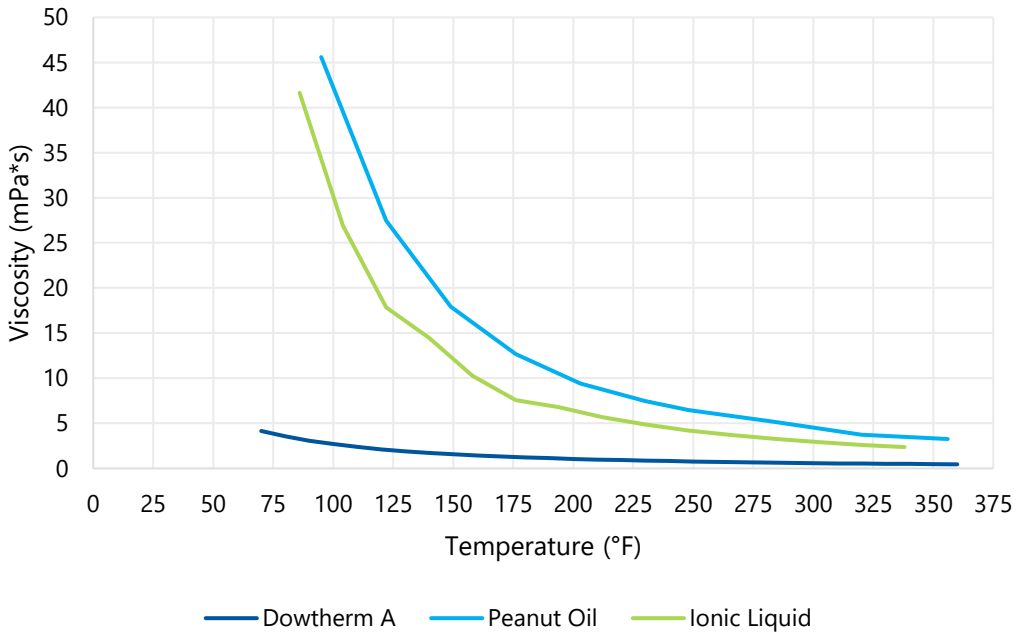

Figure 33: Viscosity of Dowtherm A, peanut oil, and ionic liquid.

Mock Desorber Design

Once the burners were procured and the custom desorber design was finalized, the remainder of the desorber test stand components were sized and selected. The test stand was designed to accommodate the desorber which includes all the ports needed to measure temperature of the heat transfer fluid, the burner and inlet flue gas manifold (burner chamber), the outlet flue gas manifold, the external plate heat exchanger needed for thermal rejection, the recirculation pump for the heat transfer fluid and a Unistrut frame to support all the components. A 3D CAD model was generated of the mock desorber assembly as shown in

Figure 34. The drawing package was submitted to an external fabrication vendor who built all components shown in the figure.

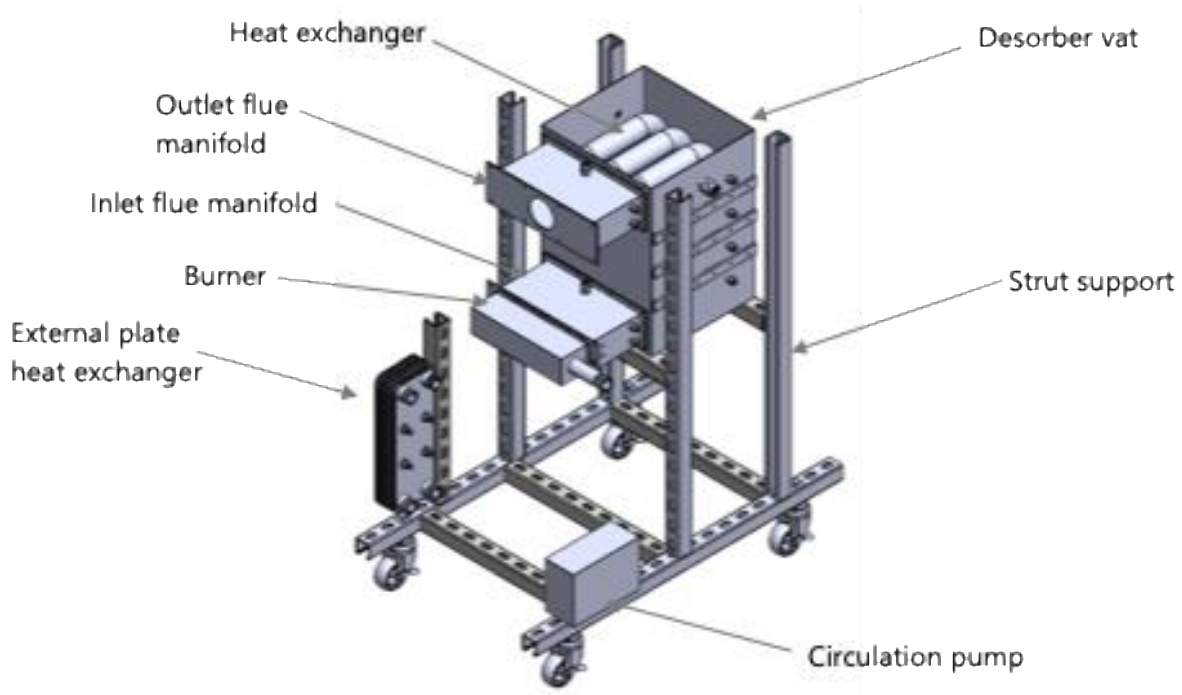

Figure 34: 3D CAD model of desorber test stand.

To capture the heat exchanger surface temperatures, a total of 48 K-type thermocouples were spot welded to the center coil and one of the outside coils. The locations of the thermocouples are shown in Figure 35 below. Based on results from previous CFD simulations, the regions of interest for potential hot spot development were the heat exchanger inlet, middle of bends, outlet of first bend, and exit. For the center heat exchanger, five additional thermocouples were placed on the straight runs of tubing in between the bends to allow for characterization of surface temperature along the coil and for calculation of heat transfer coefficient. Refer to Figure 36 to view examples of the thermocouple spot welds on the heat exchanger coil surface.

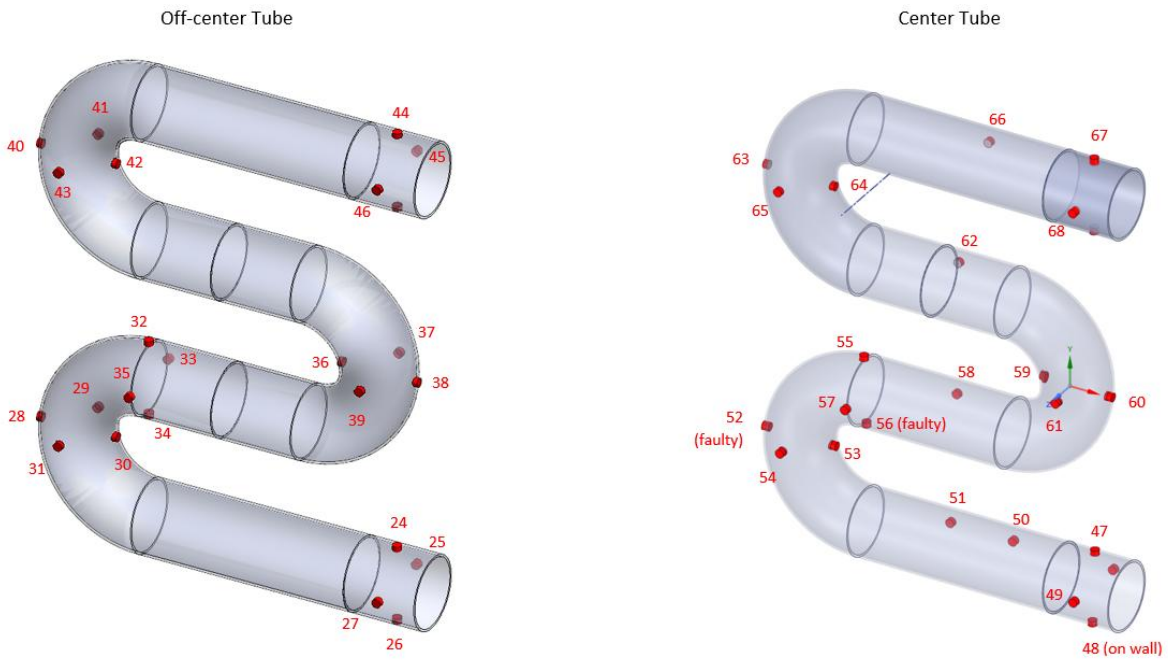

Figure 35: Heat exchanger surface thermocouples labeled in sequence with balance of experimental thermocouples.

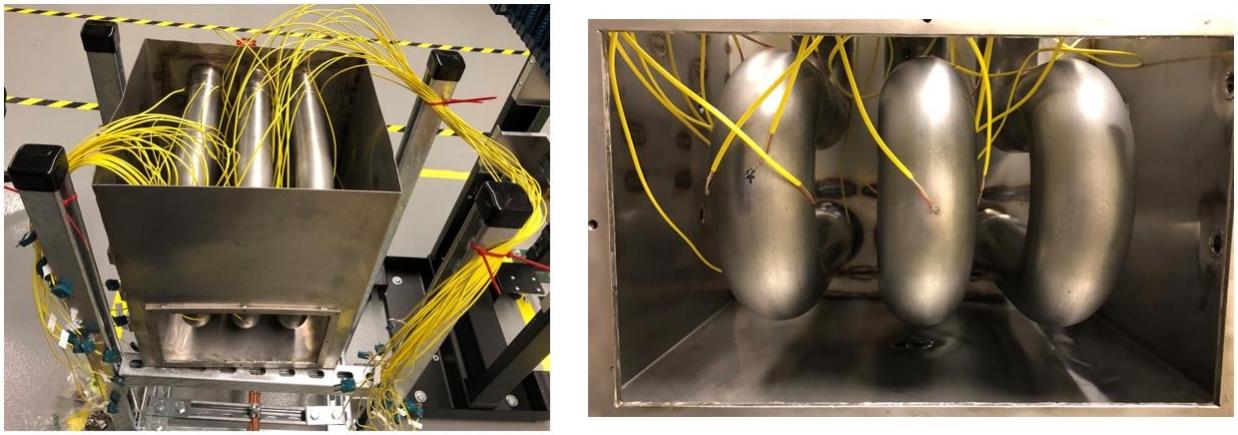

Figure 36: Thermocouple spot welds on heat exchanger coils.

Once the thermocouples were all welded to the heat exchanger coils, the remaining components of the mock desorber test stand were assembled, plumbed to the vat, and wired to the data acquisition cart. Eight T-type thermocouples were installed on each side of the vat, for a total of 16 thermocouples that would be immersed in the peanut oil during testing. Thermocouples were also installed at the inlet and outlet of the vat and external plate heat exchanger to allow for calculation of heat rejection. The thermocouples were not individually calibrated but were tested for accuracy in a water boil test, which will be discussed in the next section. A four-way crossover valve was installed downstream of the recirculation pump to allow for two flow configurations: (1) flow enters the side port of the vat and exits through the bottom drain or alternatively (2) flow enters through the drain port and exits through the side port. A side view of the desorber test

stand is shown in Figure 37 and a closeup of components in the flow loop are shown in Figure 38. Refer to the appendix for more details on the planned testing for the mock desorber.

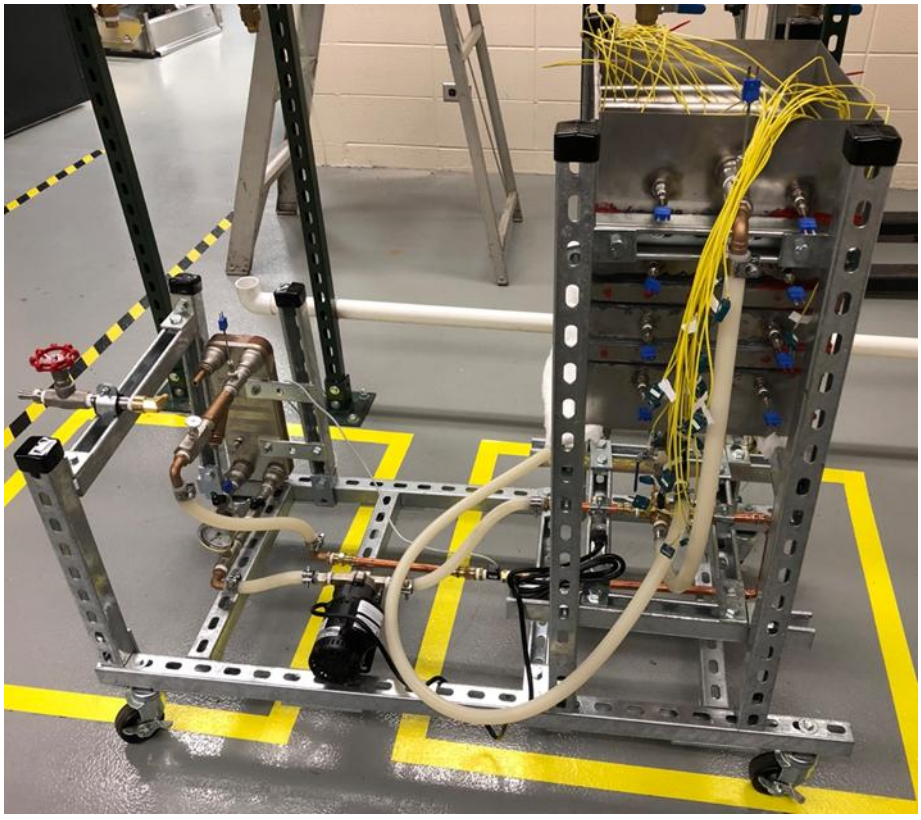

Figure 37: Mock desorber test stand with plumbing and thermocouple wiring completed.

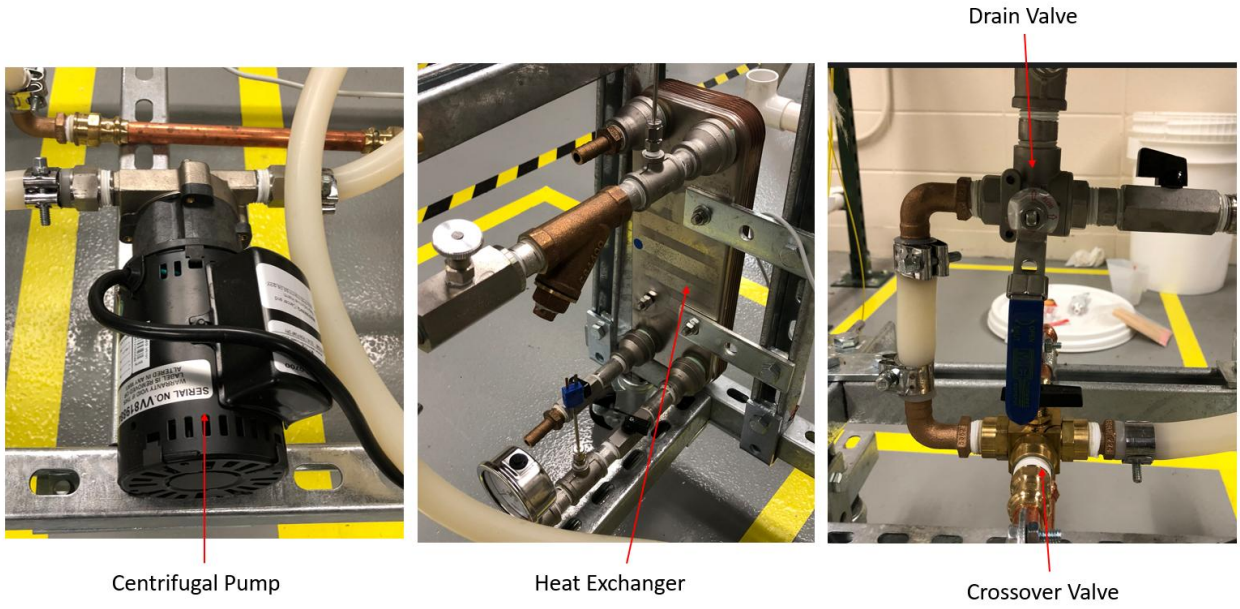

Figure 38: Balance of components in external thermal rejection flow loop for desorber.

Experimental Results

Water Boil Test

Initial testing of the desorber test stand was completed using water as a heat transfer fluid. The vat was filled with ~8.2 gal of water, reaching halfway up the heat exchanger tubes at the flue gas exit plane. The average firing rate over the duration of the experiment was 8.9 kW, with an air-equivalence ratio of 1.28 (excess air of 28%). With a starting temperature of 75°F, the water took ~30 min to reach boiling point. Boiling continued for 40 min before the experiment was shut down. The rise in heat exchanger surface thermocouple temperature measurements is shown in Figure 39.

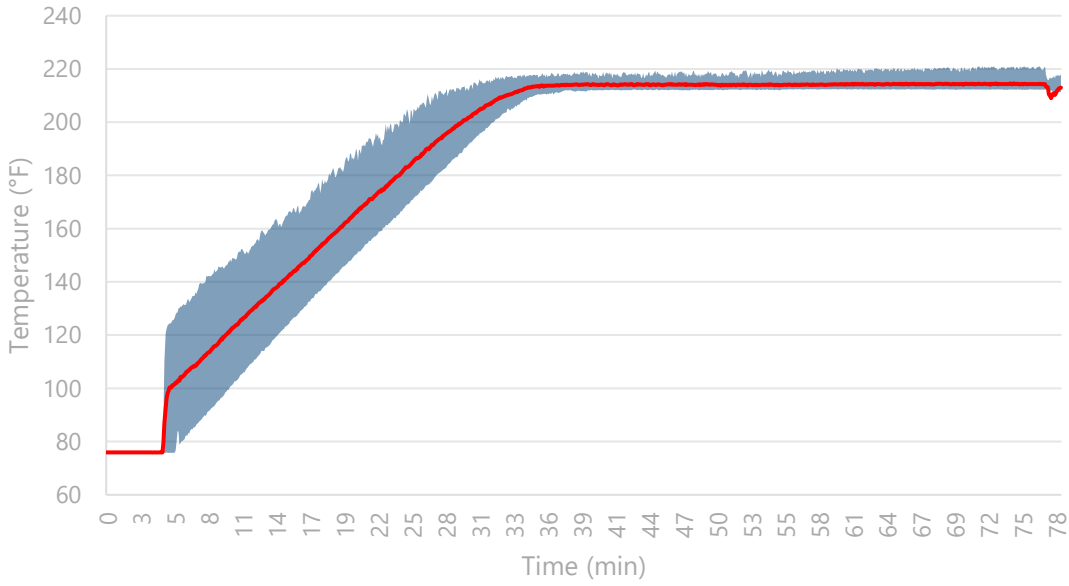

Figure 39: Temperature band of heat exchanger surface thermocouple measurements.

Due to challenges with the emissions sampling line, flue gas emissions measurements were collected only over a 15-minute window. The emissions as measured by the analyzer were averaged over this period of time as follows:

- O_2: 4.94%
- CO: 0.5 ppm
- NO_x: 27 ppm

An energy balance calculation was performed for the water boil test which showed a total heat input of 9,104 BTU (9,605 kJ) from the flue side. However, only 6,694 BTU (7,063 kJ) of energy gain was calculated from the water and steel side, leaving 2,410 BTU (2,543 kJ) which was assumed to be evaporative losses. Calculation of heat flux was performed at the 55 min mark (20 min into boiling) to be 14,359 W/m^2.

Over the span of multiple water boil shakedown experiments, a series of photographs were taken of the flame through the sight glass installed on the side of the burner chamber. The photographs shown in Figure 40 represent the appearance of the flame at varying lambda ratios, with the respective flue gas emissions measurements listed.

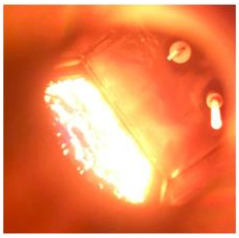

Lambda: 1.24
NOx: 30 ppm
CO: 0 ppm
CO2: 9.5%
O2: 4.4%

Lambda: 1.42
NOx: 8.2 ppm
CO: 0 ppm
CO2: 8.0%
O2: 6.9%

Lambda: 1.37
NOx: 12 ppm
CO: 0 ppm
CO2: 8.4%
O2: 6.1%

Lambda: 1.49
NOx: 4.8 ppm
CO: 0.5 ppm
CO2: 7.6%
O2: 7.5%

Figure 40: Images of flame at varying air-fuel equivalence ratios.

Peanut Oil Test

The goal for Task 3 was to test the mock desorber test stand with a surrogate heat transfer fluid, which was completed using peanut oil. A photograph of the desorber test stand during testing with peanut oil is shown in Figure 41.

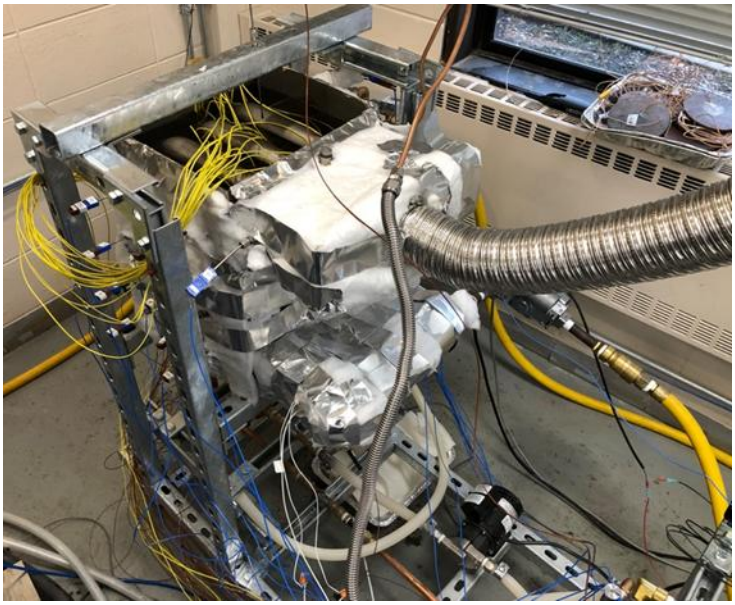

Figure 41: Insulated desorber vat filled with peanut oil.

Due to the increased viscosity of peanut oil compared to water, the flow rate of peanut oil through the external heat rejection flow loop was greatly diminished. In an attempt to improve the heat rejection capacity, a second external plate heat exchanger was installed. However, this worsened the problem due to increased pressure drop in the flow loop. As a result, the highest possible firing rate achievable to prevent thermal runaway of the heat exchanger was 48% less than for the water boil test. Furthermore, a higher air-equivalence ratio was needed to reduce the flame temperature and therefore the flue gas temperature. The final peanut oil test was performed in two parts, to allow for all the heat exchanger surface thermocouple measurements to be recorded, since the data acquisition system had a limited number of thermocouple channels. During part 1 of testing, the first hour was spent tuning the combustion blower speed and gas flow to the mixer to obtain the lowest, stable firing rate such that steady state operation could be achieved. After 60 minutes of tuning, an air-fuel equivalence ratio of 1.81 was reached. Steady state testing continued for 18.8 minutes during which the average firing rate was 4.8 kW. The average flue gas emissions during steady state, as shown in Figure 42, are listed below:

- O_2: 9.92%
- NO_x: 3.3 ppm @ 3% O_2 (1.67 ng/J)
- CO: 1.27 ppm (air free)

Due to a procedural error during testing, the emissions measurements were not recorded during part 2 of testing and were assumed to be the same as in part 1.

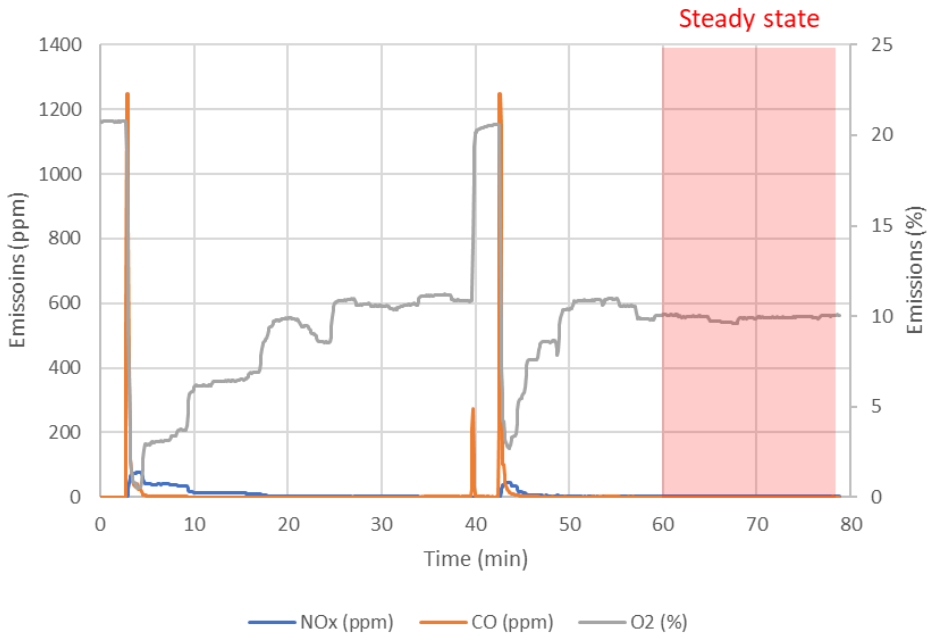

Figure 42: Flue gas emissions measurements during part 1 of peanut oil testing.

During the steady state period of part 1 of testing, the average bulk oil temperature was 271.4°F with thermal stratification in the vat ranging between 238.8°F – 302.8°F. The average coil surface temperature was 307.8°F with a range of 245.2°F – 353.2°F. Refer to Figure 43 for the temperature plots.

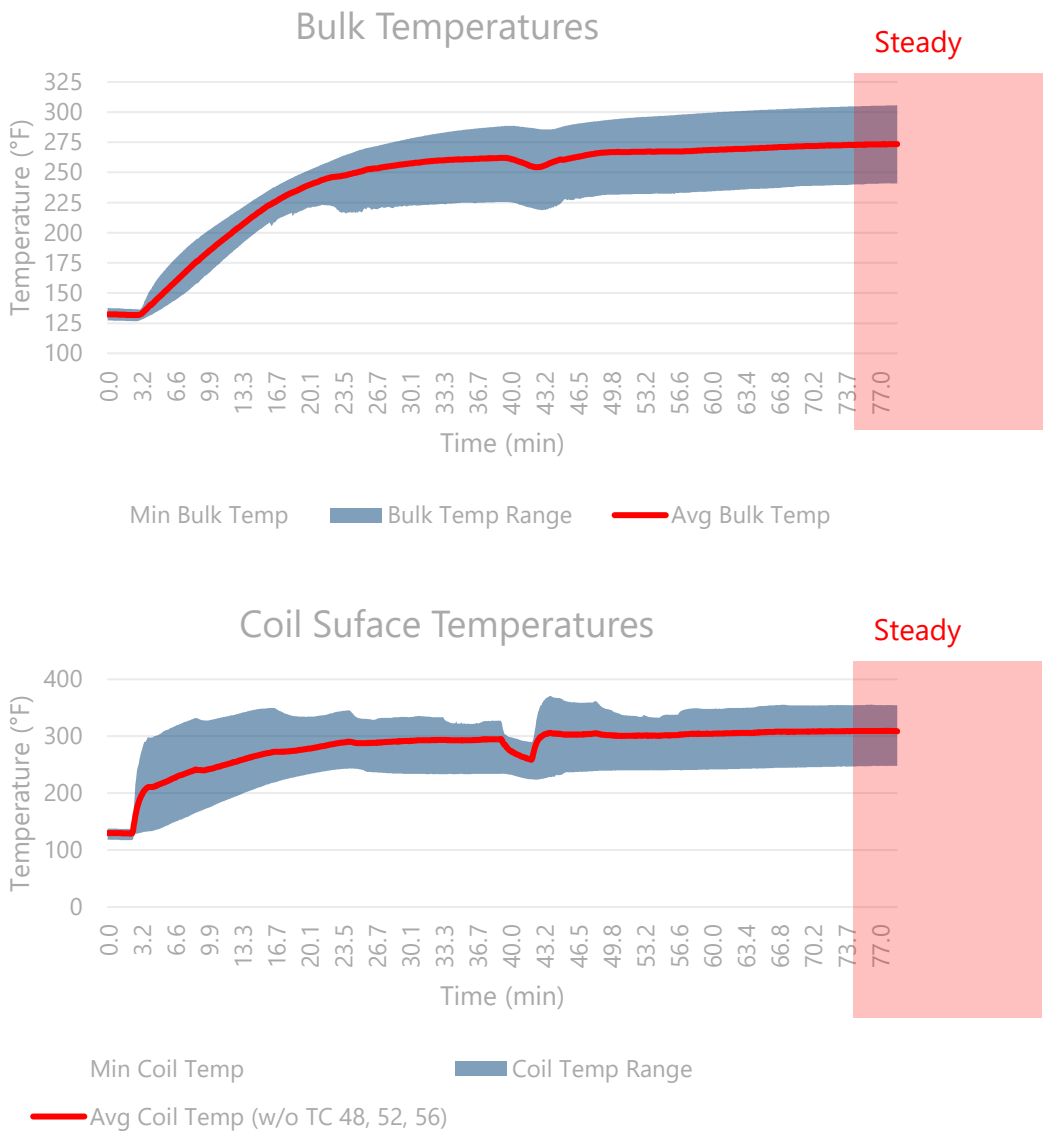

Figure 43: Peanut oil and heat exchanger surface temperatures during part 1 of peanut oil testing.

The beginning of part 2 of the peanut oil test began approximately 40 minutes after the end of Part 1 test was complete. This is the time it took to connect all the previously disconnected heat exchanger thermocouple probes to the data acquisition system, which required some of the thermocouple probes from part 1 of testing to be disconnected to free up a connector. Therefore, some thermocouples from part 1 remained connected to the data acquisition system for part 2 of testing. In this span of time, the oil and heat exchanger surface temperatures increased slightly, due to a slightly higher thermal input compared to heat rejection, which was maxed out. Part 2 of testing ran for a duration of 37 minutes of steady state operation at 4.7 kW. The average bulk oil temperature was 274.1°F with thermal stratification in the vat ranging between 244.2°F – 305.2°F. The average coil surface temperature was 319.6°F with a range of 284.9°F – 361.5°F. Refer to Figure 44 for the plots.

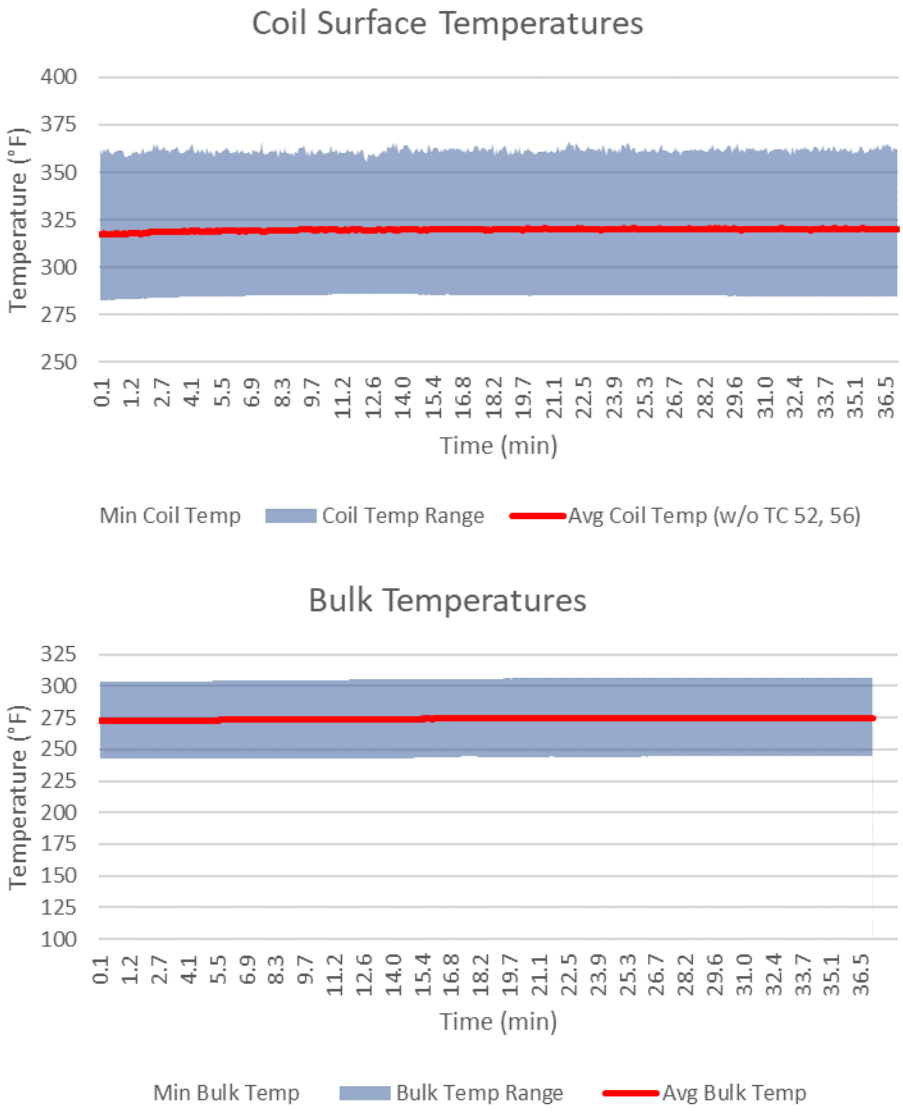

Figure 44: Peanut oil and heat exchanger surface temperatures during part 2 of peanut oil testing.

The external heat rejection loop was operating at maximum capacity with peanut oil flow rates of ~0.23 GPM. The combined average peanut oil temperature and heat exchanger surface temperature for parts 1 and 2 of testing were 272.8°F and 313.8°F, respectively. A graphical representation of the coolest and hottest regions on the heat exchanger surface along the flow path are shown in

Figure 45.

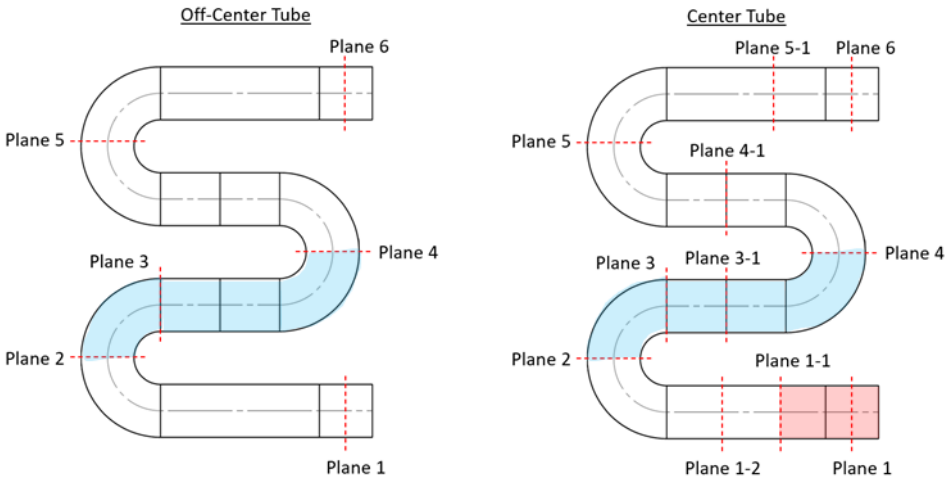

Figure 45: Hottest and coolest regions on center and off-center coils during peanut oil test.

The red shading in the figure highlights the hottest zone for both heat exchangers overall from the averages results of part 1 and 2 of testing with peanut oil. No red shading was applied to the off-center coil since there was no distinct region of elevated surface temperatures. One reason for this is the lack of surface thermocouple probes as compared to the center coil, which had an additional five thermocouples attached on the straight sections of the coil. As can be seen in the figure, the hottest surface temperatures overall were captured in the first 4 inches of flow path for the center coil. For both the center and off-center coils, the coolest region was found to occur between the middle of the first and second bends (11 – 22 inches along flow path). The lowest average surface temperature overall was captured at Plane 3-1 on the center coil, although this was the result of only one thermocouple measurement as compared to the planes coinciding with the middle of the coil bends, which averaged the temperatures of four thermocouples. The average heat exchanger surface thermocouple measurements as a function of flow path along the heat exchanger for both center and off-center coils are shown in Figure 46.

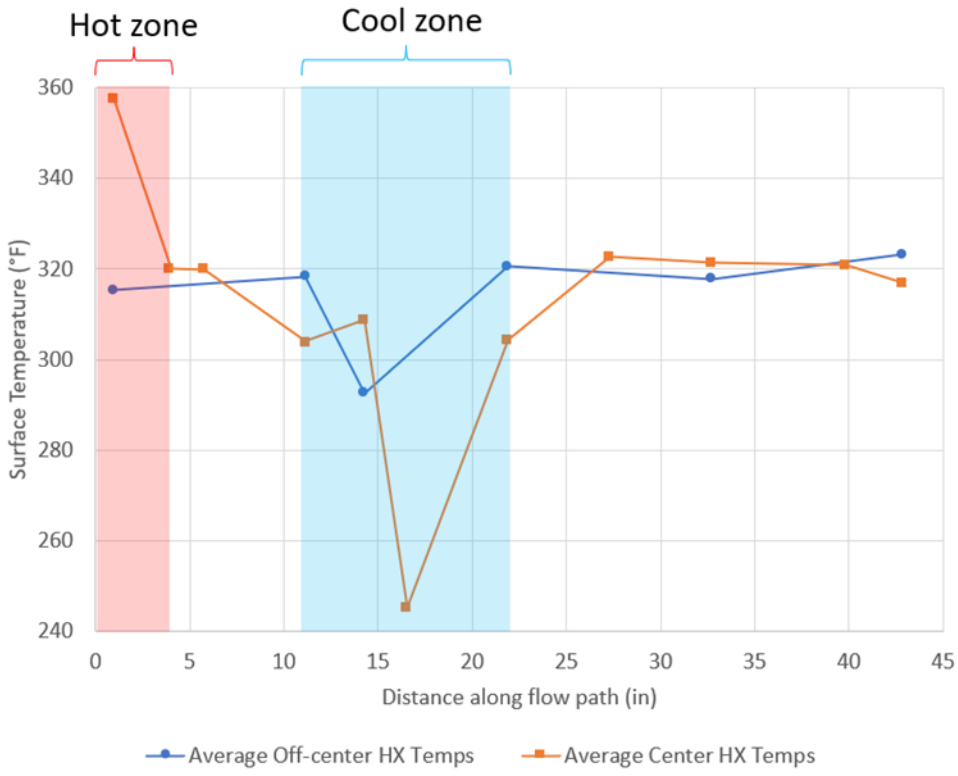

Figure 46: Heat exchanger surface thermocouple measurements along flow path for center and off-center coils.

A detailed breakdown of the average heat exchanger surface thermocouple measurements for the oil test at each cross-sectional plane as depicted in Figure 45 are shown in Table 11.

Analysis of Heat Transfer Coefficient

An analysis of the average heat exchanger heat transfer coefficient was performed using the average peanut oil and heat exchanger surface temperatures. A schematic depicting the average temperature stratification in the vat, the peanut oil inlet and outlet temperatures, and the average heat exchanger surface temperature are shown in Figure 47. The overall average peanut oil temperature in the vat was 272.8°F, which in combination with the average heat exchanger surface temperature was used to determine an average film temperature of 293.3°F. Using the peanut oil property equations presented in Figure 48, the characteristic properties of the peanut oil were calculated as follows:

- Thermal conductivity = 0.35 W/m*K
- Density = 835.1 kg/m^3
- Specific heat capacity = 2.83 KJ/kg*K
- Dynamic viscosity = 0.0046 Pa*s
- Kinematic viscosity = 5.6 x 10^{-6} m^2/s

The Prandtl number was calculated to be 30.7 and the coefficient of volume expansion was assumed to be that of olive oil, which is 0.0007 K^{-1}. From the nature of the heat exchanger geometry and the flow regime of the peanut oil, the heat transfer mechanism was assumed to be best characterized by natural convection over a horizontal cylinder. To confirm this assumption,

Table 11: Average heat exchanger thermocouple measurements for center and off-center coils at specified flow path distances

Plane	Distance (in)	Center HX Temp (°F)	Off-Center HX Temp (°F)
Plane 1	1.0	357.3	315.5
Plane 1-1	4.0	320.0	
Plane 1-2	5.8	319.9	
Plane 2	11.1	304.0	318.3
Plane 3	14.3	308.8	292.6
Plane 3-1	16.5	245.2	
Plane 4	21.9	304.3	320.5
Plane 4-1	27.3	322.7	
Plane 5	32.7	321.5	317.7
Plane 5-1	39.8	320.8	
Plane 6	42.8	317.0	323.2

the Rayleigh number needed to be calculated, which required the Grashof and Prandtl numbers. Using the heat exchanger tube diameter of 2 in. as the characteristic length, the Grashof number was calculated to be 6.6×10^5. Multiplying the Grashof and Prandtl numbers yielded a Rayleigh number of 2.0×10^7, which being $\leq 10^{12}$, indicated natural convection being the dominant heat transfer mechanism rather than forced convection. Therefore, using a model for natural convection over a horizontal cylinder, the Nusselt number was calculated to be 46.3, which yielded a heat transfer coefficient of 315 W/m^2*K. More detail on the heat transfer analysis is shown in the appendix.

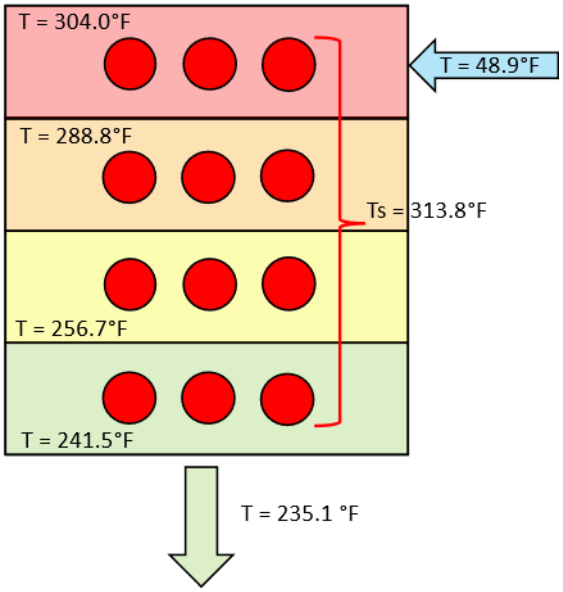

Figure 47: Average temperatures from part 1 and part 2 of testing including oil inlet, outlet and stratification and heat exchanger surface temperature.

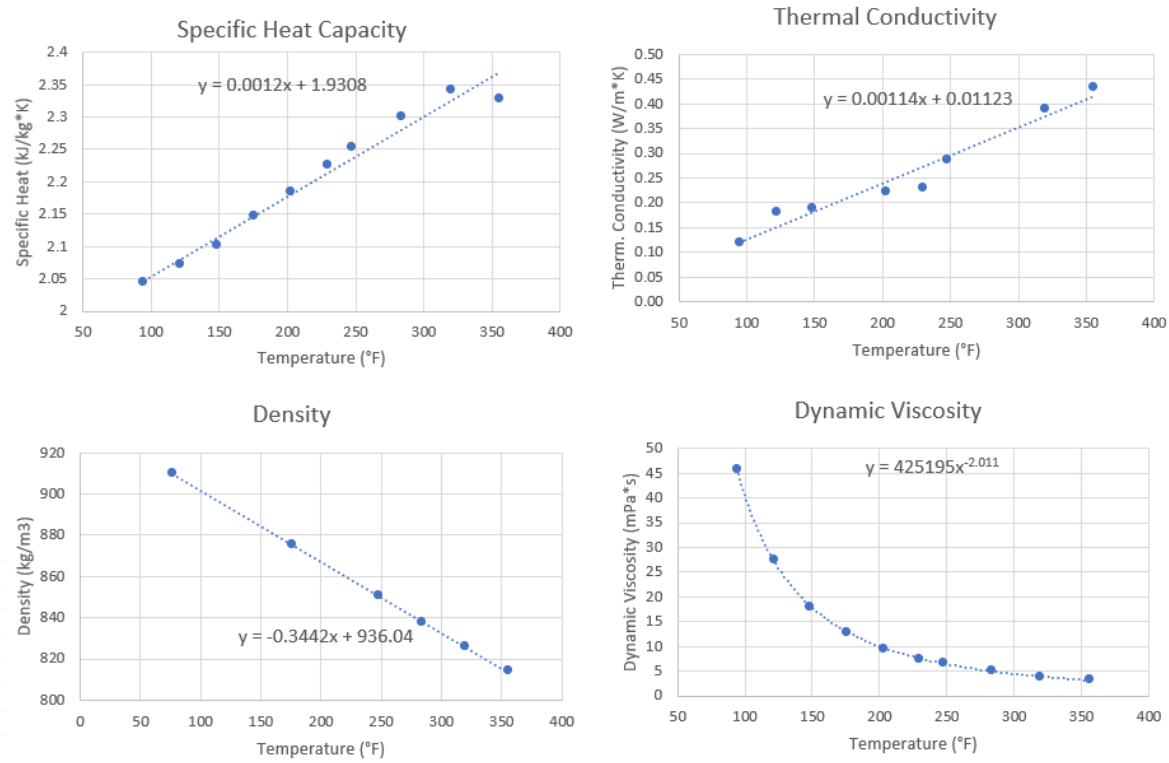

Figure 48: Peanut oil properties used for heat transfer calculations[18]

[18] Source: https://www.tandfonline.com/doi/pdf/10.1080/10942910701586273

CFD Analysis

Due to the use of a surrogate heat transfer fluid, calibrated simulation was necessary to extend to operation with an ionic liquid desiccant and a CFD model was developed of the mock desorber to allow for further parametric analyses. Similar to Task 1, ANSYS Fluent was used as the simulation environment. An initial model was created based on the experimental results from the peanut oil test. Although multiple simulations were performed, only the final simulations are presented in this section. It is important to note that the CFD models did not include multiphase flow or heat transfer with respect to water being boiled off. The simulations presented are strictly single phase with the heat transfer fluid domain initially being modeled as pure peanut oil and then as a 95% ionic liquid solution.

Peanut Oil Simulation

The first set of CFD simulations were developed based on the peanut oil experiment described in the previous sections. The intent behind these simulations was to develop a working model that could reliably predict the location of hot spots on the heat exchanger coil surface, using the experimental results as a reference point. To achieve the best possible results efficiently, a 3D, symmetrical, multi-domain model representing the same dimensions of the actual mock desorber was generated, as shown in Figure 49. The model included both the flue gas (combustion is not directly modeled) and peanut oil fluid components and were developed based on the final CAD models for the desorber and include the burner, ceramic insert, and true vat dimensions.

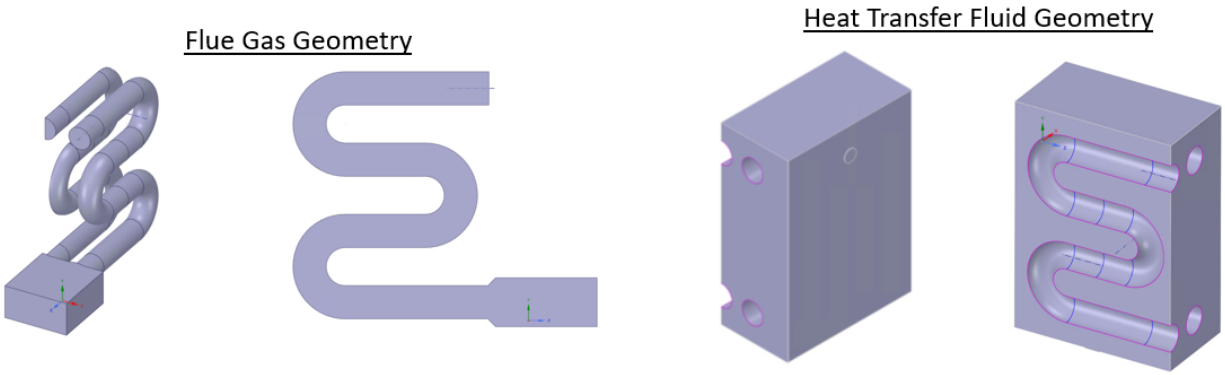

Figure 49: Model geometry for flue gas and heat transfer fluid.

Using the above geometry, a mesh was generated with tetrahedral elements measuring up to 0.005 m for the peanut oil domain and 0.003 m for the flue gas domain, as shown in Figure 50. The maximum element size for the flue gas domain was reduced to better resolve the higher temperature, higher velocity flow inside the heat exchanger, as opposed to the peanut oil in the vat, external to the heat exchanger. To better resolve the heat exchanger surface hot spots, five inflation layers were added. The total nodes and elements in the mesh were 834,324 and 3,333,043, respectively.

The model parameters for the simulation were set as follows:

Flue Gas Inlet:

- Method: Mass Flow Inlet

- Mass Flow Rate (kg/s): 0.001369 (based on 4.75 kW operating condition)
- Hydraulic Diameter: 0.0393 m
- Temperature: 1579 K
- Wet Flue Gas Species Concentrations:
    - O_2: 8.85%
    - CO_2: 5.62%
    - H_2O: 10.81%
    - N_2: 73.77%
    - Ar: 0.95%

Flue gas outlet:

- Method: Pressure Outlet
- Gauge Pressure: 0 Pa
- Hydraulic Diameter: 0.0393 m
- Temperature: 422.7 K
- Species: Same as inlet

Peanut Oil Inlet

- Method: Mass Flow Inlet
- Mass Flow Rate (kg/s): 0.0035 (based on 0.23 GPM)
- Hydraulic diameter: 0.0254 m
- Temperature: 282.6 K

Peanut Oil Outlet:

- Method: Pressure Outlet
- Gauge Pressure: 3583.3 Pa
- Hydraulic diameter: 0.0254 m
- Temperature: 386K

Peanut Oil Surface:

- Method: Pressure outlet
- Gauge Pressure: 0 Pa
- Hydraulic diameter: 0.2169 m
- Temperature: 437.3 K (assumed from averaged peanut oil part 1 and 2 test results)

Flue Gas-Peanut Oil Interface:

- Method: Wall
- Type: Coupled
- Thickness: 0.001588 m

Peanut Oil Vat Wall:

- Condition: No slip
- Heat Flux: -232 W/m^2

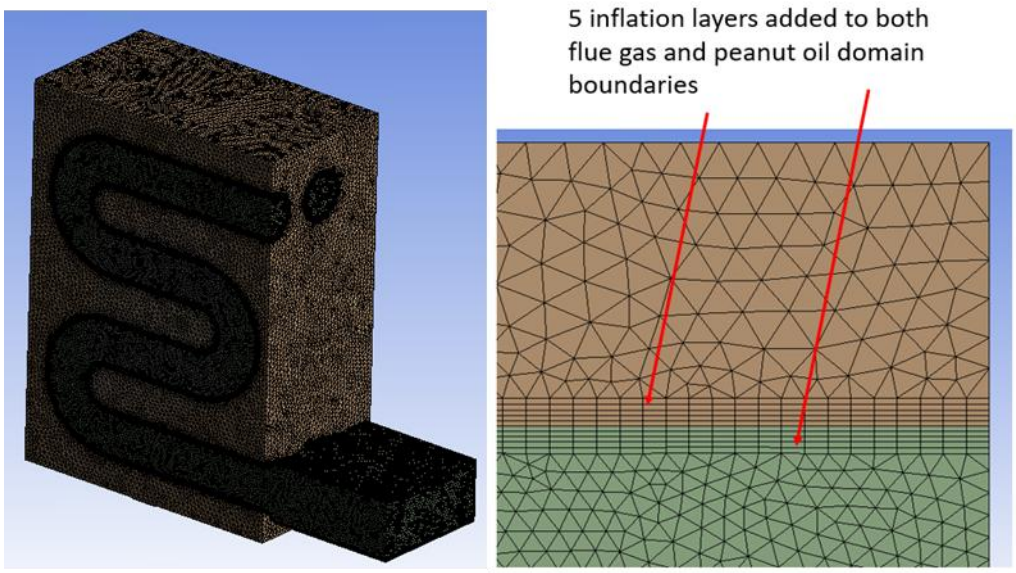

Figure 50: Isometric view of overall mesh and closeup of inflation layers added to flue gas and peanut oil domains at interface.

A solution for the model was obtained with a pseudo-steady state approach, with an initial steady state calculation of 1,000 iterations followed by a transient calculation of 1,000 time steps with time step durations of 0.01 s, for a total run time of 10 s. The resulting heat exchanger surface temperature contour was mapped on the mesh as shown in Figure 51. Multiple views of the symmetrical half of the heat exchanger are presented in the figure to highlight the hot spot locations. As can be seen in the isometric views, the highest surface temperatures occurred in three primary locations: close to the inlet at the top of the straight run of pipe, the second half of the first bend, and the center of the second bend. A hot spot also appears at the center of the third bend for the center coil. The side and bottom view also show the coldest part of the coil, which is the bottom of the straight run of pipe leading to the first bend.

Surface probes were also placed on the CFD model to track the temperatures at the intended location for the thermocouples as presented in Figure 35. As was discussed in a previous section, the process of spot welding the thermocouples to the desired locations on the heat exchanger surface was challenging due to limited access inside the vat. Therefore, the true locations of the thermocouple probes are not as precisely positioned as those in the CFD model, and have a maximum deviation from the desired location of approximately 0.25 in (6.35 mm). This partly explains some of the deviation in temperature measurements that can be seen in the charts presented in Figure 52. As shown in Figure 51, the hot spots are highly concentrated, and even a small deviation in thermocouple placement can drastically change the outcome of the measurement. Overall, the average deviation between the experimentally measured temperatures and the simulated temperatures was 7%. The

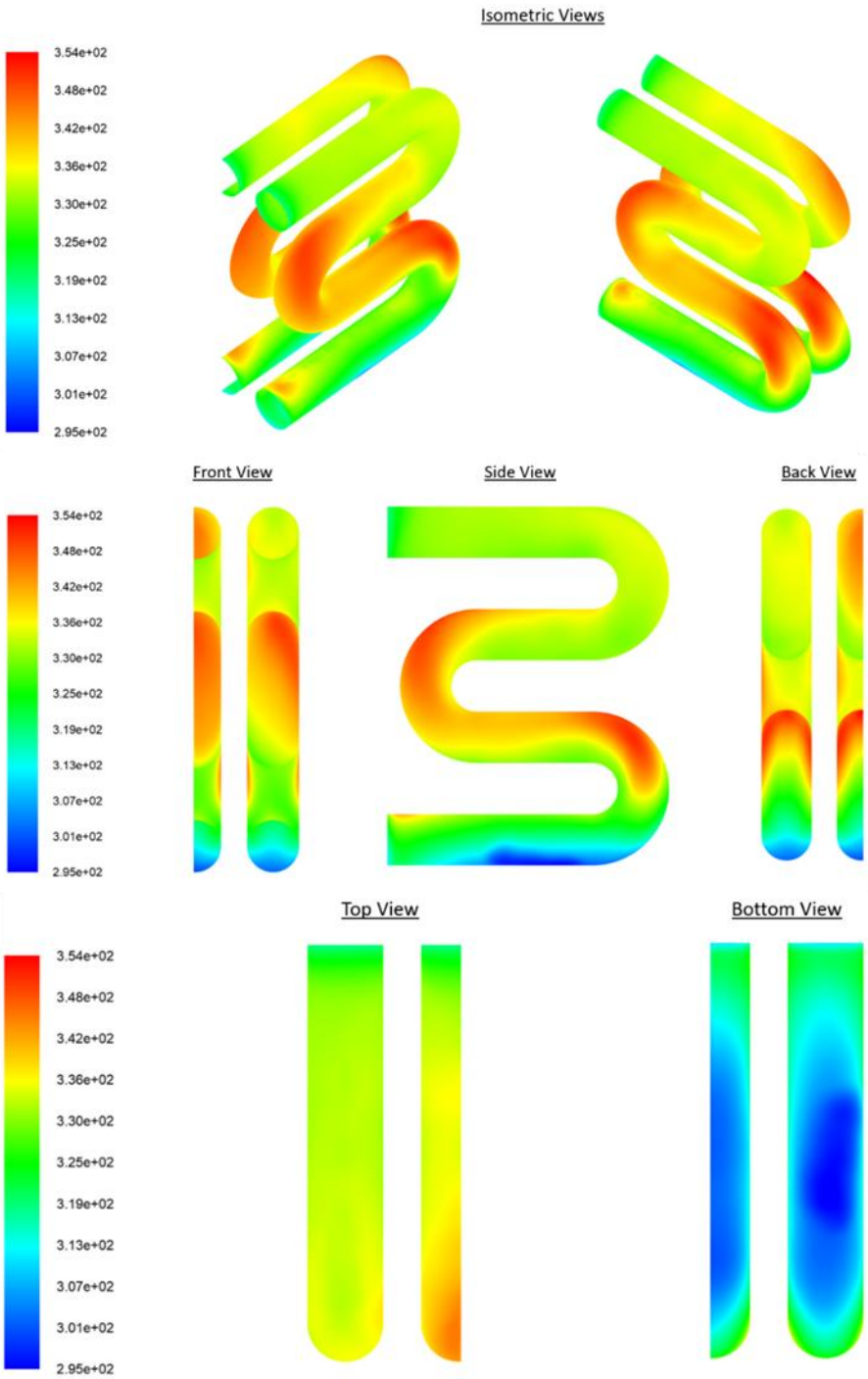

Figure 51: Surface temperature contours of center and off-center heat exchanger coils based on a simulated firing rate of 4.8 kW and peanut oil flow rate of 0.23 GPM. Temperature scale is in °F.

largest temperature deviations are highlighted in the chart in red. These deviations showed an overestimation in simulated temperature at the outlet of the first bend in the off-center coil and in the center of the second leg and center of the second bend of the center coil. The deviation in thermocouple # 48 was due to the probe being welded to the wall of the vat, due to difficulty reaching the bottom of the inlet tube of the center coil.

Off-Center Tube TC Temperatures (°F)				
TC	Experiment	CFD	ΔT	% Error
24	333.3	346.2	12.9	4%
25	310.9	337.9	27.0	8%
26	296.1	329.1	33.0	10%
27	321.5	335.6	14.1	4%
28	332.7	332.9	0.2	0%
29	337.2	346.9	9.7	3%
30	291.9	333.3	41.4	12%
31	311.5	347.9	36.4	10%
32	333.5	348.5	15.0	4%
33	285.0	339.4	54.4	16%
34	266.0	331.4	65.4	20%
35	285.8	338.7	52.9	16%
36	313.6	335.4	21.8	6%
37	335.4	344.5	9.1	3%
38	313.1	343.8	30.7	9%
39	319.9	337.4	17.5	5%
40	327.4	335.5	8.2	2%
41	331.3	333.6	2.3	1%
42	305.0	335.3	30.4	9%
43	307.2	337.0	29.8	9%
44	325.3	329.4	4.1	1%
45	325.4	330.0	4.6	1%
46	318.8	329.7	10.8	3%

Center Tube TC Temperatures (°F)				
TC	Experiment	CFD	ΔT	% Error
47	361.5	348.6	12.9	4%
48	265.7	328.6	62.9	19%
49	353.2	335.6	17.6	5%
50	320.0	330.5	10.5	3%
51	319.9	329.0	9.1	3%
52	n/a	332.7		
53	301.3	335.5	34.2	10%
54	313.8	347.8	34.0	10%
55	318.0	351.7	33.7	10%
56	n/a	329.8		
57	325.6	339.8	14.2	4%
58	245.2	336.6	91.4	27%
59	312.5	338.2	25.8	8%
60	284.9	345.4	60.6	18%
61	323.9	343.4	19.5	6%
62	322.7	335.6	12.9	4%
63	321.4	342.4	21.0	6%
64	n/a	333.1		
65	322.7	334.7	12.0	4%
66	321.9	332.9	11.1	3%
67	316.8	332.5	15.7	5%
68	317.1	330.8	13.7	4%

Off-Center Tube Error		Center Tube Error		**Total Error**	
Max:	20%	Max:	27%	**Max:**	**27%**
Min:	0%	Min:	3%	**Min:**	**0%**
Average:	7%	Average:	7%	**Average:**	**7%**

Figure 52: Experimental vs simulated heat exchanger surface thermocouple probe temperatures for firing rate of 4.8 kW and peanut oil flow rate of 0.23 GPM

Ionic Liquid Simulation

Using the same geometry shown in Figure 49, a simulation was also performed using properties of ionic liquid provided by UF. The same tetrahedral-style mesh approach was used for this model, except that the maximum ionic liquid element size was 0.0075 m and the maximum flue gas element size was 0.005 m. To improve the resolution of the temperature contour on the heat exchanger surface, a more refined inflation treatment was applied to the flue gas and ionic liquid interface. Rather than five inflations layers, ten layers were used with a growth rate of 1.1. Refer to Figure 53 for a closeup of the mesh. Some of the model parameters were upgraded to allow for the simulation of the full 10 kW firing rate with the ionic liquid flow rate of 4 LPM. The updated model parameters are as follows:

Flue gas inlet:

- Method: Mass Flow Inlet
- Mass Flow Rate (kg/s): 0.002027 (based on 10 kW operating condition. Excess air ratio has also been reduced to 25% for a more representative emissions profile)
- Hydraulic Diameter: 0.0393 m
- Temperature: 1997 K
- Wet Flue Gas Species Concentrations: (Based on theoretical calculation with excess air ratio of 25% - not based on experimental emissions testing)
    - O_2: 3.87%

- CO_2: 7.93%
- H_2O: 15.24%
- N_2: 72.04%
- Ar: 0.92%

Ionic Liquid Inlet:

- Method: Mass Flow Inlet
- Mass Flow Rate (kg/s): 0.0306 (based on 4 LPM)
- Hydraulic diameter: 0.0254 m
- Temperature: 282.6 K

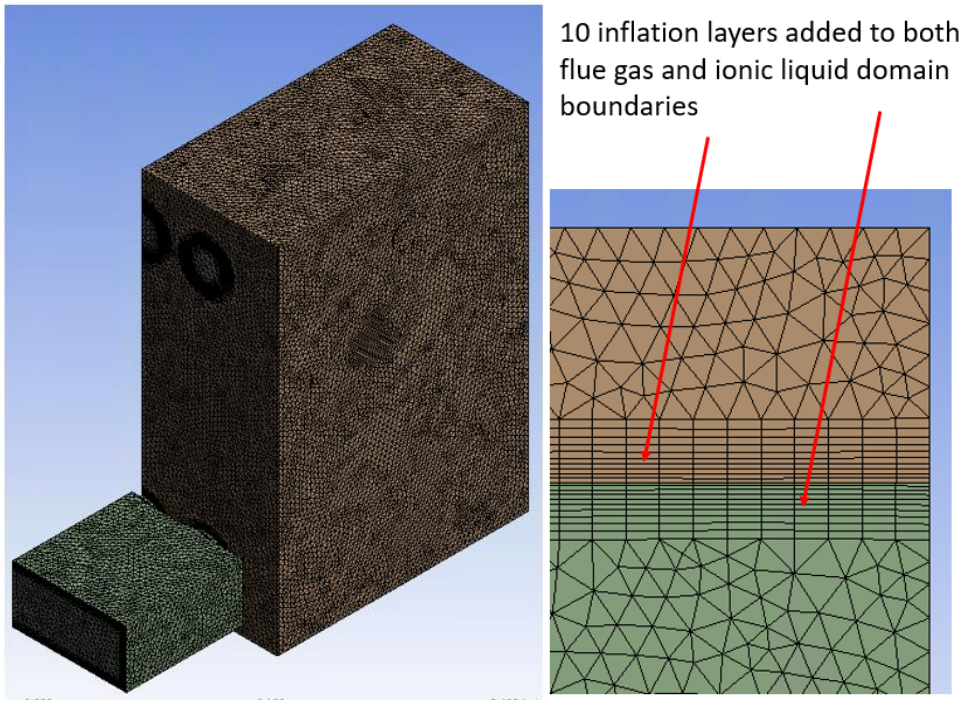

Figure 53: Isometric view of overall mesh and closeup of inflation layers added to flue gas/ionic liquid interface.

Similar to the peanut oil simulation, a solution for the model was obtained using an initial steady state calculation of 1,000 iterations followed by a transient calculation of 1,000 time-steps with time step durations of 0.01 s, for a total run time of 10 s. The resulting heat exchanger surface temperature contour was mapped on the mesh as shown in Figure 54. As can be seen in the figure, the location of the hot spots differs significantly from the previous peanut oil simulation performed at a firing rate of 4.8 kW and oil flow rate of 0.23 GPM (equivalent to 0.87 LPM). Generally, the hot spots have migrated further downstream, with minimal hot spots visible at the inlet pipe and a smaller hot spot on the first bend. On the surface of the second bend of the two coils, the hot spot seems to be similar to that of the previous simulation. However, the most obvious deviation from the previous simulation is seen at the second half of the third bend and top of the outlet pipe for both coils. This same region in the previous simulation was shown to have moderate temperatures that were in the middle of the temperature scale. The cool zone does persist in the same region for the ionic liquid simulation as for the peanut oil simulation.

One explanation for the difference in hot spot location is the higher flue gas velocity, and therefore shorter residence time, which allows the hot spots to be pushed further downstream the flow path.

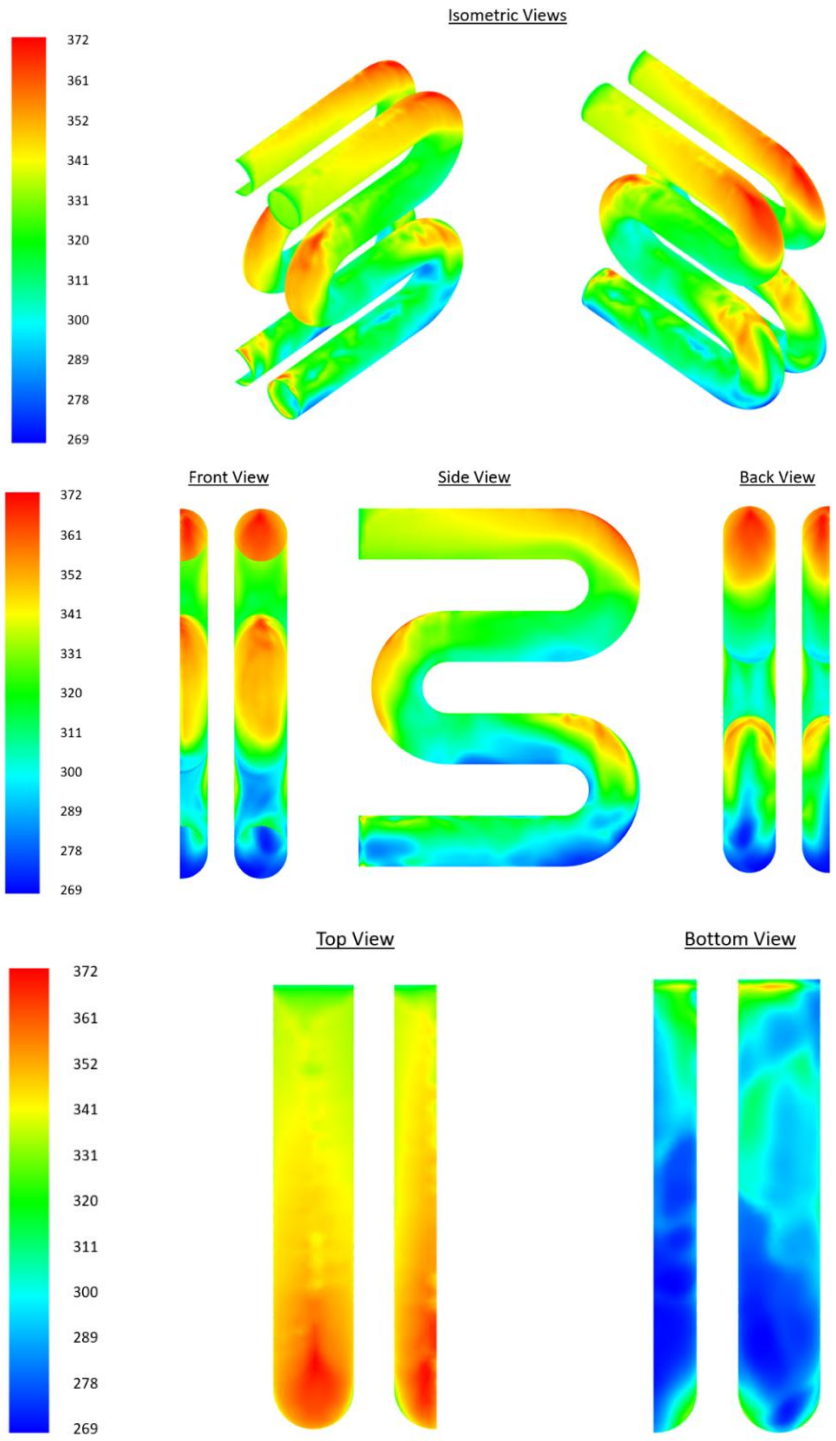

Figure 54: Surface temperature contours of center and off-center heat exchanger coils based on a simulated firing rate of 10 kW and ionic liquid flow rate of 4 LPM. Temperature scale is in °F.

Steam-powered Desorber

The design of the steam-powered desorber is inspired by our fundamental studies, in which we developed surface features that significantly enhance the desorption rate at low surface temperatures. This approach reduces both the size of the desorber and the temperature required to drive the desorption process. Figure 55 summarizes these findings: the flow of ionic liquid on a smooth vertical surface forms streaks of liquid sliding down the surface (Figure 55a) rather than a continuous thin film. In contrast, the structured surface in Figure 55b spreads the ionic liquid uniformly across the entire surface by subjecting the fluid to asymmetric flow resistance. Finally, Figure 55c presents test results demonstrating a threefold increase in desorption rate compared with prior studies.

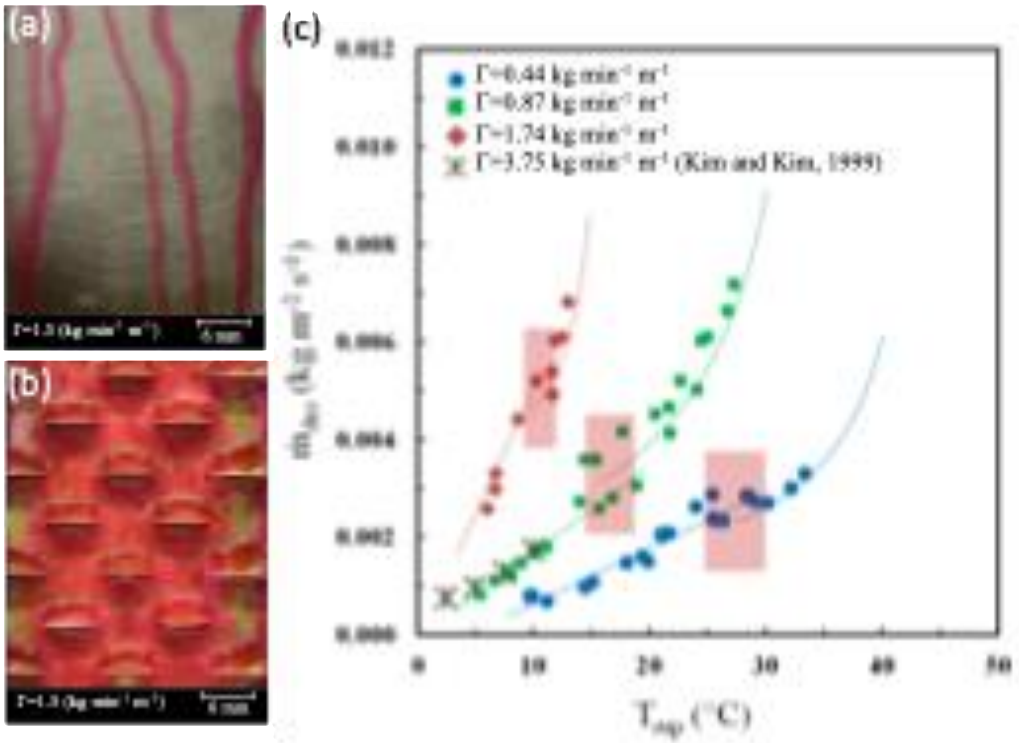

Figure 55: Colored ionic liquid flow over a smooth vertical plate (a) and a plate with surface structures (b) showing significant improvement in liquid distribution over the entire surface resulting in 3x increase in desorption rate relative to previous work.

The lessons learned from these studies were applied to the design of the desorber for the 1000 CFM system. The desorber is designed to deliver a capacity of 10 kW under the system's nominal design conditions. Figure 56 illustrates the desorber at various stages of preparation: Figure 56a shows a 3D model consisting of three two-sided panels over which the ionic liquid flows, Figure 56b presents the fabricated desorber produced by high-temperature vacuum brazing of both flat and formed metal sheets followed by final electroplating of the assembly, and Figure 56c depicts the completed desorber undergoing ionic liquid flow test.

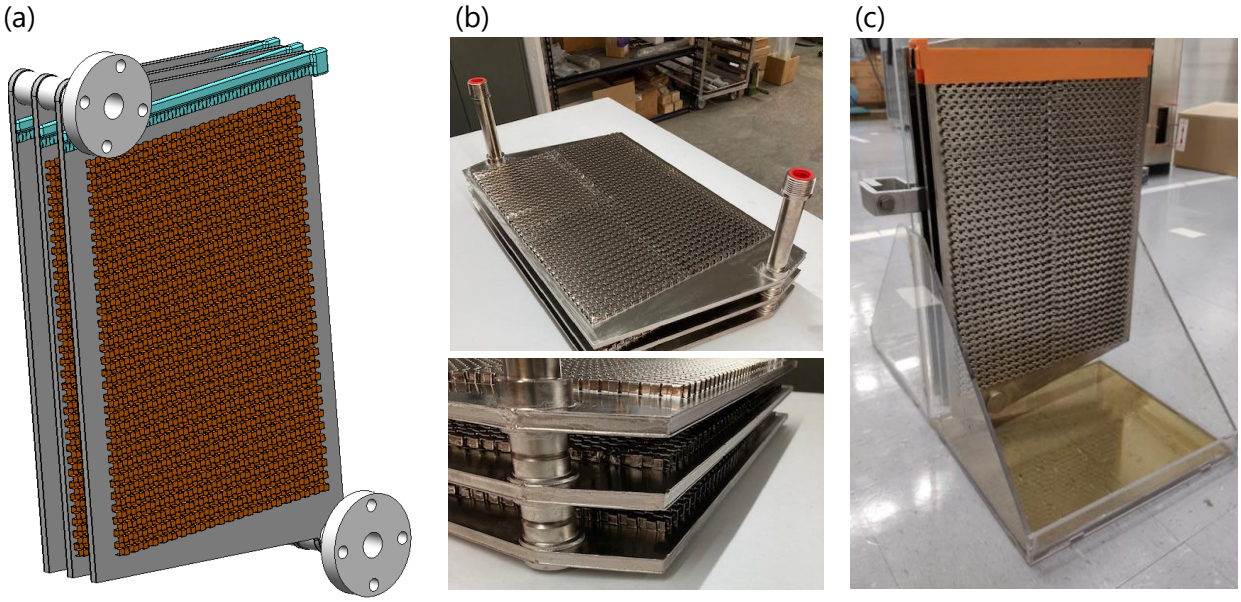

Figure 56: Steam-powered falling film desorber 3D design (a), manufactured (b), and installed within the ionic liquid flow test setup (c).

Desorber and Condenser Assembly

The condenser section of the system's hot side was fabricated by forming metal sheets followed by vacuum brazing. Figure 57 presents both a schematic cross-section of the integrated desorber–condenser assembly and the manufactured full-scale condenser.

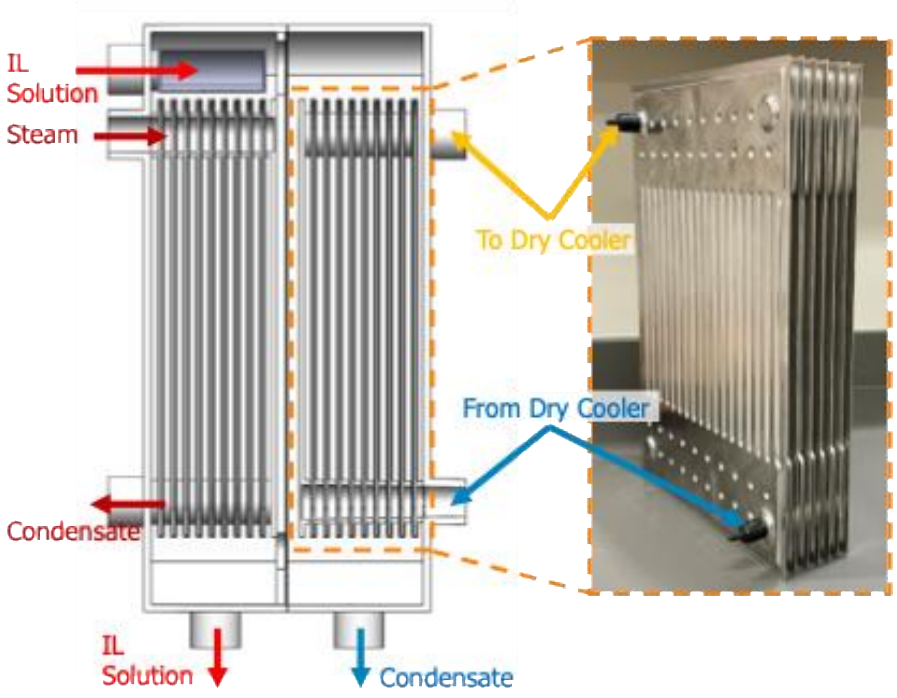

Figure 57: Multiplate condenser of the semi-open system built through forming and high temperature vacuum brazing process.

The hot-side models, including the condenser and desorber, were validated using a benchtop test suite designed to confirm both the sizing and operation of these components. Figure 58 shows the final test configuration, which consisted of a seven-panel double-sided condenser paired with a three-panel double-sided desorber. The multi-panel desorber used in these tests was electrically heated. The results demonstrated the capability of the assembly to exceed 5 kW of capacity at low solution flow rates.

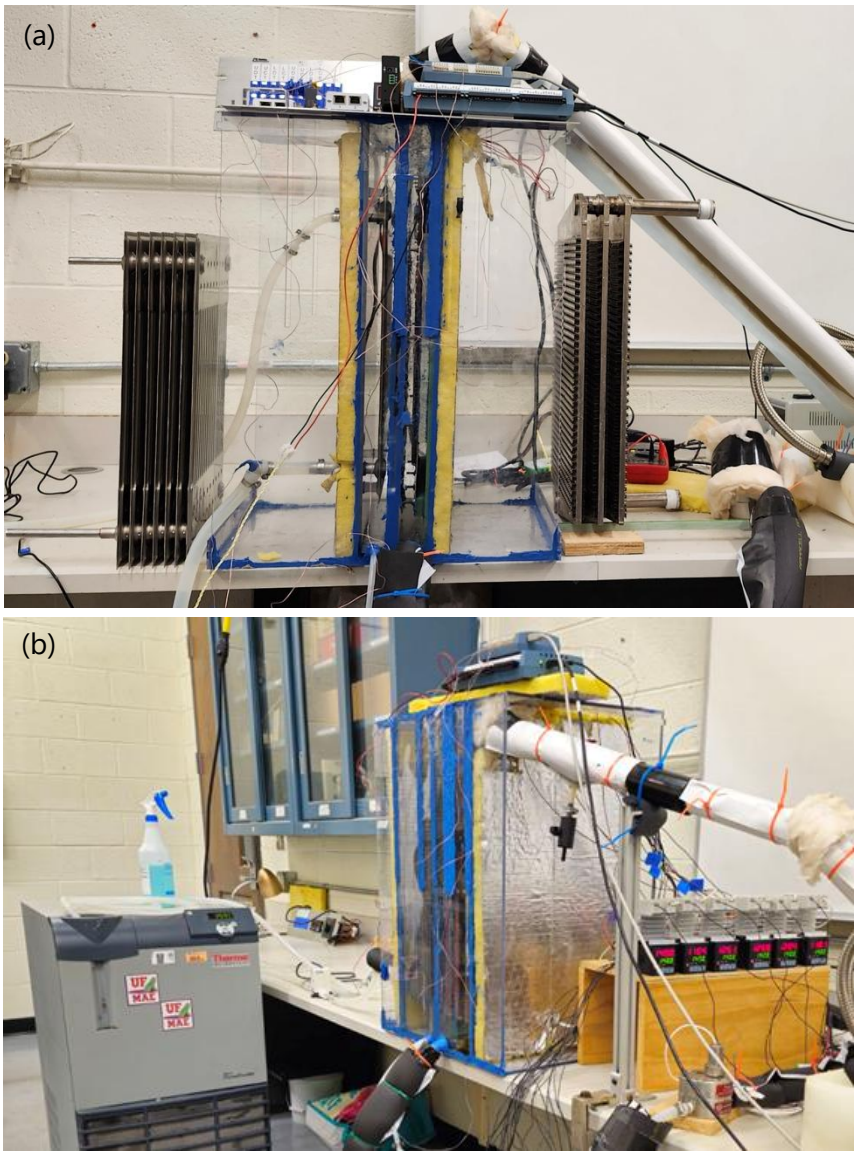

Figure 58: Multi-panel condenser (7 panel) and desorber (3 panel) test setup before installation of the condenser and desorber within the setup (a) and after installation of the condenser and desorber and during testing (b).

This configuration also enabled experimental evaluation of the desorbed steam flow distribution within the assembly predicted by our COMSOL model, which had been used to establish the appropriate inter-panel spacing. As shown in Figure 59, visual inspection confirmed that the desorbed steam flow was flowing across all panels with a close velocity, supporting the model predictions.

Figure 59: An image of the bottom of the condenser during testing showing air with some moisture content returning to the desorber.

To test the desorber-condenser assembly at the design capacity of 10 kW, we developed a 15 kW steam generator and associated controller in our laboratory. Figure 60 shows a diagram of the system. Figure 61 illustrates the completed system, with Figure 61a showing the blueprint and Figure 61b presenting the actual system photograph. The water supply/steam loop was designed, the required components were installed, and the assembly was successfully sealed and commissioned. The final configuration of the steam loop included the 15 kW steam generator, steam flow meter, steam trap, and associated plumbing. Additional pressure and temperature sensors were incorporated to ensure that the test loop replicated the testing and heat balance measurement requirements of ANSI/ASHRAE Standard 139-2022. Following reassembly with an improved pipe/joint sealant, the system operated reliably without leakage and was capable of steady-state operation under constant load.

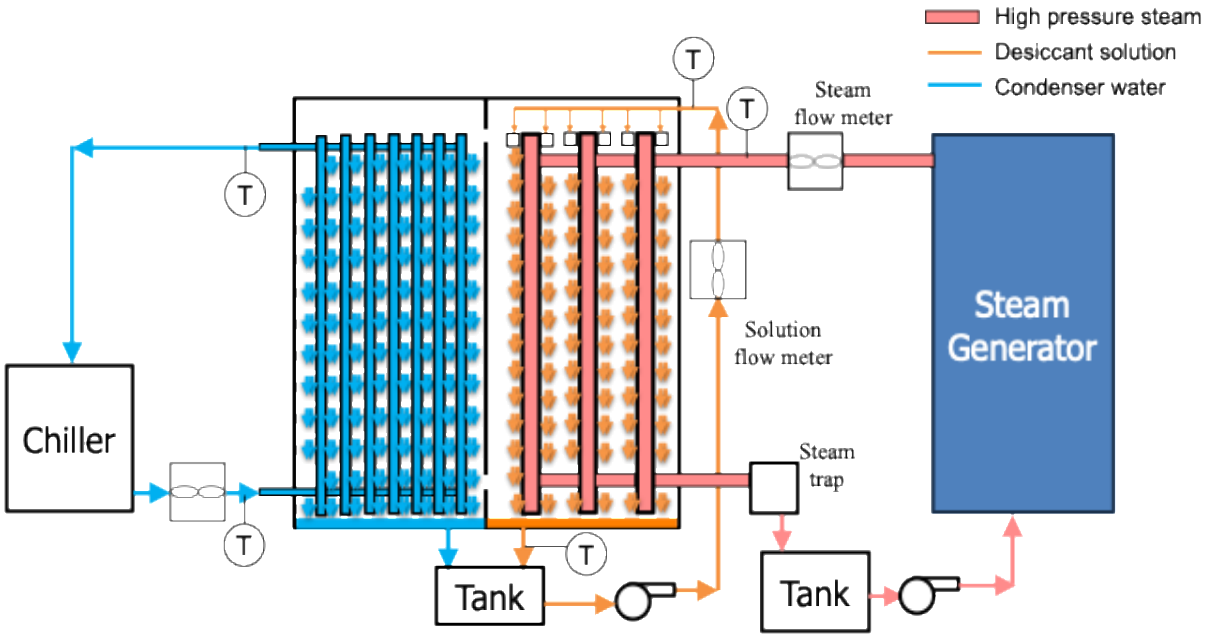

Figure 60: Diagram of the desorber-condenser assembly and integration with the steam generation system.

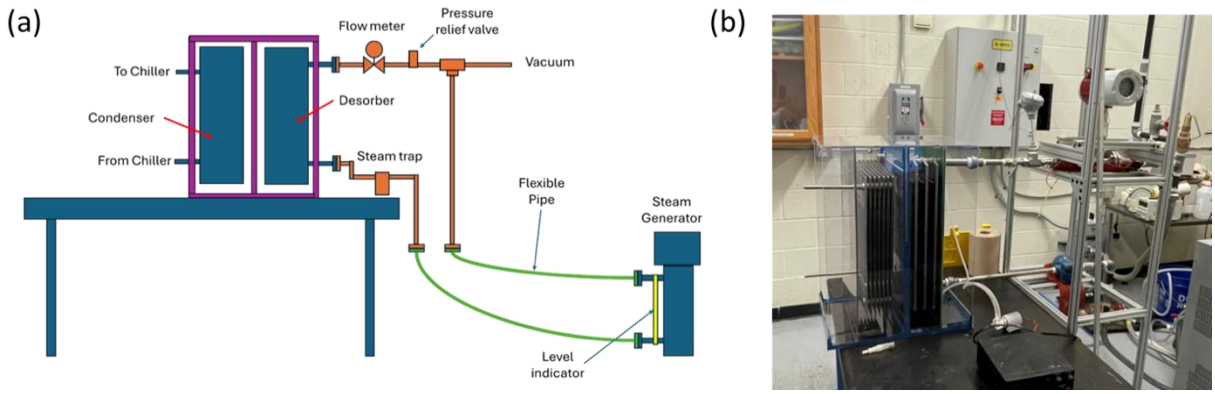

Figure 61: System blueprint (a) and actual picture of the system (b).

The initial operational tests employed a three-panel desorber to validate loop performance, followed by integration of the seven-panel condenser into the hot-side test chamber. These tests confirmed the ability of the steam loop to support the operation of the integrated steam condenser–desorber module and provided insight into loop startup procedures, including the role of the steam trap in stable operation. The testing also demonstrated the ability of the GTI steam flow meter to accurately measure steam flow at the desired rates and confirmed the feasibility of capturing and reusing steam condensate. To support further testing, we fabricated a set of custom test manifolds for the legacy desorber configuration, which proved effective in distributing flow within the test suite.

Absorber

We completed the fabrication of two 50-panel prototype absorber modules to support controls testing within the operational prototype system. These modules (Figure 62) incorporated the newly developed injection-molded absorber panel together with our redesigned manifold. Unlike the proof-of-concept dryer absorber, the new manifold design positioned the solution inlet port at the center of the top header to improve flow distribution. Assembly of the modules led to minor design modifications that simplified fabrication and improved assembly for future builds. The modules were installed in the operational prototype unit (Figure 62), where they supported flow distribution and controls testing. The results of these tests confirmed the viability of the new manifold design and provided the basis for completing the full 200-panel absorber design.

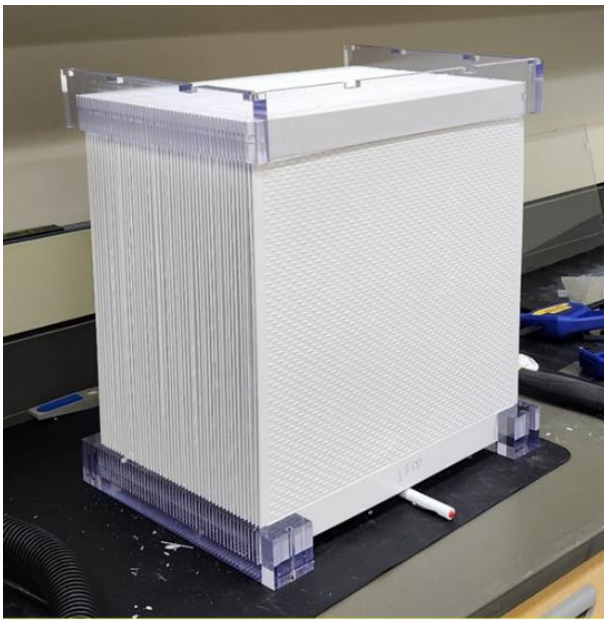

Figure 62: Fifty panels absorber module fabricated from ABS through injection molding.

Design and Building of the System Test Facility

We completed the design, fabrication, and integration of a full-scale 1000 CFM thermally driven Dedicated Outdoor Air System (DOAS) semi-open absorption testing system. The system was developed to evaluate the performance of our ionic liquid–based cycle under representative operating conditions and to validate the viability of the technology at the commercial scale. The steam generator, hydronic loops, and air-handling infrastructure were designed and assembled to provide the necessary boundary conditions for testing. Instrumentation for flow, temperature, pressure, humidity, and power measurement was installed to enable both system-level performance evaluation and component-level analysis of the absorber and desorber.

Figure 63 presents the schematic diagram of the packaged unit, while Figure 64 shows the completed system. The prototype was fabricated, commissioned, and installed in the test facility to support flow distribution, controls development, and performance evaluation. Testing of the unit is planned across a range of operating conditions to determine the coefficient of performance (COP), cooling capacity, and latent effectiveness, while also verifying the performance of key innovations such as the membrane absorber, desorber, and advanced manifold design.

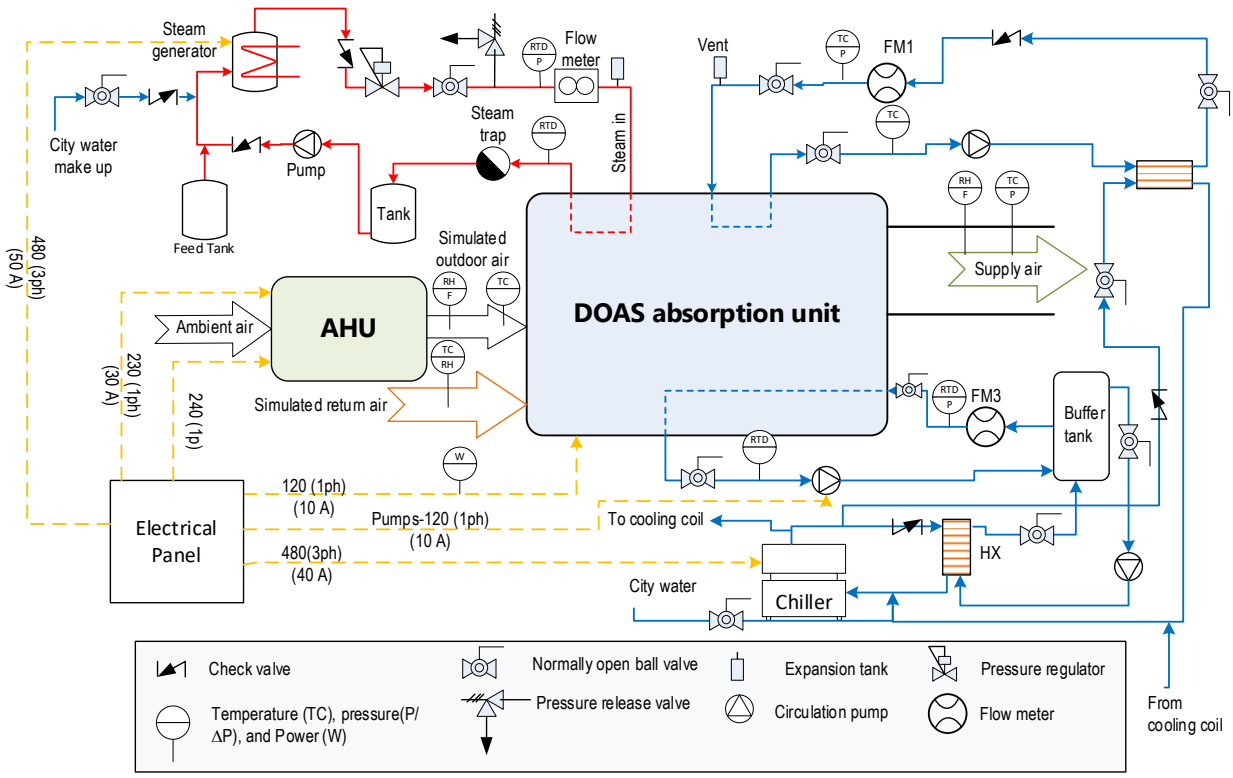

Figure 63: Diagram of the 1000 CFM test system.

Figure 64: Photograph of the 1000 CFM test system.

Data Analysis

Recorded Datapoints

The following data points will be measured and reported for each testing point. If test data is not logical or consistent, the setup and instrumentation will be revised, and the test will be repeated.

- **Air Conditions:** Dry-bulb temperature, flow rate, relative humidity, and barometric pressure around the system.
- **Steam Conditions:** The temperatures, pressure, and flow rate of steam.
- **Power Usage:** Power (W) and Energy (kWh) consumed by the steam generator, the absorption unit, and chillers.

Data Sampling Rate and Test Run Data Collection Duration

A data acquisition system shall record all data continuously throughout the data collection period. A maximum data sample interval of 5 seconds and minimum data collection period of at least 15 minutes shall be used for each steady state evaluation.

Calculated Values

The performance of the absorption unit will be evaluated at the system and component level based on the testing points mentioned in this test plan.

1. Energy and mass balance:

During the shake-down (commissioning) testing, the energy and mass balance across the system should be verified using the following equations.

$$(\dot{m}_o h_{air,o} + \dot{m}_{air,r} h_r - \dot{m}_{air,s} h_s) + \dot{m}_{st} \left(h_{st,in} - h_{st,out}\right) = \dot{m}_{w,cond} C_{p,w} \, \Delta T_{w,cond} + \dot{m}_{w,cc} C_{p,w} \, \Delta T_{w,cc} + \dot{m}_d h_f \quad (1)$$

$$\dot{m}_o \omega_{air,o} + \dot{m}_r \omega_{air,r} - \dot{m}_s \omega_{air,s} = \dot{m}_{water,c} \quad (2)$$

where

$\dot{m}_o$	Simulated outdoor air flow rate, kg/s.
$\dot{m}_r$	Simulated return air flow rate, kg/s.
$\dot{m}_s$	Simulated supply air flow rate, kg/s.
h_o	Simulated outdoor specific enthalpy, kJ/kg.
h_r	Simulated return specific enthalpy, kJ/kg.
h_s	Simulated supply specific enthalpy, kJ/kg.
$\dot{m}_{st}$	Steam mass flow rate, kg/s.
$h_{st,in}$	Specific enthalpy of inlet steam, kJ/kg.

$h_{st,out}$	Specific enthalpy of outlet steam, kJ/kg.
$\Delta T_{w,cond}$	Temperature difference of water across the condenser, °C.
$\Delta T_{w,cc}$	Temperature difference of water across the cooling coil, °C.
ω_{air}	Humidity ratio of air, g of water vapor/g of dry air.
$\dot{m}_{water,c}$	Water condensed over the cooling coil, kg/s.

Note that the mass balance across the absorber and desorber could be calculated if the packaged unit shipped to GTI Energy has sensors to measure the air humidity ratio and solution concentration across the absorber.

The specific enthalpy and humidity ratio (moisture content) of air will be estimated from the dry-bulb temperature and humidity using the database of Engineering Equation Solver (EES).

2. Electrical Energy Input:

Electricity consumption of the absorption unit and steam generator will be directly measured using a wattnode. Each test point will be evaluated and converted to power and energy demand for the given test periods.

3. Cooling Energy Output:

The useful energy output (unit's cooling capacity, sensible and latent heat) can be calculated from the enthalpy of the inlet and outlet air streams across the unit. Also, the moisture removal rate across the heat pump can be estimated. They will be calculated using the following equation:

$$\dot{Q}_{u,total} = \dot{m}_o h_o + \dot{m}_r h_r - \dot{m}_s h_s \quad (3)$$

$$MRR_{total} = \dot{m}_o \omega_o + \dot{m}_r \omega_r - \dot{m}_s \omega_s \quad (4)$$

The sensible cooling energy and sensible heat ratio can be estimated from the following equations:

$$\dot{Q}_{u,sensible} = \dot{m}_o C_{p,o} T_o + \dot{m}_r C_{p,r} T_r - \dot{m}_s C_{p,s} T_s \quad (5)$$

$$\dot{Q}_{u,latent} = \dot{Q}_{u,total} - \dot{Q}_{u,sensible} \quad (6)$$

$$SHR = \frac{\dot{Q}_{u,sensible}}{\dot{Q}_{u,total}} \quad (7)$$

where

$\dot{Q}_{u,total}$	Useful total cooling output energy, kW.
$\dot{Q}_{u,sensible}$	Useful sensible cooling output energy, kW.
C_p	Dry air specific heat capacity, kJ/kg.K.

4. Desorption Energy:

The energy required for the desorption process will be calculated by measuring the steam flow rate and temperatures across the desorber.

$$\dot{Q}_{in} = \dot{m}_{st}\left(h_{st,in} - h_{st,out}\right)$$

where

$\dot{Q}_{in}$ Inlet power to the desorber, kW.

5. Absorber Capacity

The capacity of the absorber can be estimated from the following equations:

$$\dot{Q}_{absorber} = \dot{m}_o(h_{in} - h_{out}) \quad (8)$$

$$MRR_{abs} = \dot{m}_{air}\left(\omega_{air,in} - \omega_{air,out}\right) \quad (9)$$

where

h_{in} Specific enthalpy of air entering the absorber, kJ/kg.

h_{out} Specific enthalpy of air exiting the absorber, kJ/kg.

The specific enthalpy of air exiting the absorber will be calculated from EES using the internal sensors provided by the UF, and therefore, the share of the absorber in the cooling energy can be calculated as follows:

$$\%Share = 100 \times \frac{\dot{Q}_{absorber}}{\dot{Q}_{u,total}} \quad (10)$$

$$\%ShareLatent = 100 \times \frac{\dot{Q}_{absorber}}{\dot{Q}_{u,latent}} \quad (11)$$

6. Efficiency:

- *System-level performance*

The Coefficient of Performance (COP) will be calculated for each test point when steady conditions are realized. The COP of the absorption system and the overall COP of the entire system are defined as:

$$COP_{HP} = \frac{\dot{Q}_u}{\dot{Q}_{in}} \quad (12)$$

$$COP_{overall} = \frac{\dot{Q}_u}{\sum \dot{E}_{in}} \quad (13)$$

$$MRR_{abs} = \dot{m}_{air}\left(\omega_{air,in} - \omega_{air,out}\right) \quad (14)$$

where

$\sum \dot{E}_{in}$ Inlet electrical energy used to drive the system, which is the electrical energy used to power the steam generator, the condenser chiller and cooling loop chiller, kW.

- *Component-level performance*

The absorber's performance is evaluated by its dehumidification COP, and latent effectiveness. The latent effectiveness is the ratio between the actual and maximum possible mass transfer in the absorber during dehumidification. These evaluation parameters are computed using the following equations:

$$COP_{deh} = \frac{MRR_{abs} \times h_{fg}}{\dot{Q}_{in}} \quad (15)$$

$$\epsilon_{latent,abs} = \frac{\omega_{air,inlet-} \omega_{air,outlet}}{\omega_{air,inlet-} \omega_{s,max}} \quad (16)$$

where

$\omega_{s,max}$ The equivalent specific humidity calculated as a function of desiccant temperature and concentration.

7. Uncertainty:

The propagation of systematic uncertainty was computed using Engineering Equation Solver (EES)[19], which uses an uncertainty propagation solver based on the Kline & McClintock method[20].

Table 12 Uncertainties of instrumentation and propagated uncertainties for derived quantities.

	Quantity	Uncertainty
Measurement	Temperature	0.5 °C
	Mass flow rate (water)	±1.4 GPM
	Air relative humidity	±1.0% RH & ±0.18 °F
	Velocity pressure	±0.25% Reading
Derived quantity	COP_{HP}	±3 – 4%
	$Q_{cooling}$	±3 – 5%
	$Q_{desorption}$	±1%
	MRR_{total}	±4 – 7%

[19] Klein S. Engineering Equation Solver. F-Chart Softw 2016.
[20] Kline S, Mcclintock F. Describing Uncertainties in Single-Sample Experimentstle. Mech Eng 1953;75:3–8.

Appendix A: Desorber Experimental Test Plan

As part of Task 3.0 of the DOE project, GTI will evaluate the technical feasibility and comparative performance of options for direct (preferred) and indirect-fired (steam/oil) desorbers. With design guidance from the project team, GTI will design and fabricate "simulators" for the desorber(s) to evaluate multiple combustion system design options and to assess the ability to meet or exceed performance and emission targets. In addition to this test plan, GTI will develop simulator design, "hot side" design options, and measurement schemes. Upon team approval, GTI will construct the simulator test rig, procure cost-effective options for the combustion system (burner, gas valve/controls, ignition system, blower/inducer), and shakedown the test rig. This test rig will be designed for flexible operation, as it will later be used in Task 6.0.

The purpose of this test plan is to outline the design of a desorber simulator and experimental methodology to evaluate a direct-fired approach. The combustion system will be optimized to maximize the performance of the desorber to remain within specified temperature limits of the ionic liquid solution while meeting emissions targets (e.g., California ultra-low NOx limit of 14 ng/J for gas-fired residential appliances). Together with CFD simulation results, the outcome of experimental testing will inform further design iterations of the desorber.

Background

The central component of the desorber system is a serpentine, multiple pass, plate heat exchanger design provided by UF, as shown in the figure below, as per the Milestone 1.2 activity.

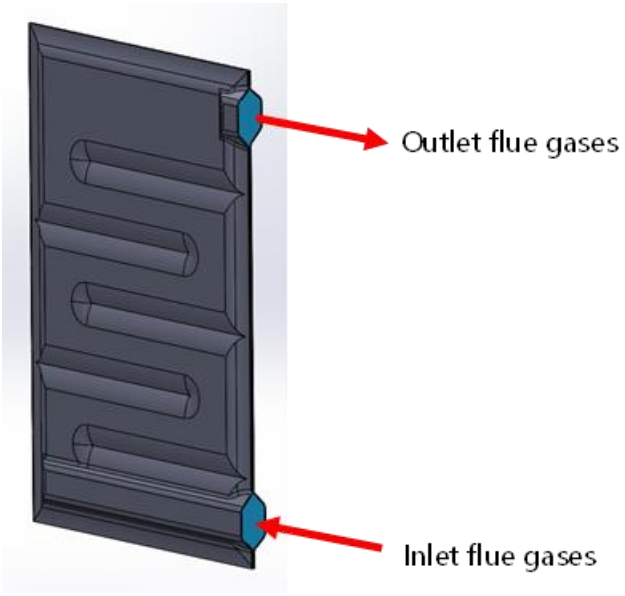

Figure 65: Heat exchanger component of desorber system

The following parameters were used to define boundary conditions based on theoretical calculations by GTI and experimental observations by UF:

- Firing rate: 10 kW (~34,000 BTU/hr)
- Excess air range: 20-50%

- Flame temperature: 1,650°C
- Film: Heat transfer coefficient = 200 W/m^{2}K, T = 140°C
- Pool: Heat transfer coefficient = 500 W/m^{2}K, T = 180°C

The heat exchanger design shown in Figure 65 and parameters listed above were used to perform CFD simulations to determine the severity and location of hot spot development on the surface. Simulation results yielded a flue gas outlet temperature of 232°C and combustion efficiency of 78%. The results also showed that hot spots exceeding the limit of 190°C (to avoid degradation of the ionic liquid) covered a significant area of the plate heat exchanger despite full immersion in the ionic liquid solution and increased plate numbers. To verify the outcome of the simulation campaign, a bench-scale experiment will need to be performed.

Research Questions

In evaluating a direct-fired desorber system, the following research questions will be addressed:

- How closely will experimental results align with simulation results?
    - What combustion efficiency will the fully premixed, surface stabilized burner system yield?
    - How many heat exchanger plates will be needed to provide sufficient heat dissipation?
    - Will a single inlet heat exchanger be sufficient or will a dual inlet design be necessary to avoid surface hot spots as suggested by the simulation results?
- How will back pressure generated by the heat exchangers affect combustion stability?
    - What is the minimum number of heat exchangers needed to avoid stability issues?
- Ultimately, this task seeks to answer the following primary questions:
    - Can the desorber be successfully operated in a direct-fired manner, achieving < 14 ng/J NO_x, while avoiding 'hot spots' of 190°C or greater?
    - How does the impact of a flooded or a partially-flooded desorber translate impact the aforementioned question?

Methodology

The experimental apparatus will comprise of five components:

1. Flue gas-to-ionic liquid solution heat exchanger
2. Tank for holding reservoir of ionic liquid solution (or surrogate fluid)
3. Radiant, forced-draft type burner to achieve Ultra-low NOx performance
4. Gas train
    a. Blower
    b. Fuel/air mixer
    c. Gas Valve
5. Combustion controls

The impact of these components, as designed and simulated for this experimental task, are as follows:

#1 and #2: Heat Exchanger and Solution Tank

To reduce manufacturing costs and lead time, an in-house fabrication procedure was devised that involved 3D printing of dies for stamping out the heat exchanger plates. PLA filament will be used

as the 3D printing material to minimize warping of the die. The hollow spaces within the 3D printed dies will be filled with a polyester resin to harden the die and allow for use with a hydraulic press. To maximize the success of this fabrication process, the sharp edges and corners in the original design of the heat exchanger from Figure 65 were replaced with rounded edges and sweeping corners. The 3D printed male die and female die design as well as the resulting heat exchanger assembly are shown in the following figure.

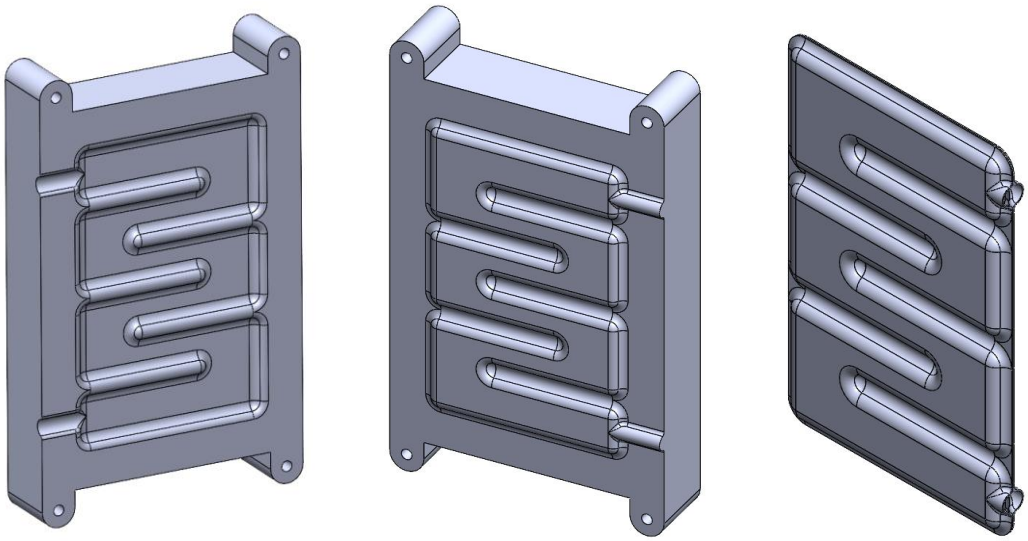

Figure 66: Female die, male die, and stamped out heat exchanger

Due to the limited area of the 3D printing surface, the width and height of the heat exchanger will be reduced by 25% from the original dimensions provided by UF, to a height and width of 8.9 in and 5.9 in, respectively. For initial testing, six plates will be stamped out to make three identical heat exchangers. The heat exchanger plates will be joined together by welding around the outside perimeter. Spot welding will also be performed on the concave surfaces separating the multiple passes of the heat exchanger to ensure flue gases follow the serpentine pathway.

If this manufacturing process is not successful, as judged by material integrity and leak tests, the project team will document the manufacturing process and will pivot to an off-the-shelf heat exchanger. Assuming that testing will be performed using a flooded design, the project team will utilize a forced-air heating type tubular heat exchanger, common in furnaces and unit heaters. The heat exchanger will be a 4-tube heat exchanger that is installed in some 80% efficient, 90,000 BTU/hr Goodman residential furnaces (e.g., model GMS80903BNA), as shown below. Generally, furnace heat exchangers can be divided into two types: "clamshell" and tubular. Although clamshell style heat exchangers can offer greater surface areas than tubular heat exchangers, they are typically designed for induced draft operation, and thus do not have a sealed construction. Rather, the heat exchanger plates are crimped together, making them incompatible for flooded operation.

Figure 67: Goodman furnace 4-tube heat exchanger (model # 4021309S)

The heat exchangers will be immersed inside an ionic liquid solution (or surrogate fluid) contained in a stainless steel batch can, as shown below. Insulation will be added to the outside of the tank to eliminate convective cooling of the fluid. A loose-fitting lid will also be placed over the tank opening with holes drilled out for temperature sensors. A drain port in the bottom will allow for easy disposal of the coolant.

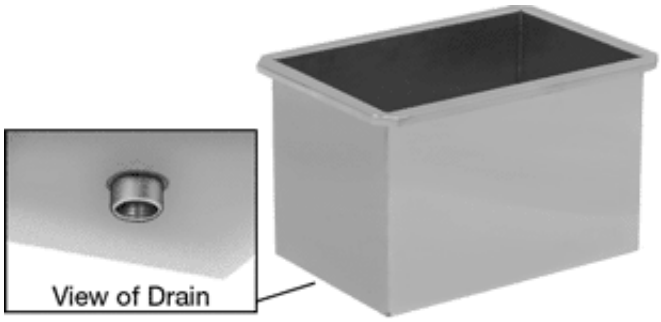

Figure 68: 7 gal. stainless steel batch can (McMaster-Carr item # 3763K252)

The experimental surrogate for the ionic liquid solution is DOWTHERM™ A, which is a synthetic organic heat transfer fluid developed by Dow that is suitable for applications between 60°F and 750°F (15°C to 400°C). At atmospheric conditions, however, the fluid has a boiling point of 495°F (257°C), which means that precautions need to be taken to ensure the fluid is not overheated. A plot of the fluid's specific heat with respect to temperature is shown in the figure below.

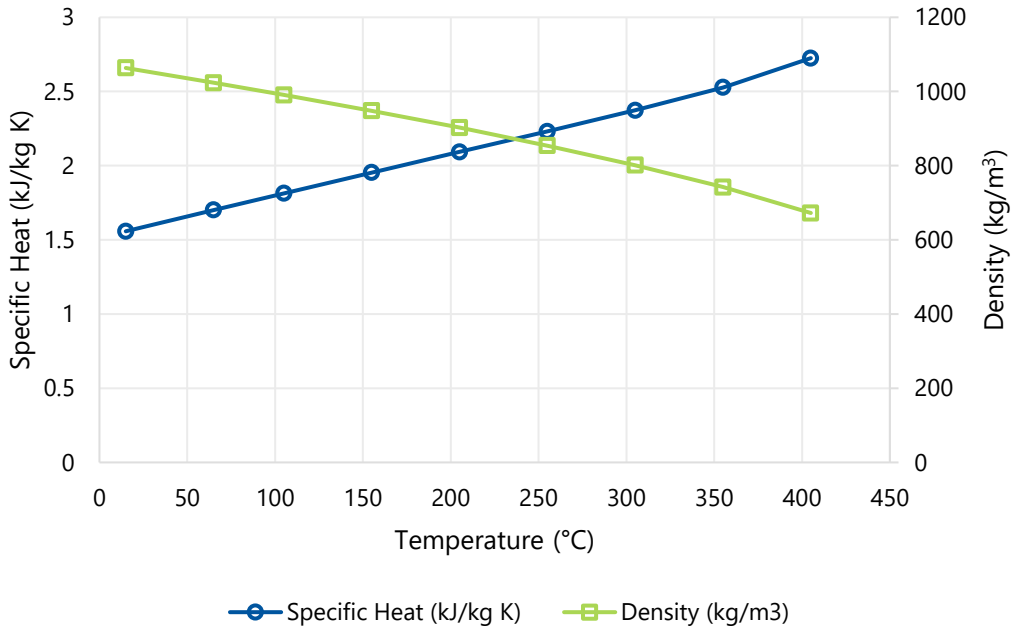

Figure 69: Saturated liquid properties of Dowtherm A Fluid

#3: Burner

Integral to determining if a direct-fired desorber is technically feasible is the design of the burner and how it mates with the desorber itself. In preliminary discussions, the project team has opted to go with a single, flat mesh-type burner. The burner will be mounted to a manifold, which will be mated to the tank surface. The manifold will carry the flue gases from the burner surface and through the openings in the tank for the tubular heat exchanger. An advantage of having a manifold system is that it will allow for burners of various sizes to be tested while only making modifications to the manifold and not the tank. The manifold will have multiple ports to accommodate thermocouples as well as the injection of dilution air to decrease the flue gas temperature entering the heat exchangers. This will provide a safeguard against the development of hot spots on the heat exchangers, as predicted by the CFD simulations.

The use of a radiant burner has several advantages when operating in this environment as compared to jet flames. The surface-stabilized flame limits surface impingement and ensures more efficient combustion and therefore less products of incomplete combustion such as CO. Mesh-type burners are also highly flexible with respect to operating conditions and can be operated in either orange or blue flame mode. This can help reduce NOx emissions for applications requiring strict adherence to emissions regulations (e.g., such as water heaters in California being limited to no more than 20 ppm of NOx). Furthermore, mesh-type burners can be designed to operate at high turndown ratios which are necessary for modulating applications. A possible challenge associated with the use of a mesh-type burner is the radiant energy output of the burner and potential hot spots that may form on the surface of the tank. A possible solution to this problem is to apply a radiant barrier to the tank surface facing the mesh surface of the burner.

#4 and #5: Gas Train and Combustion Controls

The combustion system that will be assembled for the desorber simulator is a fully premixed combustion system with a flat radiant burner, wherein the fuel and combustion air are mixed upstream of the burner and pressurized with a blower. Some of the advantages for this combustion system are as follows:

- Modulation: Variable speed blower control permits variation of the heating rate to the process, allowing for 5:1 turndown or greater to facilitate continuous process modulation. This fine control is often advantageous over discrete staging of individual or multiple burners, as is common with induced/natural draft equipment.
- Emissions: Pressurizing the fuel/air mixture allows the use of low-NOx burner designs whose flameholders have appreciable pressure drops, including woven/knitted fiber sheets, sintered fiber mats, ceramic/metallic foams, and other flameholders intended to decrease flame temperatures and NOx emissions.
- Efficiency: Similarly, the pressurization permits the use of more tortuous heat exchangers and the aforementioned premix burners with increased surface heat flux permits compact, more efficient heat transfer.

With these advantages, premix combustion systems are commonly deployed as part of high-efficiency gas-fired equipment, primarily for condensing boilers. These premixed combustion systems are comprised of five main components: the gas valve/regulator assembly, the blower, the fuel/air mixer, the premix burner, and the combustion controls (including ignition, gas valve, and blower speed controls). While the premix burner can vary widely from application to application, the modulating gas train (gas valve, blower, fuel/air mixer, ignition sense/control) is typically one of two configurations: pneumatic control and electronic control. Both cases permit modulation by adjusting the natural gas flow with the blower speed, in an attempt to maintain the air/fuel ratio (lambda, λ) over the modulation range. A schematic of a premixed combustion system with pneumatic control is shown below.

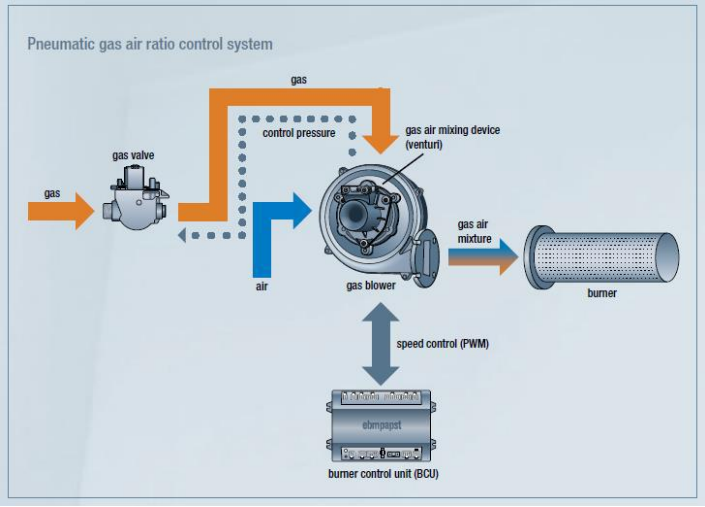

Figure 70: Premixed combustion system with pneumatic control (Source: ebm-Papst)

The complete combustion system, including burners, will be evaluated in both open air testing and optional closed chamber testing to determine the suitability of the combustion system based on the following criteria: (1) stable combustion at firing rate of 10 kW and throughout modulation with turndown ratio of at least 2:1, in which stability is characterized by proximity of the flame to the flameholder and absence of flashback (2) low CO (e.g., < 50 ppm at 0% oxygen) and NOx emissions (e.g., < 20 ppm at 0% oxygen) at a firing rate of 10 kW, and (3) stable combustion when dilution air is injected and back pressure is introduced. The open air testing will act as an initial screening to rank the burners from most to least suitable. Due to the difficulty in capturing accurate emissions in open air burner testing, the relative performance between the various burners will be used to judge the overall rank. Depending on how well the burners meet the above three criteria, the burners deemed most feasible for the direct-fired desorber application will advance to a second test phase with the burner being enclosed by a manifold, provided that a representative environment can be assured. On an as-needed basis, to further investigate burner dynamics based on in-situ testing (next section), second phase testing will use a damper or blast gate in the venting system to manipulate the back pressure according to estimates provided by CFD analysis. The combustion stability and emissions of the burner at a fixed firing rate will be examined at increasing back pressure, representing 3, 4, and 5 tube heat exchangers. Since both open air and closed burner testing will be operated without a load, accurate emissions measurements will be difficult to make. Therefore, a relative comparison of burner performance will be made to judge between them (i.e., the burner(s) that consistently produce the lowest CO and NOx emissions regardless of environment will rank highest).

For phase one of testing, a water-cooled probe will be placed approximately one inch above the flame holder material to obtain flue gas emissions at 0% or near-0% dilution. For phase two of testing on an as-needed basis, a suction pyrometer will be used to draw flue gas samples through a long tube and across an exposed bead thermocouple to measure the flue gas temperature inside the manifold.

Experimental Apparatus and Instrumentation

Once phase one and, as needed, two of burner testing is completed, the best performing burner based on the criteria discussed before will be selected for testing in the desorber test apparatus. A basic schematic outlining the general layout of the experimental apparatus is shown below. A 3D mockup of the apparatus is also shown.

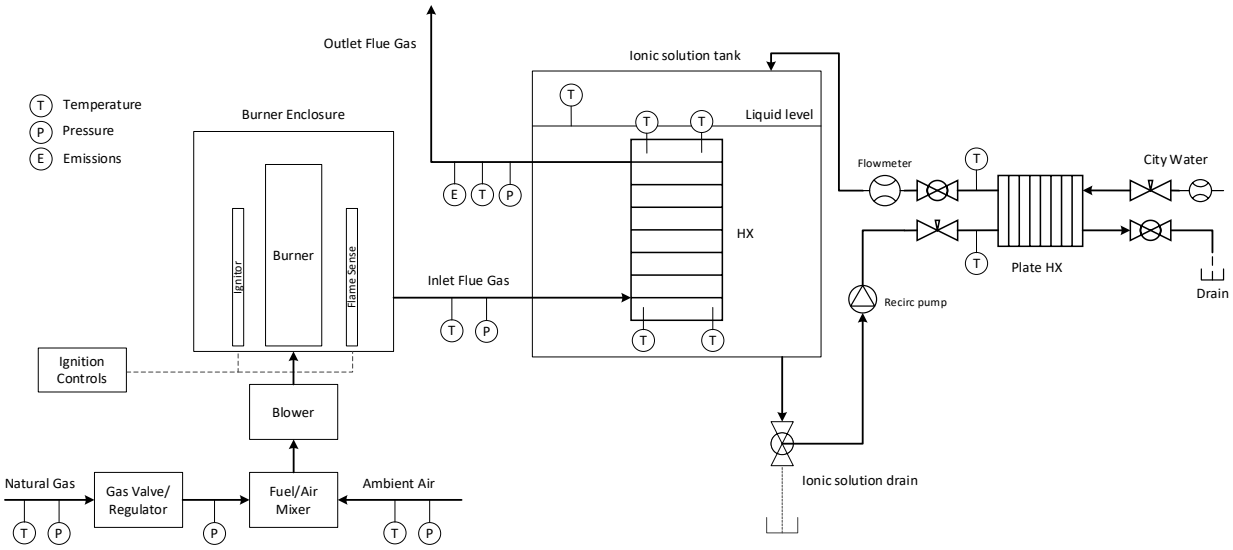

Figure 71: Desorber test apparatus

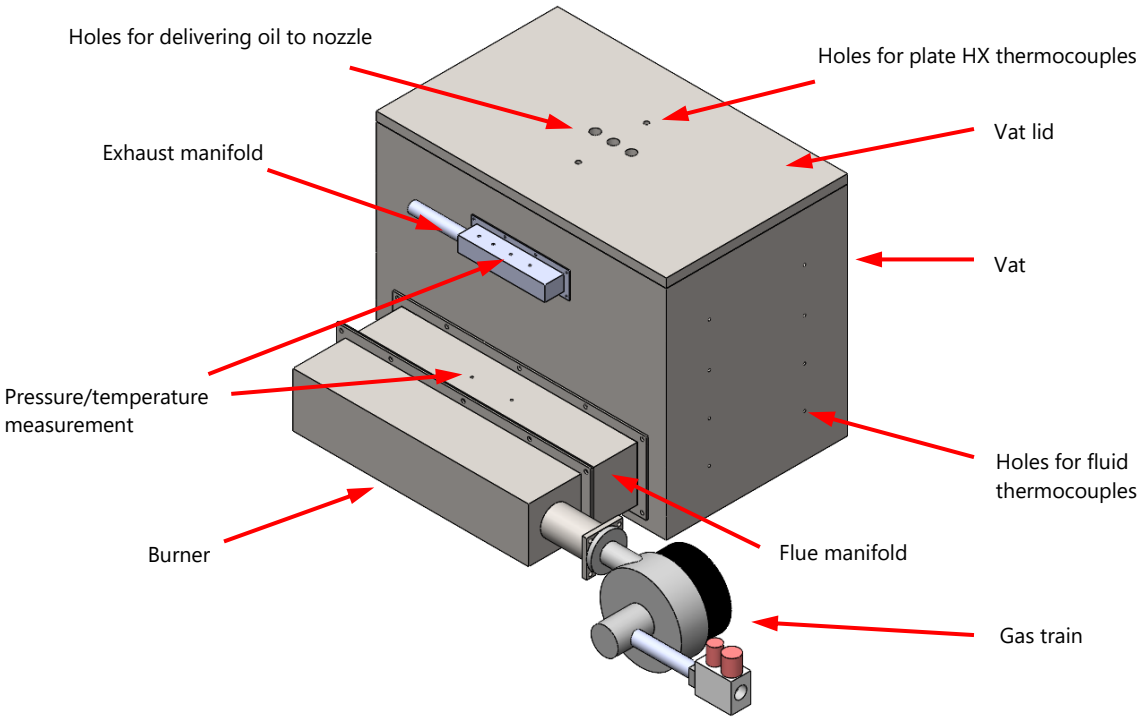

Figure 72: Figure 73: 3D representation of experimental apparatus - enclosed

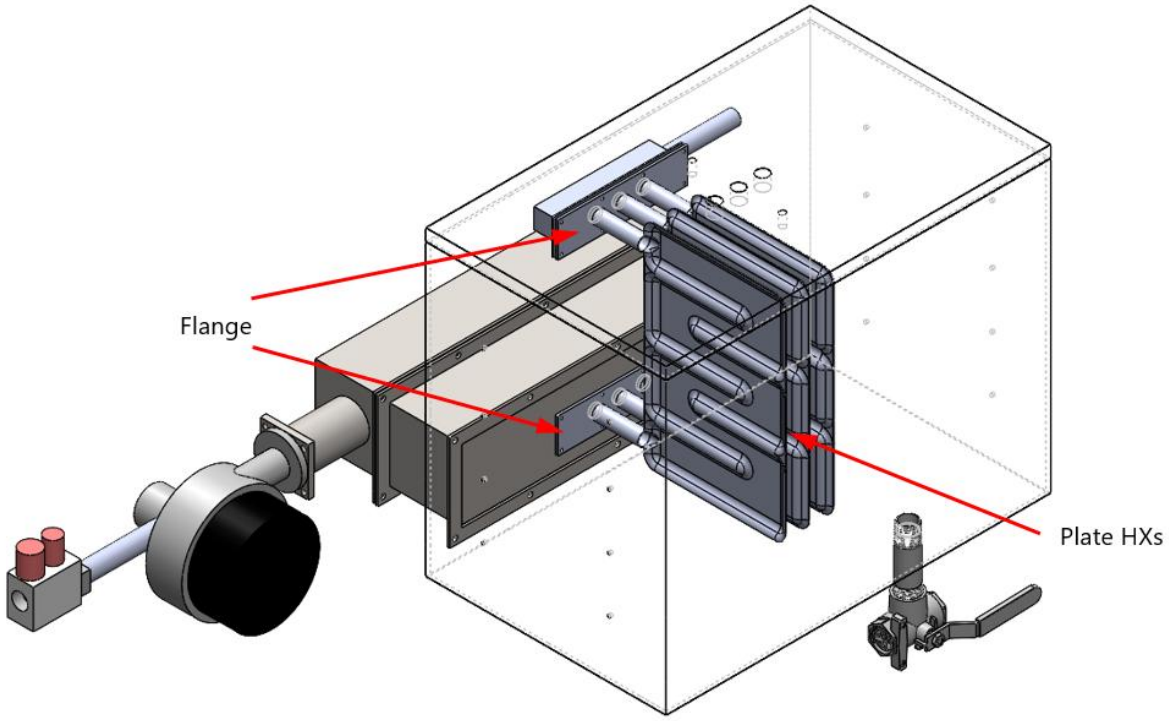

Figure 74: 3D representation of experimental apparatus - open

As shown in the figures above, the radiant burner will be a rectangular box with a woven/knitted metal fiber welded onto the open face of the box. The burner will be bolted to a manifold which will direct the flue gases into the heat exchangers inside the vat. The burner will be fed by a gas train manufactured by Honeywell and composed of the following parts:

- A FIME blower, PX118 model, with a max speed of 7,000 rpm, 56 CFM, and max outlet pressure of 10.4" W.C.
- A VK81 series gas valve, with pneumatic 1:1 air/fuel control
- A standard venturi 45.900.444-003 model, with an output range from 5 to 27 kW (17,000 to 92,000 Btu/hr)

The above components are labeled in the following figure.

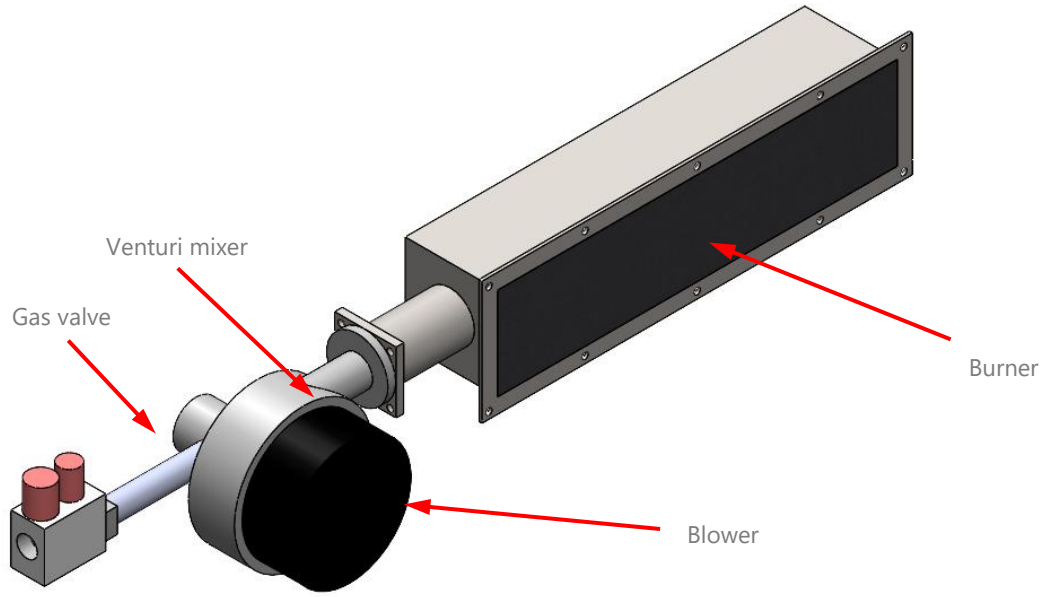

Figure 75: Burner assembly

Downstream of the burner, the flue gases will diverge at a manifold and be carried to the individual heat exchangers inside the tank. Temperature and pressure measurements will be taken of the gas train to monitor firing rate. The flue gas entering and leaving the heat exchangers will also be monitored for temperature and pressure to evaluate combustion efficiency and back pressure, respectively. A sample line will carry flue gases to a gas analyzer to monitor species composition and excess air. For the heat transfer fluid tank, a series of temperature probes will be submerged in the fluid to obtain an average temperature. Multiple thermocouples will also be attached to the heat exchanger surface at critical locations to detect hot spots.

To maintain the heat transfer fluid at a constant temperature of ~160°C, the heat transfer fluid will be recirculated at a flow rate of ~0.2 gal/min through a cooling loop with plate heat exchanger. Municipal water will be used as the coolant with a flow rate of ~0.13 gal/min to shed thermal load from the burner. Refer to the table below for a list of instrumentation.

Table 13: Summary of instrumentation

Measurement Type	Measurement Point	Instrument
Natural Gas	Dry Test Meter	Model: Elster AC-250
	Pressure Transducer	Model: Dwyer 668-7
	Thermocouple	K-Type Thermocouple Model: KQXL-116U-12
Ambient Air	Thermocouple	K-Type Thermocouple Model: KQXL-116U-12
	Relative Humidity	Model: TE HPP809A033
Combustion Blower	Pressure Transducer	Model: Dwyer 616D
	Embedded Tachometer	N/A
Exhaust Gases	Thermocouple	K-Type Thermocouple Model: KQXL-116U-12
	Pressure Transducer	Model: Dwyer 620
	Horiba Gas Analyzer	Model: PG-300
Desorber Simulator	Thermocouple	K-Type Thermocouple Model: KQXL-116U-12
	Water Flowmeter	Model: Omega FTB4607
	Thermal Fluid Flowmeter	Model: Omega FP-5061

Test Procedure

Phase one of burner testing will include preliminary testing of the combustion system using the various procured flameholder materials and burners. Each of the burners will be tested in turn to obtain the following:

- Qualitative assessment of flame stability at firing rate of 10kW down to 5 kW observing
    - Flame lift-off or flash back
    - Radiant vs blue flame operating mode
    - Uniformity of blue-flame or radiant combustion and prevalence of dark spots
- Quantitative assessment of CO and NOx emissions
    - CO < 50 ppm (at 0% oxygen)

- NOx < 22 ppm (at 3% oxygen)

Each of the burners will be tested at two firing rates and equivalence ratios as shown in the table below.

Table 14: Phase one burner test points

Test Point	Firing Rate	Equivalence Ratio
1	10 kW	1.2
2	10 kW	1.5
3	5 kW	1.2
4	5 kW	1.5

Based on the performance of the burners in phase one testing, those that demonstrate high levels of stability at varying firing rates and equivalence ratios while maintaining low levels of CO and NOx will proceed to in-situ testing within the desorber simulator. If issues are observed, on an as-needed basis, a second phase of burner testing will be used for further investigation and calibration of the combustion system parameters. In the second phase, test conditions will mimic the actual conditions of the mock desorber while still allowing for ease of testing on a burner table. The burner(s) will be tested at a constant firing rate of 10 kW and equivalence ratio of 1.5 (or highest achievable equivalence ratio without compromising on emissions) while varying the dilution air injection and back pressure. Test points are outlined in the table below.

Table 15: Phase two burner test points

Test Point	Dilution Air (Fraction of Stoich. AFR)	Back Pressure (inWC)
1	0	0.1
2	0	0.2
3	0	0.4
4	0.1	0.1
5	0.1	0.2
6	0.1	0.4
7	0.3	0.1
8	0.3	0.2
9	0.3	0.4

The back pressures listed in Table 14 are only an estimation of the expected pressure drops from the heat exchangers based on results from CFD simulations. The 3-tube heat exchanger yielded a

steady-state pressure drop of 30 Pa (0.12 inWC) from CFD simulations, whereas the 3-plate heat exchanger yielded a steady-state pressure drop of 100 Pa (0.4 inWC). Both CFD-based pressure drops were a result of using an equivalence ratio of 1.5 for the inlet mass flow condition. The criteria that will be used to judge the performance of the burner will be the extent to which flue gas temperatures can be reduced with increasing dilution air while adhering to emission limits for CO and NOx. The burner(s) that can withstand the greatest injection of dilution air while meet the emissions requirements at increased back pressure will be used for final testing in the mock desorber.

The main goals of testing within the desorber simulator will be a) to demonstrate the feasibility of direct-firing the desorber, while b) tuning of the combustion system to achieve low CO and NOx emissions while avoiding hot spot development on the heat exchanger. This will involve firing of the burner at the full 10 kW capacity with the (highest) equivalence ratio that was found to generate acceptable CO and NOx emissions based on phase one burner testing. As the thermal fluid begins to heat up, the thermal fluid and cooling water flow rates will be set to a nominal rate of 0.6 gal/min and 1.3 gal/min, respectively, based on an estimate using Dowtherm A fluid properties, to prevent overheating of the fluid and obtain a constant thermal fluid temperature. Thermocouples attached to the most susceptible regions of the heat exchanger (i.e., pipe entrance and outside radius of first and second pipe bends) will be used to monitor the heat exchanger surface temperature rise and potential hot spot formation. Once a steady state surface temperature is obtained, dilution air will be injected into the burner chamber/manifold to decrease the flue gas temperature entering the heat exchanger. At each nominal increase in dilution air (as a fraction of the stoichiometric air-fuel ratio) the steady-state surface temperature of the susceptible regions of the heat exchanger will be monitored at the same thermal fluid and cooling water flow rates. If at the highest possible dilution air injection there is still found to be persistent hot spots on the heat exchanger, the heat exchanger may be modified by attaching extended surfaces to enhance flue-to-liquid heat transfer in and around the hot spot zones or replaced entirely by a heat exchanger with more surface area. An example test matrix for the mock desorber experiment is outlined below. Actual dilution injection rates will depend on the outcome of phase two of burner testing.

Table 16: Combustion system test points for heat exchanger hot spot evaluation

Test Point	Dilution Air (Fraction of Stoich. AFR)
1	0
2	0.1
3	0.2
4	0.3
5	0.4
6	0.5

For each of the test points in Table 16, combustion efficiency will be calculated as follows using the burner firing rate and enthalpy of the outlet flue gas stream:

$$CE = \frac{\dot{V}_{NG} \times HHV_{NG} - \dot{m}_{flue,gas} \times h_{flue,out}}{\dot{V}_{NG} \times HHV_{NG}}$$

where $\dot{V}_{NG}$ is the flow rate of the natural gas feeding the burner based on the dry test diaphragm gas meter, HHV_{NG} is the gross calorific value of the natural gas, $\dot{m}_{flue,gas}$ is the estimated mass flow rate of the flue gas stream based on the combustion stoichiometry and fuel constituents, and $h_{flue,out}$ is the specific enthalpy of the outlet flue gas stream based on flue gas composition. A reference temperature of 60°F will be used for the calculation of the natural gas HHV which will be determined using ASTM D1945 - Standard Test Method for Analysis of Natural Gas by Gas Chromatography. Since the gas analyzers only provide mole fractions of gas species on a dry-basis, an approximation of the flue gas vapor content will be made based on the O2 and CO2 dry-basis concentrations and fuel composition. The heat input to the desorber can therefore be characterized as follows:

$$\dot{Q}_{in} = \dot{V}_{NG} \times HHV_{NG} - \dot{m}_{flue,gas} \times h_{flue,out}$$

To evaluate the heat output from the heat exchanger to the thermal fluid, the following equation will be used:

$$\dot{Q}_{out} = \dot{m} c_p (T_{out} - T_{in})$$

where $\dot{m}$ is the mass flow rate of the thermal fluid through the external heat exchanger, c_p is the specific capacity of the thermal fluid, and T_{out} and T_{in} are the temperatures of the thermal fluid leaving and returning to the tank, over a sufficiently long steady-state period to account for fluctuations of the stored fluid temperature. Due to the large thermal fluid volume compared to flow rate (i.e., ~30 gal vs. 0.6 gal/min) reaching a perfectly steady-state temperature may not be practical. Therefore, an approximation of heat output will be made once inlet and outlet thermal fluid temperatures are within +/- 2°F for at least 5 minutes. The efficiency of the desorber heat transfer process can then be characterized as follows:

$$\eta = \frac{\dot{Q}_{out}}{\dot{Q}_{in}}$$

Multiple plots will be generated of the heat exchanger surface temperatures at the hot spot locations with respect to desorber heat input, heat output, and efficiency to demonstrate the flue conditions required to achieve sub-190°C surface temperatures and therefore safe desorber operation.

Appendix B: Desorber Heat Transfer Analysis

Heat Transfer from Desorber Heat Exchanger to Oil

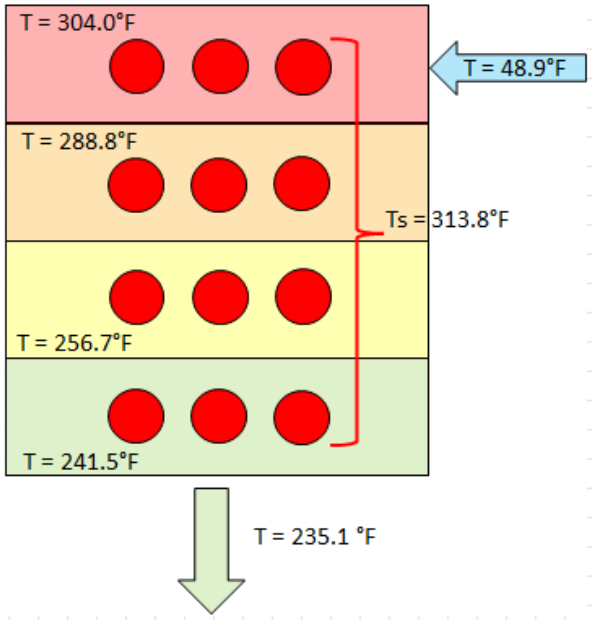

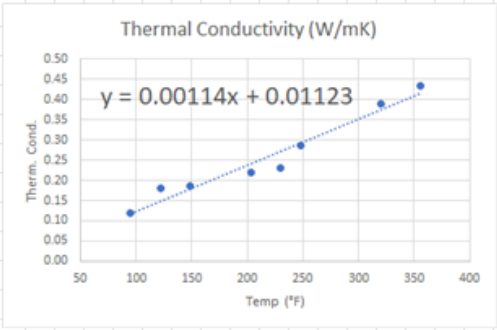

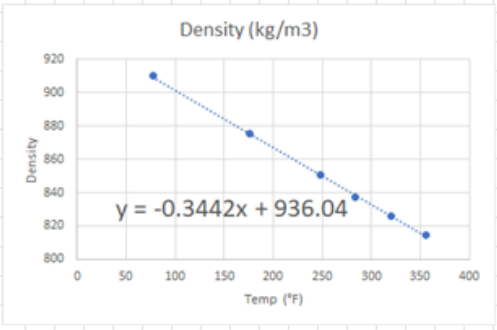

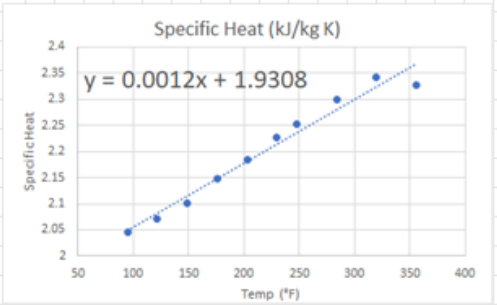

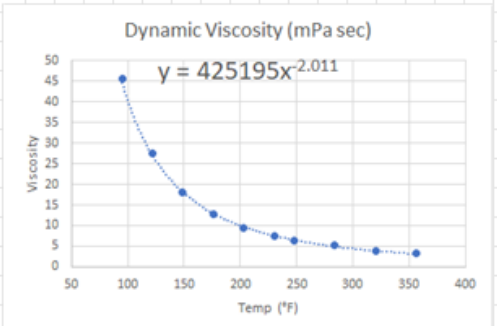

Steady-state Peanut Oil Properties

Peanut Oil Temperatures from 1/9/2023 – Part 1 & 2 Test

Average fluid temperature: $T_{inf} := 272.8\ °F$

Average heat exchanger surface temperature: $T_s := 313.8\ °F$

Average film temperature: $T_f := \frac{T_s + T_{inf}}{2} = 293.3\ °F$

Fluid properties at film temperature (natural convection):

Thermal conductivity:

$$k_f := \left(0.00114 \cdot \frac{T_f}{°F} + 0.01123\right) \frac{W}{m\ K} = 0.3456\ \frac{W}{m\ K}$$

Density:

$$\rho_f := \left(-0.3442 \cdot \frac{T_f}{°F} + 936.04\right) \frac{kg}{m^3} = 835.0861\ \frac{kg}{m^3}$$

Specific Heat Capacity

$$C_{p,f} := \left(0.0012 \cdot \frac{T_f}{°F} + 1.9308\right) \frac{kJ}{kg\ K} = 2.2828\ \frac{kJ}{kg\ K}$$

Dynamic Viscosity

$$\mu_f := \left(425195 \cdot \left(\frac{T_f}{°F}\right)^{-2.011}\right) \cdot 0.001\ Pa\ s = 0.0046\ s\ Pa$$

Kinematic Viscosity:

$$\nu_f := \frac{\mu_f}{\rho_f} = 5.5602 \cdot 10^{-6}\ \frac{m^2}{s}$$

Prandtl Number:

$$Pr_f := \frac{C_{p,f} \cdot \mu_f}{k_f} = 30.6705$$

Coefficient of volume expansion (olive oil):

$$\beta := 0.0007\ K^{-1}$$

Natural Convection over Horizontal Cylinder

The equations and figures from this section have been taken from Heat Transfer: A Practical Approach 2nd Edition by Y.A. Cengel and M.A. Boles (pg 468)

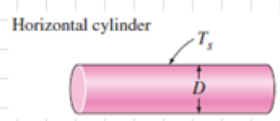

D | $Ra_D \le 10^{12}$ | $Nu = \left\{0.6 + \frac{0.387Ra_D^{1/6}}{[1 + (0.559/Pr)^{9/16}]^{8/27}}\right\}^2$

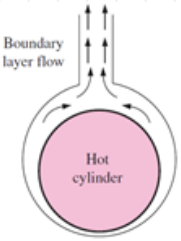

FIGURE 9–12
Natural convection flow over a horizontal hot cylinder.

Characteristic Length: $L_c := 2\ in$ $D := 2\ in$

$$Gr := \frac{g_e \cdot \beta \cdot \left(T_s - T_{inf}\right) \cdot L_c^3}{\nu_f^2} = 6.6304 \cdot 10^5$$

Rayleigh number:

$$Ra_D := Gr \cdot Pr_f = 2.0336 \cdot 10^7$$

Nusselt number:

$$Nu := \left(0.6 + \frac{0.387 \cdot Ra_D^{\frac{1}{6}}}{\left(1 + \left(\frac{0.559}{Pr_f}\right)^{\frac{9}{16}}\right)^{\frac{8}{27}}}\right)^2 = 46.3374$$

$$h_{HX,nat.conv.} := \frac{k_f}{D} \cdot Nu = 315.2332\ \frac{W}{m^2\ K}$$

HX Surface Area: $SA := 826.56\ in^2$

$$Q_{nat.conv} := h_{HX,nat.conv.} \cdot SA \cdot \left(T_s - T_{inf}\right) = 3828.9983\ W$$

$$q_{flux} := \frac{Q_{nat.conv}}{SA} = 7180.3126\ \frac{W}{m^2}$$

Wall Thickness: $\frac{2\ in - 1.875\ in}{2} = 0.001588\ m$

Actual energy input from burner: $Q_{burner} := 3.918\ kW$

$$Error := \frac{Q_{burner} - Q_{nat.conv}}{Q_{burner}} = 2.3\ \%$$

Appendix C: IEA Heat Pump Conference 2023 Paper

The following conference paper is attached here for UTD member reference:

Bhagwat, R.; Schmid, M.; Ahsan, A.; Kumar, N.; Glanville, P.; Moghaddam, S.; *Ionic liquid absorption system for dehumidification and IAQ enhancement in built environment*, Proceedings of the 14th IEA Heat Pump Conference (2023), Chicago, IL.